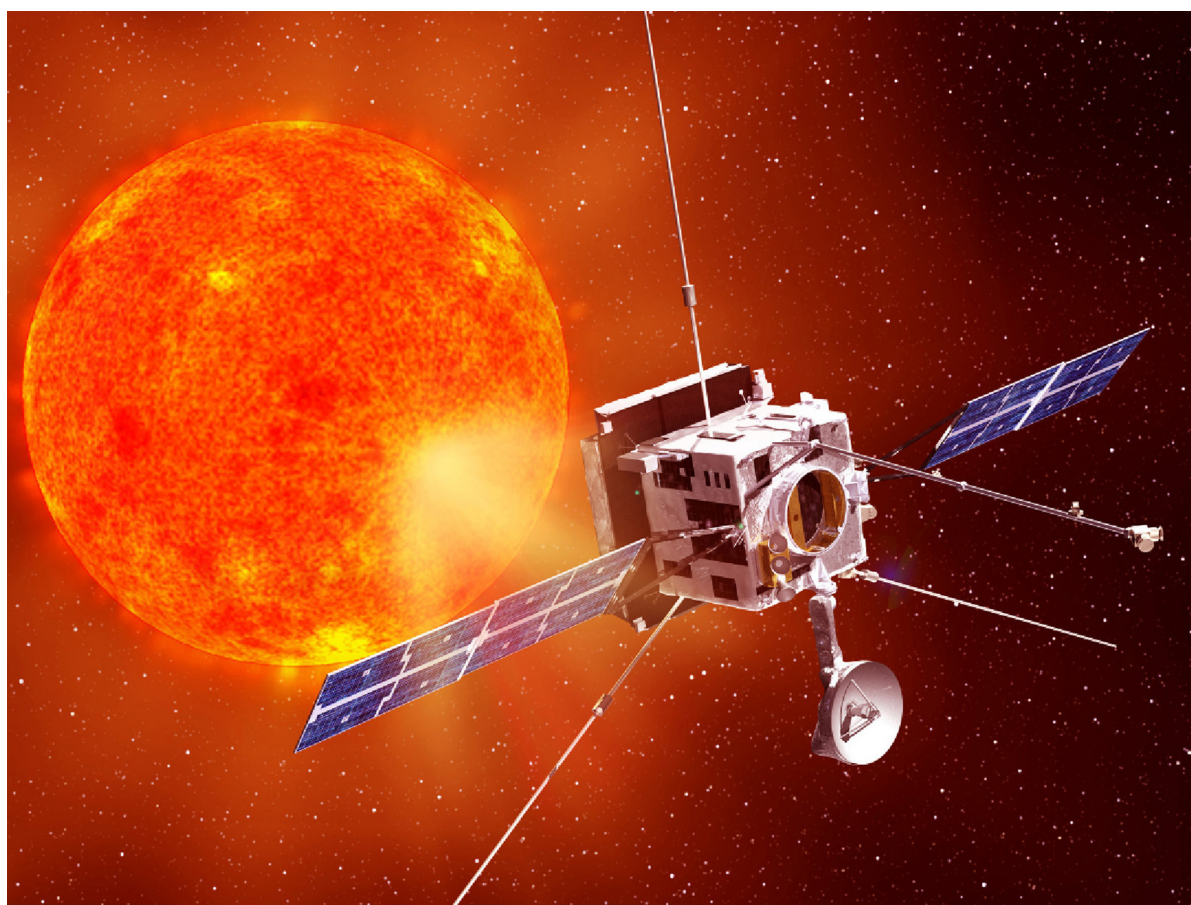


Solar Orbiter

Exploring the Sun-heliosphere connection



Assessment Study Report

This page left intentionally blank

Table of Contents

Foreword.....	iv
Authorship and Acknowledgements.....	v
1.0 Executive Summary	1
2.0 Science Objectives.....	5
2.1 How and where do the solar wind plasma and magnetic field originate in the corona?.....	7
2.1.1 What are the source regions of the solar wind and the heliospheric magnetic field?	8
2.1.2 What mechanisms heat and accelerate the solar wind?	12
2.1.3 What are the sources of turbulence in the solar wind and how does it evolve?	14
2.2 How do solar transients drive heliospheric variability?.....	15
2.2.1 How do CMEs evolve through the corona and inner heliosphere?	15
2.2.2 How do CMEs contribute to the solar magnetic flux and helicity balance?	17
2.2.3 How and where do shocks form in the corona and inner heliosphere?	19
2.3 How do solar eruptions produce energetic particle radiation that fills the heliosphere?	21
2.3.1 How and where are energetic particles accelerated at the Sun?	21
2.3.2 How are energetic particles released from their sources and distributed in space and time?	25
2.3.3 What are the seed populations for energetic particles?	26
2.4. How does the solar dynamo work and drive the connections between the Sun and heliosphere?.....	27
2.4.1. How is magnetic flux transported to and reprocessed at high solar latitudes?	28
2.4.2. What are the properties of the magnetic field at high solar latitudes?	30
2.4.3. Are there separate dynamo processes acting in the Sun?	31
3.0 Science Implementation: Scientific Requirements and Payload.....	33
3.1. Observations, Measurements, and Orbital Characteristics	33
3.1.1 Measurement Requirements and Instrument Capabilities	33
3.1.2 Orbit Requirements.....	35
3.1.3 Summary of Requirements on the Solar Orbiter Spacecraft	48
3.2 Selected Payload Summary	49
3.2.1 In-Situ Instruments	49
3.2.2 Remote-Sensing Instruments	57
3.3 Science Operations Coordination and Science Planning.....	63
3.3.1 Data Rates, Telemetry, Inter-Instrument Communication & Burst Mode	63
3.3.2. Sample Science Orbits.....	64
3.4. Supporting Observations.....	64
3.4.1. Space-Based Observations Supporting Solar Orbiter Science	64
3.4.2. Ground-Based Observations Supporting Solar Orbiter Science.....	65
3.5. Theory, Modelling, and Scientific Closure	66
4.0 Mission Implementation: Mission Design and Operations	67
4.1 Baseline Mission Design	67
4.1.1 Launch and Launch Vehicle Selection.....	68
4.1.2 Baseline Mission Trajectory (2017 Launch).....	68
4.1.3 Back-up Mission (2018 Launch)	68
4.2 Spacecraft Overview	69
4.2.1 Spacecraft Description.....	70

4.2.2 BepiColombo Technology Re-use	72
4.2.3 Spacecraft Subsystems.....	72
4.3 System Budgets.....	76
4.3.1 Mass Budget	77
4.3.2 Power Budget.....	77
4.3.3 Link Budget	78
4.3.4 Data Storage Budget.....	78
4.3.5 Pointing Budget	78
4.4 Technical Challenges	79
4.5 Mission Environment.....	80
4.6 Mission Operations Concept.....	81
4.6.1 Ground Segment Architecture	82
4.6.2 Spacecraft Operations Approach	84
4.7 Science Operations Concept	84
4.7.1 Science Operations Centre.....	84
4.7.2 Payload Operations Approach	84
4.7.3 Science Management Plan.....	85
5.0 Management	87
5.1 Industrial Organization	87
5.2 Payload Procurement	87
5.3 Solar Orbiter Schedule.....	87
6.0 References	89
7.0 Acronyms	91

Mission Description

Solar Orbiter Mission Summary	
Top-level Science Questions	<ul style="list-style-type: none"> • How and where do the solar wind plasma and magnetic field originate in the corona? • How do solar transients drive heliospheric variability? • How do solar eruptions produce energetic particle radiation that fills the heliosphere? • How does the solar dynamo work and drive connections between the Sun and the heliosphere?
Science Payload	<ul style="list-style-type: none"> • Heliospheric In-Situ Instruments: <ul style="list-style-type: none"> • Solar Wind Analyser (SWA) • Energetic Particle Detector (EPD) • Magnetometer (MAG) • Radio and Plasma Wave analyser (RPW) • Solar Remote-Sensing Instruments: <ul style="list-style-type: none"> • Polarimetric and Helioseismic Imager (PHI) • EUV full-Sun and high-resolution Imager (EUI) • EUV spectral Imager (SPICE) • X-ray spectrometer/telescope (STIX) • Coronagraph (METIS/COR) • Heliospheric Imager (SoloHI)
Mission Profile	<ul style="list-style-type: none"> • Launch on NASA-provided Evolved Expendable Launch Vehicle (Soyuz-Fregat 2-1B as back-up) • Interplanetary cruise with chemical propulsion and gravity assists at Earth and Venus. • Operational orbit in 3:2 resonance with Venus with multiple Venus gravity assists to increase inclination
Spacecraft	3-axis stabilised platform, heat shield, two adjustable, 2-sided solar arrays, dimensions: 2.5 x 3.0 x 2.5 m ³ (launch configuration)
Orientation	Sun-pointing
TM band	X/Ka
Data downlink	150 kbps (at 1 AU S/C-Earth distance)
Launch date	Jan-2017 (Jul-2018 back-up)
Nominal Mission duration	7.5 yr (incl. cruise phase)
Extended Mission duration	2.4 yr
Post-ops & Archiving	2.0 yr
Ground TM station	New Norcia (Australia) or Cebreros (Spain), 35-m antenna, 4 to 8 hrs/day (effective)
Programmatic	<ul style="list-style-type: none"> • ESA is responsible for the Solar Orbiter spacecraft, transfer to nominal science orbit, mission operations. • NASA is responsible for launch vehicle provision and launch operations. • Science payload provided by ESA Member States and NASA (already selected via competitive AO process in 2008/9)

Foreword

Over the last 10 years since the first Solar Orbiter mission studies were conducted, results from new missions have become available that show that the scientific relevance and timeliness of the mission have only increased, making the broad international community support for the mission stronger than ever. At the time of this writing, we are experiencing a solar minimum much deeper than any in the space age; indeed it is almost a century since the Sun has been so devoid of active regions. This development was not predicted and serves to illustrate both the complexity of solar activity and the challenges remaining in our quest to understand the Sun.

The Solar Orbiter mission has its origins in a proposal called “Messenger” that was submitted by Richter et al. in 1982 in response to an ESA call for mission ideas. At the meeting “Crossroads for European Solar and Heliospheric Physics” held on Tenerife in March 1998, the heliophysics community recommended to “Launch an ESA Solar Orbiter as ESA’s [next flexible] mission, with possible international participation, [for launch] around 2007.” The kick-off meeting for a pre-assessment study of the “ESA Solar Orbiter” concept was held at ESTEC on 25 March 1999.

Solar Orbiter was subsequently proposed in 2000 by E. Marsch et al., and was selected by the Science Programme Committee (SPC) in October 2000 as a Flexi-mission for launch after BepiColombo (in the 2008-2013 timeframe). A number of internal and industrial studies were then carried out, including parallel system-level Assessment Studies performed in industry between April and December 2004. At its 107th meeting in June 2004, the SPC confirmed Solar Orbiter’s place in the Horizon 2000+ programme, with the goal of a launch in October 2013 and no later than May 2015.

Work continued on the mission and payload definition throughout 2005 and 2006, and at its meeting in February 2007, SPC instructed the Executive to find ways to implement Solar Orbiter within a financial envelope of 300 M€ (at 2006 EC), while keeping a realistic contingency margin. In response to this request, a Joint Science and Technology Definition Team (JSTDT) comprising scientists and engineers appointed by ESA and NASA, studied the benefits to be gained by combining ESA’s Solar Orbiter mission and NASA’s Solar Sentinels into a joint programme.

This led to the release of an ESA Announcement of Opportunity (AO) for the Solar Orbiter Payload on 18 September 2007 and a NASA Small Explorer Focused Opportunity for Solar Orbiter (SMEX/FOSO) AO that was issued on 22 October 2007. In total, 14 proposals were received by ESA in response to the Payload AO. The final report of the Payload Review Committee (PRC), giving a recommended payload for selection, was issued on 24 May 2008. Meanwhile, at its meeting in November 2007, SPC gave approval to start an 18-month industrial Phase B1 study lead by Astrium UK and this was kicked off in March 2008.

A major change in the progress of Solar Orbiter occurred in November 2008, when the SPC decided to integrate Solar Orbiter into the first planning cycle of Cosmic Vision 2015-25 as an M-mission candidate for the first launch opportunity in 2017. In addition, in view of NASA’s high prioritization of Solar Probe Plus (SPP) in its Living With a Star programme (compared with Sentinels), and the strong science synergies between Solar Orbiter and SPP, ESA called for an independent review of the PRC’s recommended payload, now in the context of a joint Solar Orbiter-SPP scientific programme. The joint ESA-NASA review panel confirmed the validity of the recommended payload in its report of March 2009. As a result, the instrument selections, as recommended by the PRC in 2008, were formally announced on 20 March 2009. In parallel, NASA announced the results of the FOSO selection, and selected 2 instruments and portions of 2 instruments to be included in the Solar Orbiter payload. A Design Status Review, being the final review of the industrial Phase B1 study conducted by Astrium UK as prime, was held in ESTEC in June 2009.

This report presents an overview of the Solar Orbiter mission in its present state of advanced definition, based largely on the recent industrial study activities, and demonstrates the scientific importance of the mission as the next logical step in solar and heliospheric physics.

Authorship and Acknowledgements

The material for this report was provided by the members of the Solar Orbiter Science Working Team, together with the ESA Solar Orbiter Project Team, the ESA Study Scientists, the industrial study team led by Astrium UK, and members of the science community. The final document was compiled and edited by:

Don Hassler (SWRI, Boulder)
 Timothy Horbury (ICSTM, London)
 William Lewis (SWRI, San Antonio)
 Glenn Mason (JHU/APL, Laurel)
 Chris Owen (UCL/MSSL)
 Sami Solanki (MPS, Lindau)
 Marco Velli (JPL/U. Firenze)
 Robert Wimmer-Schweingruber (U. Kiel)

Key contributions to the science and payload sections were provided by:

Ester Antonucci (Obs. Torino)	Eckart Marsch (MPS, Lindau)
Arnold Benz (ETH Zürich)	Valentin Martinez Pillet (IAC)
Craig DeForest (SWRI, Boulder)	Pierre Rochus (CSL)
Richard Harrison (RAL)	Javier Rodriguez-Pacheco (U. Alcalá)
Russ Howard (NRL)	Angelos Vourlidas (NRL)
Milan Maksimovic (Obs. Meudon)	

Technical content was provided by:

Philippe Kletzkine (Project Manager, ESA)
 Danielle Renton (Payload Engineer, ESA)
 Javier Marti Canales (System Engineer, ESA)
 Jose Rodriguez-Canabal (Mission Operations, ESA)
 Jose-Luis Pellon-Bailon (Mission Operations, ESA)
 Ivan Ferrario (Project Manager, Astrium UK)

ESA planning and coordination office:

Marcello Coradini
 Philippe Escoubet
 Fabio Favata
 Timo Prusti

The valuable input provided by the members of the Red Team led by Len Fisk, who reviewed an earlier draft of this report, is gratefully acknowledged. Thanks go to NASA for its support in the preparation of this report, in particular to Richard Fisher, Madhulika Guhathakurta, Haydee Maldonado, and Chris St.Cyr. Thanks also go to Rosemary Ryan (SWRI, Rockville) for support during the reviewing and writing of this report. Finally, we wish to acknowledge the important contribution of the Organizing Committees of the three Solar Orbiter Workshops, in particular: Eckart Marsch, Valentin Martinez Pillet (chair, 1st Solar Orbiter Workshop), Kanaris Tsinganos (chair, 2nd Solar Orbiter Workshop), and Ester Antonucci (chair, 3rd Solar Orbiter Workshop). These Workshops were essential in defining the mission's science and for maintaining the community involvement over the years.

Richard G. Marsden (Study Scientist, ESA)
 Daniel Müller (Deputy Study Scientist, ESA)

This page left intentionally blank.

1.0 Executive Summary

We live in the extended atmosphere of the Sun, a region of space known as the heliosphere. Understanding the connections and the coupling between the Sun and the heliosphere is of fundamental importance to addressing one of the major scientific questions of Cosmic Vision 2020: “How does the Solar System work?” The heliosphere also represents a uniquely accessible domain of space, where fundamental physical processes common to solar, astrophysical and laboratory plasmas can be studied under conditions impossible to reproduce on Earth, or to study from astronomical distances.

The results from missions such as Helios, Ulysses, Yohkoh, SOHO, TRACE and RHESSI, as well as the recently launched Hinode and STEREO missions, have formed the foundation of our understanding of the solar corona, the solar wind, and the three-dimensional heliosphere. Each of these missions had a specific focus, being part of an overall strategy of coordinated solar and heliospheric research. However, an important element of this strategy has yet to be implemented. None of these missions have been able to fully explore the interface region where the solar wind is born and heliospheric structures are formed with sufficient instrumentation to link solar wind structures back to their source regions at the Sun. For example, Helios 1 and 2 carried no imaging instruments. With previously unavailable observational capabilities provided by the powerful combination of in-situ and remote-sensing instruments and the unique inner-heliospheric mission design specifically tailored for the task, Solar Orbiter will address the central question of heliophysics: ***How does the Sun create and control the heliosphere?***

This primary, overarching scientific objective can be broken down into four interrelated scientific questions, all of which have strong, direct relevance to the Cosmic Vision theme “How does the Solar System work?” The four top-level scientific questions being addressed by Solar Orbiter are:

- How and where do the solar wind plasma and magnetic field originate in the corona?
- How do solar transients drive heliospheric variability?
- How do solar eruptions produce energetic particle radiation that fills the heliosphere?
- How does the solar dynamo work and drive connections between the Sun and the heliosphere?

These are outstanding fundamental questions in solar and heliophysics today. By addressing them, we will make major breakthroughs in our understanding of how the inner solar system works and is driven by solar activity.

To answer these questions, it is essential to make in-situ measurements of the solar wind plasma, fields, waves, and energetic particles close enough to the Sun that they are still relatively pristine and have not had their properties modified by subsequent transport and propagation processes. This is one of the fundamental drivers for the Solar Orbiter mission, which will approach the Sun to within 0.25 AU.

Relating these in-situ measurements back to their source regions and structures on the Sun requires simultaneous, high-resolution imaging and spectroscopic observations of the Sun in and out of the ecliptic plane. The resulting combination of in-situ and remote sensing instruments on the same spacecraft, together with the new, inner-heliospheric perspective, distinguishes Solar Orbiter from all previous and current missions, enabling breakthrough science which can be achieved in no other way.

Mission Design. A mission profile for Solar Orbiter has been developed that will, for the first time, make it possible to study the Sun with a full suite of in-situ and remote-sensing instruments from inside 0.25 AU and provide imaging and spectral observations of the Sun’s polar regions from out of the ecliptic. This proximity to the Sun will also have the significant advantage that the spacecraft will fly in near synchronization with the Sun’s rotation, allowing observations of the solar surface and heliosphere to be studied from a near co-rotating vantage point for almost a complete solar rotation.

The baseline mission is planned to start on 4 January 2017 with a launch on a NASA-provided launch vehicle from Cape Canaveral, placing the spacecraft on a ballistic trajectory that will be combined with planetary gravity assist manoeuvres (GAM) at Earth and Venus. The initial resonance with Venus is 4:3, switching to 3:2 after the third Venus GAM. The resultant operational orbit has an orbital period of 150 days, a perihelion radius of 0.23 AU and an initial solar inclination of 7.7°. A series of Venus gravity assists (every 450 days) will then increase the solar inclination. The end of the nominal mission occurs 7.5 years after launch, when the

orbit inclination relative to the solar equator exceeds 25° . The inclination may be further increased during an extended mission phase using additional Venus GAMs, to reach a maximum of 34° .

Scientific Payload. The scientific payload of Solar Orbiter will be provided by ESA member states and NASA, and has already been selected and funded for the definition phase through a competitive AO selection process. The 10 principal investigator-led hardware investigations are:

The in-situ instruments:

- The Solar Wind Analyser (SWA) instrument suite (C. J. Owen, PI, UK) will fully characterize the major constituents of the solar wind plasma (protons, alpha particles, electrons, heavy ions) between 0.23 and 1.4 AU.
- The Energetic Particle Detector (EPD) experiment (J. R. Pacheco, PI, Spain) will measure the properties of suprathermal ions and energetic particles in the energy range of a few keV/n to relativistic electrons and high-energy ions (100 MeV/n protons, 200 MeV/n heavy ions).
- The Magnetometer (MAG) experiment (T. S. Horbury, PI, UK) will provide detailed in-situ measurements of the heliospheric magnetic field.
- The Radio and Plasma Waves (RPW) experiment (M. Maksimovic, PI, France) will measure magnetic and electric fields at high time resolution and determine the characteristics of electromagnetic and electrostatic waves in the solar wind from almost DC to 20 MHz.

The remote-sensing instruments:

- The Polarimetric and Helioseismic Imager (PHI) (S. K. Solanki, PI, Germany) will provide high-resolution and full-disk measurements of the photospheric vector magnetic field and line-of-sight velocity as well as the continuum intensity in the visible wavelength range.
- The Extreme Ultraviolet Imager (EUI) (P. Rochus, PI, Belgium) will provide image sequences of the solar atmospheric layers from the photosphere into the corona.
- The Spectral Imaging of the Coronal Environment (SPICE) EUV Spectrograph (D. M. Hassler, PI, U.S.) will provide spectral imaging of both the solar disk and in the corona to remotely characterize plasma properties of regions at and near the Sun.
- The Spectrometer/Telescope for Imaging x-rays (STIX) (A. O. Benz, PI, Switzerland) provides imaging spectroscopy of solar thermal and non-thermal x-ray emission from ~ 4 to 150 keV.
- The Multi Element Telescope for Imaging and Spectroscopy (METIS/COR) Coronagraph (E. Antonucci, PI, Italy) will perform broad-band and polarized imaging of the visible K-corona and narrow-band imaging of the UV and EUV corona.
- The Solar Orbiter Heliospheric Imager (SoloHI) (R. A. Howard, PI, U.S.) will image both the quasi-steady flow and transient disturbances in the solar wind over a wide field of view by observing visible sunlight scattered by solar wind electrons.

Spacecraft. The Solar Orbiter spacecraft is a Sun-pointed, 3-axis stabilized platform, with a dedicated heat shield to provide protection from the high levels of solar flux near perihelion. Feed-throughs in the heat shield (with individual doors) provide the remote-sensing instruments with their required fields-of-view to the Sun. Two-sided solar arrays provide the capability to produce the required power throughout the mission over the wide range of distances from the Sun using rotation about their longitudinal axis to allow switching between faces, as well as control of the solar aspect angle to allow management of the array temperature throughout the mission, particularly during closest approach to the Sun. An articulated high temperature high gain antenna provides nominal communication with the ground station, and a medium gain antenna and two low gain antennas are included for use as backup. The design drivers for the Solar Orbiter spacecraft come not only from the need to satisfy the mission's technical and performance requirements, but also from the need to minimize the total cost of the mission. The adopted philosophy is therefore to avoid technology development as far as possible, in order to maintain the cost-cap of the mission in keeping with its M-class status. The design of Solar Orbiter has therefore incorporated BepiColombo technology items where appropriate. Furthermore, design heritage from the Express series of missions, with their goal of rapid and streamlined development, has also featured heavily in the Solar Orbiter spacecraft design.

Mission Operations. One of the strengths of the Solar Orbiter mission is the synergy between in-situ and remote-sensing observations, and each science objective requires coordinated observations between several

in-situ and remote-sensing instruments. Another unique aspect of Solar Orbiter, in contrast to near-Earth observatory missions like SOHO, is that Solar Orbiter will operate much like a planetary encounter mission, with the main scientific activity and planning taking place during the near-Sun encounter part of each orbit. Specifically, observations with the remote-sensing instruments will be organized into three 10-day intervals centered around perihelion and either maximum latitude or maximum co-rotation passages. As a baseline, the in-situ instruments will operate continuously during normal operations. Another important aspect of this mission, from a science operations standpoint, is that every science orbit is different, with different orbital characteristics (Sun-spacecraft distance, Earth-spacecraft distance, etc.). Science and operations planning for each orbit is therefore critical, with specific orbits expected to be dedicated to specific science problems. This will be similar to what has been used successfully in ESA's SOHO mission's Joint Observation Programs (JOPs).

Science Management and Data Archiving. Planning for Solar Orbiter is already quite mature, with science planning in particular already under way. Science teams have been formed for each science problem, which includes representatives from each instrument team, as well as theorists and modelers from the broader international scientific community. Data archiving will follow the same model as previous ESA PI-led solar and heliospheric missions, such as SOHO, with data made available to the scientific community through the ESA science data archive.

International Cooperation. Solar Orbiter is an ESA-led mission, but has strong NASA participation and substantial funded commitment. Specifically, NASA plans to provide the launch on an evolved expendable launch vehicle (EELV), and significant parts (2 complete instruments, and portions of 2 instrument suites) of the scientific payload. The mission also has important synergies with NASA's Solar Probe Plus mission, and coordinated observations are expected to enhance greatly the scientific return of both missions. In the overall international context, Solar Orbiter is ESA's primary contribution to the International Living With a Star (ILWS) initiative, and joint studies incorporating data from all missions operating in the inner heliosphere (or providing remote-sensing observations of the near-Sun environment) will contribute greatly to our understanding of the Sun and its environment.

Conclusion. Solar Orbiter is a mature mission with focused and timely scientific objectives directly relevant and important to the Cosmic Vision science programme. Its powerful combination of in-situ and remote-sensing instruments and unique mission design make Solar Orbiter ideally suited to answer several of the outstanding, fundamental questions in solar and heliophysics today. By addressing them, Solar Orbiter will achieve major breakthroughs in our understanding of how the inner solar system works and how it is driven by solar activity, as well as improve our understanding of fundamental physical processes common to all solar, astrophysical, and laboratory plasmas.

This page left intentionally blank.

2.0 Science Objectives

Solar Orbiter's mission is to address the central question of heliophysics: ***How does the Sun create and control the heliosphere?*** This, in turn, is a fundamental part of the second science question of ESA's Cosmic Vision: ***"How does the solar system work?"***¹ Solar Orbiter is specifically designed to identify the origins and causes of the solar wind, the heliospheric magnetic field, solar energetic particles, transient interplanetary disturbances, and even the Sun's magnetic field itself.

The supersonic solar wind, driven by dynamic plasma and magnetic processes at the Sun's surface, expands to surround the solar system's planets and the space far beyond. Below the surface, the solar dynamo drives magnetic fields whose buoyancy brings them to the surface where they form huge arcades of loops which contain enormous amounts of stored energy. These magnetic loops are stretched and sheared by the Sun's differential rotation and unknown surface processes, eventually erupting in explosions which eject magnetic structures that fly into the solar system, occasionally impacting the Earth and its magnetic shield with disruptive effects on space and terrestrial systems. Understanding the complex physical processes at work in this system is the central goal of heliophysics. Since the Sun and presumably the heliosphere are typical of less massive stars and their stellar spheres, these studies are relevant to astrophysics, but are unique since the Sun alone is close enough for detailed study.

Over the past ~15 years, an international effort to understand the Sun and heliosphere has been undertaken with an array of spacecraft carrying out both remote observations at visible, UV, and x-ray wavelengths, as well as in-situ observations of interplanetary plasmas, particles, and fields. Combined and coordinated observations from missions such as Ulysses, Yohkoh, SOHO, TRACE, RHESSI, Hinode, and STEREO have resulted in an enormous advance in our understanding of the Sun and heliosphere and have proven that critical progress in understanding the physics underlying the Sun-heliosphere connection requires both remote and in-situ observations working together.

Although our vantage point at 1 AU is close by astrophysical measures, it has been long known that much of the crucial physics in the formation and activity of the heliosphere takes place much closer to the Sun, and that by the time magnetic structures, shocks, energetic particles and solar wind pass by Earth they have already evolved and in many cases mixed so as to blur the signatures of their origin (**Figure 2.1**). With the proven effectiveness of combined remote and in-situ studies on the missions cited above, it is clear that ***the critical new advances will be achieved by flying a spacecraft combining remote and in-situ observations into the inner solar system.*** From this inner heliospheric vantage point, solar sources can be identified and studied accurately and combined with in-situ observations of solar wind, shocks, energetic particles, etc., before they evolve significantly. The expertise gained by the international scientific community on our existing missions has been used to design Solar Orbiter to provide the complete set of required measurements. Solar Orbiter is the next critical step in our exploration of the Sun and heliosphere.

Here we outline the major physical problems that Solar Orbiter will address; subsequent sections expand on each major question and demonstrate how Solar Orbiter will address them.

How and where do the solar wind plasma and magnetic field originate in the corona? The solar corona continuously expands and develops into a supersonic wind that extends outward, interacting with itself and with the Earth and other planets, to the heliopause boundary with interstellar space, far beyond Pluto's orbit. The solar wind has profound effects on planetary environments and on the planets themselves – for example, it is responsible for many of the phenomena in Earth's magnetosphere and is thought to have played a role in the evolution of Venus and Mars through the erosion of their upper atmospheres.

Two classes of solar wind—'fast' and 'slow'—fill the heliosphere, and the balance between them is modulated by the 11-year solar cycle. The fast solar wind (~700 km/s and comparatively steady) is known to arise from coronal holes. The slow solar wind (~400-500 km/s) permeates the plane of the ecliptic during most of the solar cycle so it is important to Earth's space environment. The slow solar wind shows different mass flux and composition than the fast wind, consistent with confined plasma in the solar corona. The specific escape mechanism through the largely closed magnetic field is not known since candidate sites and mechanisms cannot be resolved from 1 AU. Fast and slow wind carry embedded turbulent fluctuations, and these also

¹ Solar Orbiter also has direct, primary relevance to Cosmic Vision Goal #3, and secondary relevance to Cosmic Visions Goal #1.

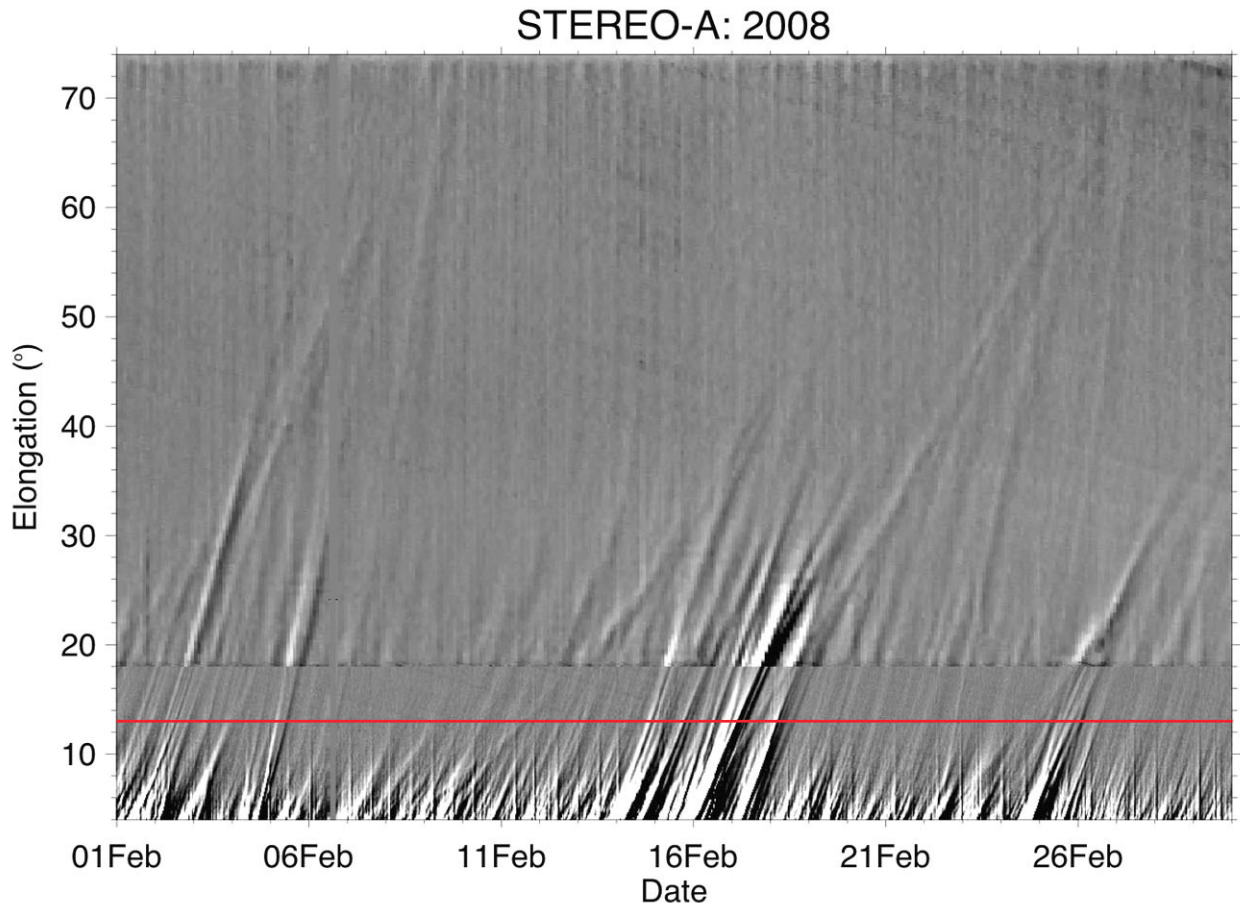


Figure 2.1. Small-scale structures flowing in the solar wind are visible as diagonal lines in this plot from the STEREO Heliospheric Imager instrument, moving further from the Sun (elongation) with time. Structures moving at different speeds collide and merge, smoothing out the flow and removing information about their relative origins. Solar Orbiter will travel to 0.23 AU, corresponding to an elongation of 13° (red horizontal line), making it possible to measure unevolved small-scale solar wind structures for the first time. (Figure courtesy J. Davies, Rutherford Appleton Laboratory, UK.)

display different properties compatible with different solar origins. It is thought that such fluctuations may be responsible for the difference in heating and acceleration between different solar wind streams.

Understanding the physics relating the plasma at the solar surface and the heating and acceleration of the escaping solar wind is crucial to understanding both the effects of the Sun on the heliosphere and how stars in general lose mass and angular momentum to stellar winds.

How do solar transients drive heliospheric variability? The largest transient events from the Sun are coronal mass ejections (CMEs), large structures of magnetic field and material that are ejected from the Sun at speeds up to 3000 km/s. CMEs are also of astrophysical interest since they are the dominant way that stars shed both magnetic flux and magnetic helicity that build up as a result of the stellar dynamo. Interplanetary CMEs (ICMEs) are the major cause of interplanetary shocks, but the locations and mechanisms by which shocks form around them is not known since this occurs in the inner solar system. Similarly, the longitudinal structure of ICMEs is not observable from the ecliptic, while its extent has a large impact on the acceleration of energetic particles. ICMEs are a major cause of geomagnetic storms but their effectiveness at disrupting the magnetosphere is only loosely related to the parent CME, because the evolution of the propagating cloud with the surrounding heliosphere is complex and has not been well studied. These unknowns have direct impact on our ability to predict transient ‘space weather’ events that affect Earth.

How do solar eruptions produce energetic particle radiation that fills the heliosphere? Like many astrophysical systems, the Sun is an effective particle accelerator. Large solar energetic particle (SEP) events produce highly energetic particles that fill the solar system with ionizing radiation. CME driven shocks can produce relativistic particles on time scales of minutes, and many CMEs convert ~10% of their kinetic energy into energetic particles. Other processes produce high-energy particles on magnetic loops without involving

shocks. The multiple processes operating in SEP events are not well understood or distinguishable from observations at 1 AU. In particular, particles accelerated in the corona and inner heliosphere are scattered by inhomogeneities in the interplanetary magnetic field (IMF) before they arrive at Earth, destroying much of the information they carry about the processes that accelerated them. Particle transport and scattering in the inner solar system are poorly understood since the turbulence properties cannot be determined from 1 AU. The actual seed population of particles energized by CME-driven shocks in the inner solar system is unexplored, and needs to be understood to construct a complete picture of particle acceleration in shock-related events.

How does the solar dynamo work and drive connections between the Sun and the heliosphere? The Sun's magnetic field connects the interior of the star to interplanetary space and its evolution is dominated by a quasi-periodic 11-year activity cycle that modulates the form of the heliosphere and strongly affects the space environment throughout the solar system. The large-scale solar field is generated in the Sun's interior, within the convection zone, by a dynamo driven by complex three-dimensional mass flows that transport and process magnetic flux. Despite notable advances in our knowledge and understanding of solar magnetism made possible by Ulysses, SOHO, and Hinode observations as well as by recent theoretical models and numerical simulations, fundamental questions remain about the operation of the solar dynamo and the cyclic nature of solar magnetic activity. Of paramount importance to answering these questions is detailed knowledge of the transport of flux at high latitudes and the properties of the polar magnetic field. To date, however, the solar high latitudes remain poorly known owing to our dependence on observations made from the ecliptic. In addition to questions about the global dynamo and the generation of the large-scale field, there are unanswered questions about the origin of the small-scale internetwork field observed in the quiet photosphere. Is this weak field produced by turbulent local dynamo action near the solar surface?

2.1 How and where do the solar wind plasma and magnetic field originate in the corona?

Significance of the question. Hot plasma in the Sun's atmosphere flows radially outward into interplanetary space to form the solar wind, filling the solar system and blowing a cavity in the interstellar medium known as the heliosphere. During solar minimum, large-scale regions of a single magnetic polarity in the Sun's atmosphere—polar coronal holes—open into space and are the source of high speed (~ 700 km/s), rather steady solar wind flows (**Figure 2.2**). There is also a slow (300–500 km/s) wind that emanates from magnetically complex regions at low latitudes and is highly variable in speed, composition, and charge state. The origin of the slow wind is not known. At solar maximum, this stable bimodal configuration gives way to a more complex mixture of slow and fast streams emitted at all latitudes, depending on the distribution of open and closed magnetic regions and the highly tilted magnetic polarity inversion line.

The fast wind from the polar coronal holes carries magnetic fields of opposite polarity into the heliosphere, which are then separated by the heliospheric current sheet (HCS) embedded in the slow wind. Measurements over a range of latitudes far from the Sun show that this boundary is not symmetric around the Sun's equator, but is on average displaced southward. This offset must reflect an asymmetry on the Sun; but since there cannot be a mismatch between the inward and outward magnetic flux on the Sun, its origin is unclear. In situ, the HCS is warped and deformed by the combined effects of solar rotation and inclination of the Sun's magnetic axis, effects that are even more prominent at solar maximum.

The energy that heats the corona and drives the wind comes from the mechanical energy of convective photospheric motions, which is converted into magnetic and/or wave energy. In particular, both turbulence and magnetic reconnection are implicated theoretically and observationally in coronal heating and acceleration. However, existing observations cannot adequately constrain these theories, and the identity of the mechanisms that heat the corona and accelerate the solar wind remains one of the unsolved mysteries of solar and heliospheric physics. How the coronal plasma is generated, energized, and the way in which it breaks loose from the confining coronal magnetic field are fundamental physical questions with crucial implications for predicting our own space environment, as well as for the understanding of the natural plasma physics of other astrophysical objects, from other stars, to accretion disks and their coronae, to energetic phenomena such as jets, x- and gamma-ray bursts, and cosmic-ray acceleration.

The solar wind contains waves and turbulence on scales from millions of kilometres to below the electron

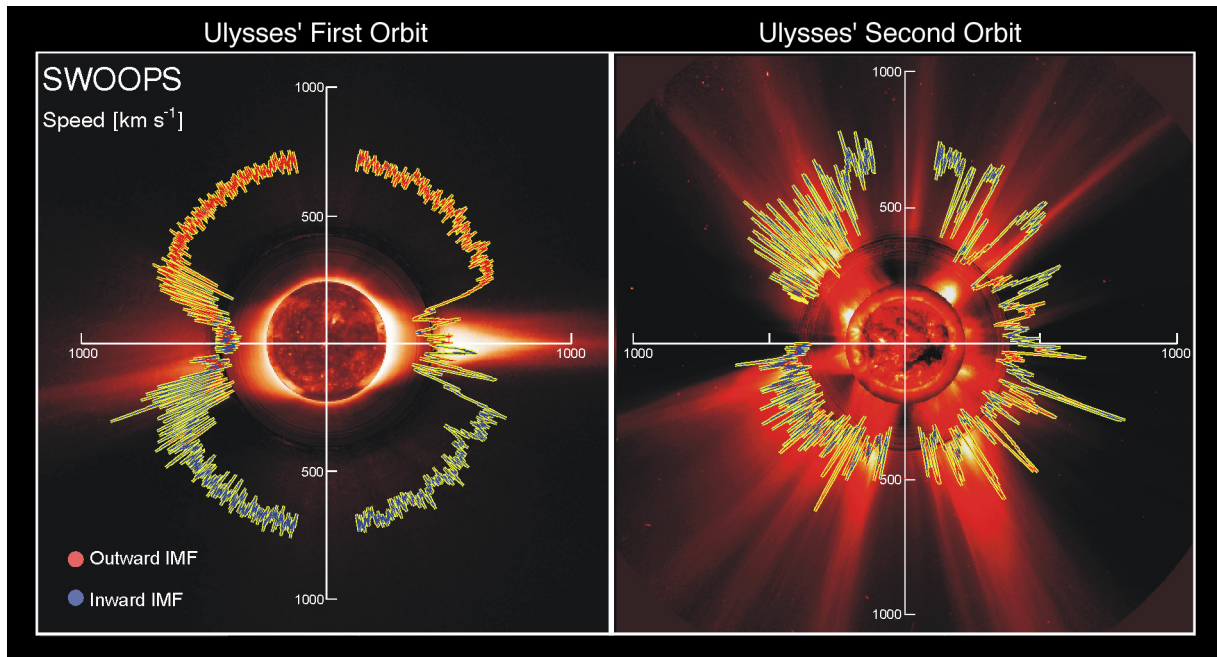


Figure 2.2. Polar plots of the solar wind speed, colored by IMF polarity for Ulysses' first two polar orbits. The earliest times are on the left (nine o'clock position) and progress around counterclockwise. The characteristic solar images for solar minimum for cycle 22 (left), solar maximum for cycle 23 (right) are from SOHO EIT and C2 coronagraph and the Mauna Loa K coronameter. Through a unique combination of remote-sensing and in-situ measurements, Solar Orbiter will map structures measured in the inner heliosphere to features observed in the corona. (Figure from McComas et al. 2008)

gyroradius. The turbulence scatters energetic particles, affecting the flux of particles that arrives at the Earth; local kinetic processes dissipate the turbulent fluctuations and heat the plasma. Properties of the turbulence vary with solar wind stream structure, reflecting its origins near the Sun, but the turbulence also evolves as it is carried into space with the solar wind, blurring the imprint of coronal conditions and making it difficult to determine its physical origin. The inner heliosphere, where Solar Orbiter will conduct its combination of remote-sensing and in-situ observations, provides the ideal laboratory for understanding the magnetohydrodynamic turbulence of natural plasmas expected to be ubiquitous in astrophysical environments.

Below we discuss in more detail three interrelated questions which flow down from this top-level question: What are the source regions of the solar wind and the heliospheric magnetic field? What mechanisms heat and accelerate the solar wind? What are the sources of turbulence in the solar wind and how does it evolve?

2.1.1 What are the source regions of the solar wind and the heliospheric magnetic field?

Present state of knowledge. At large scales, the structure of the solar wind and heliospheric magnetic field and their mapping to the solar corona are reasonably well understood. However, extending this global understanding of the overall connection between the corona and the solar wind deeper into the solar atmosphere and to the photosphere where the magnetic field can be measured has been difficult due to the dynamically evolved state of the plasma measured in situ at 1 AU and to the lack of simultaneous in-situ measurements and high-cadence, high-resolution remote sensing of solar plasma. A number of fundamental questions remain unanswered both about the source of the fast and slow solar wind and about the source of the magnetic field that the solar wind carries into the heliosphere.

Source regions of the solar wind. The speed of the solar wind is empirically anti-correlated with the (modelled) expansion rate of the magnetic field with radial distance close to the Sun (Wang and Sheeley 2006), where central areas of polar coronal holes give rise to the fastest solar wind streams, while regions closer to the coronal hole boundary give rise to progressively slower wind. Within coronal holes, strong outflows are well correlated with the intense flux elements found at the intersection of the photospheric supergranular cells; these expand into the corona as 'funnels,' preferentially from regions dominated by flux of the dominant hole

polarity (Tu et al. 2005; McIntosh et al. 2006).

The source region of the wind, at chromospheric and transition region heights, is extremely structured and dynamic (**Figure 2.3**). The chromosphere is permeated by spicules, cool and dense jets of chromospheric plasma. Spicules have been thought to be too slow and cold to contribute significantly to the solar wind, but a more dynamic type of spicule, with shorter lifetimes, faster motions, and a hotter plasma component has recently been discovered by Hinode. Such spicules also support waves, possibly with sufficient energy to accelerate fast wind streams in coronal holes (De Pontieu et al. 2009).

Hinode has also observed the frequent occurrence of very small-scale x-ray jets in polar coronal holes (Cirtain et al., 2007). Given the high velocities and frequency of these events, it has been suggested that they contribute to the fast solar wind. Their relation to the photospheric magnetic field, however, has not been established as the high latitudes at which they are observed hamper the accurate determination of their photospheric footpoints from the ecliptic plane. Other fine-scale ray-like structures—coronal plumes—permeate coronal holes and are correlated with small-scale bipolar structures inside the hole. Ultraviolet measurements show that these structures are cooler than the surrounding background hole plasma, and have slower, but denser outflows. In-situ measurements reveal the existence of faster and slower microstreams within the fast wind (Neugebauer et al. 1995) as well as other fine-scale structures (Thieme et al. 1990), but the two have not been unambiguously linked to coronal features.

The anticorrelation of expansion/wind speed suggests that the slow wind is accelerated along those open field lines with the greatest expansion rate, notably corresponding to the bright rays at the edges of coronal holes (e.g., Wang et al. 2007). However, composition measurements tend to call this notion into question: a significant elemental fractionation is observed in the solar wind plasma relative to that of the photosphere (e.g.,

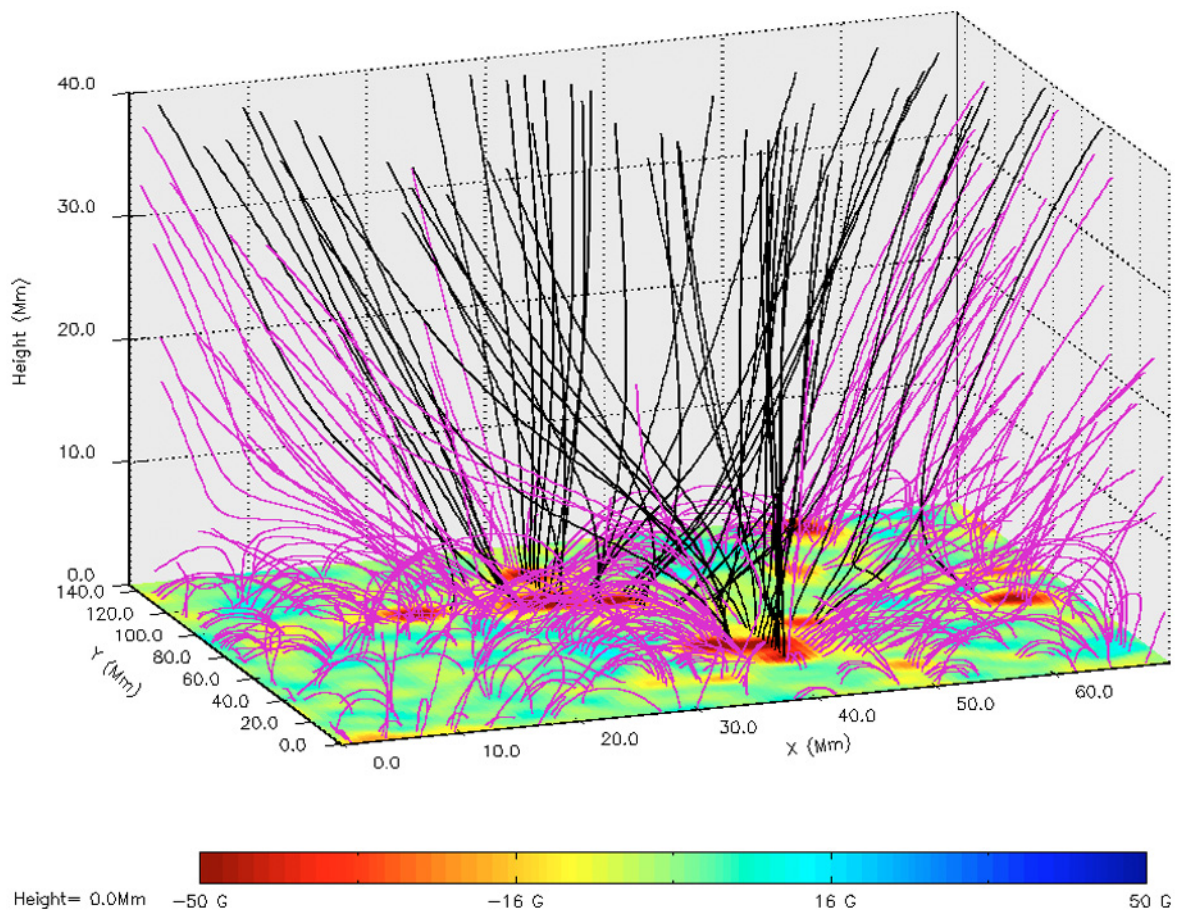


Figure 2.3. The modelled magnetic field of the transition region and lower corona in a polar coronal hole based on measurements of the photospheric magnetic field strength. The figure illustrates the complex connections between the solar surface and space: only the black lines extend far from the surface. A central goal of Solar Orbiter is to establish the links between the observed solar wind streams and their sources back on the Sun. Understanding the dynamics of the Sun's magnetic atmosphere and its signatures in the measured solar wind holds the key to understanding the origin of all solar wind flows. (Figure from Marsch et al. 2006)

Geiss and Bochsler 1985), which scales with the first ionisation potential (FIP). Metallic ions, with low FIP, are more abundant in the solar wind than mid- or high-FIP elements, when compared with their photospheric compositions (von Steiger et al. 1997). Ulysses has revealed a systematic difference in the degree of fractionation depending on the solar wind type. Fast wind associated with coronal holes has a composition similar to that of the photosphere, whereas the slow solar wind is characterized by a substantially larger degree of fractionation.

The alternative is that magnetic reconnection between closed and open field lines plays a fundamental role in slow wind generation. Closed magnetic fields lines close to the Sun confine the plasma in loops, where the compositional differentiation occurs, but these are continuously destroyed when neighbouring open field lines are advected into them. Interchange reconnection between the open and closed field allows the plasma to flow outwards into space (**Figure 2.4**). This process should occur predominantly at the coronal hole boundary, but may also be active in the intermediate areas of quiet Sun.

Additional contributions to the slow wind could arise from the opening of previously closed field lines in the middle and lower corona, from the tops of helmet streamers or the complex magnetic fields around active regions (**Figure 2.5**), for example, releasing plasma blobs or plasmoids into the heliosphere. White-light coronagraph observations show streamer blobs that might be plasmoids or might be pile-up from reconnection high in the corona. Finally, there might be a continuous outward leakage of plasma from high in the solar corona where the plasma pressure becomes comparable to the magnetic pressure in the weak field at the apex of closed loops.

Source regions of the heliospheric magnetic field. Our current knowledge of the surface magnetic field of the Sun and its extension into the solar atmosphere and interplanetary space is based on measurements of the photospheric line-of-sight—and recently, vector—magnetic field, coupled with spacecraft measurements of the field in situ. The vast majority of the magnetic flux from the Sun closes in the lower layers of the solar atmosphere, within the chromosphere and lower corona, in multiple small scale bipolar regions with strong local fields, and it is only a small fraction which extends high enough in the solar atmosphere to be dragged out into the heliosphere by the solar wind. In addition, the intense magnetic fields in the lower atmosphere are highly variable and dynamic at scales extending down to instrument resolution limits in both time and space, continuously reconnecting and contributing to the intense activity, spicules and jets in the chromosphere and lower corona. The magnetic connection between the solar wind and the solar source therefore hinges on understanding what determines the amount of open flux from the Sun, how open field lines are distributed at the solar surface at any given time, and how these open field lines reconnect and change their connection across the solar surface in time, processes which are controlled by interchange reconnection.

The HCS is embedded in slow solar wind and, like the slow wind, is full of small-scale structure. The origin of fine-scale structure in the magnetic field is therefore directly related to the origin of the slow solar wind. One of the most surprising results regarding the heliospheric current sheet is that it is not symmetric around the

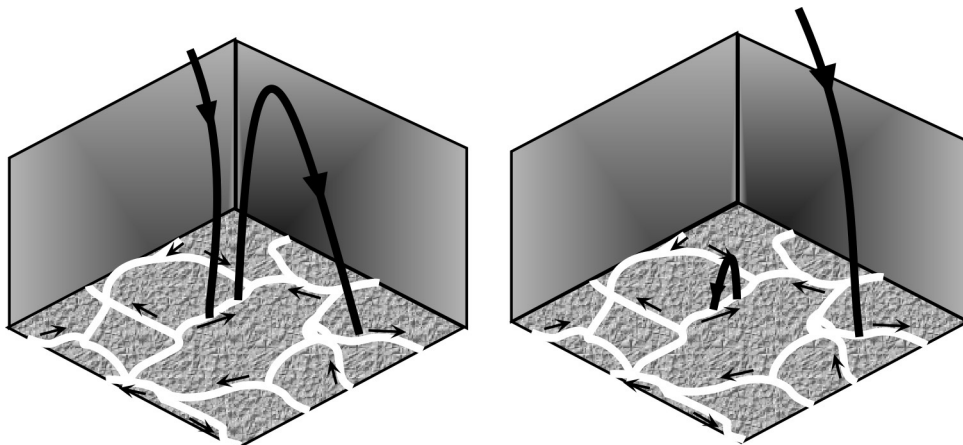


Figure 2.4. Convective cells (white lines) in the photosphere can bring together oppositely directed magnetic field lines (left). These can undergo ‘interchange reconnection,’ altering which field lines open into space and which close back to the surface (right). This process is thought to be important in generating the slow solar wind flow, as well as moving magnetic flux over the solar cycle, but observational evidence for it is currently weak. Solar Orbiter will combine high resolution observations of photospheric motion and magnetic fields with measurements of the solar wind and magnetic field flowing outward to determine the quantitative effects of interchange reconnection for the first time. (Figure from Fisk and Zurbuchen 2006)

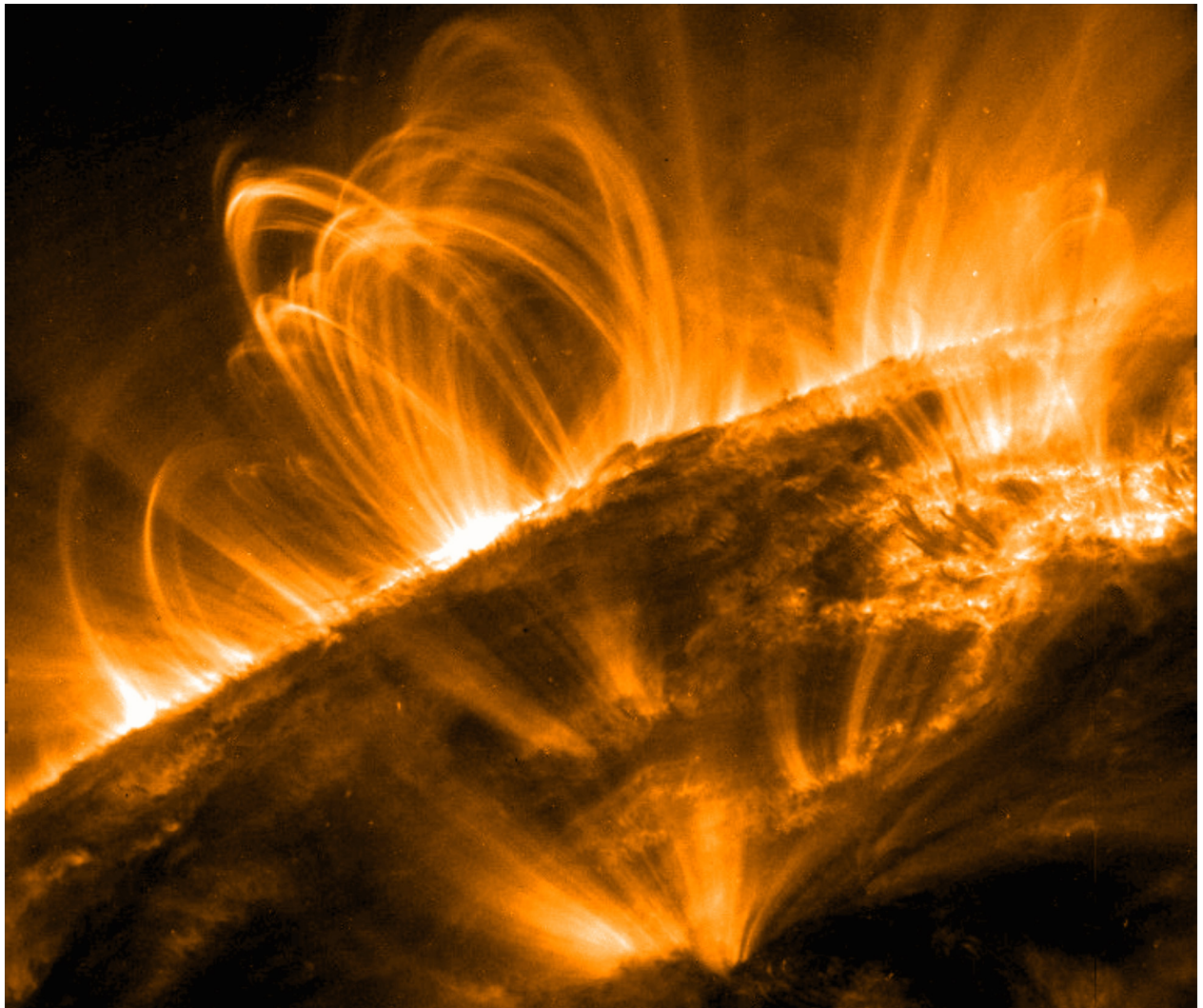


Figure 2.5. Ultraviolet emission from plasma in the Sun's atmosphere, revealing the complex magnetic field structures around active regions. Solar Orbiter will test theories of solar wind plasma emerging from such regions. (TRACE image)

equator, but appears to be displaced southward by around 10° (Smith et al. 2000) during solar minima, causing a difference in cosmic ray fluxes between hemispheres. Similar asymmetries exist in the Sun's polar magnetic fields and even sunspot numbers, but what is the origin of this asymmetry, and how does the Sun produce it in space?

How Solar Orbiter will address the question. Solar Orbiter will measure the solar wind plasma and magnetic field in situ while simultaneously performing remote-sensing measurements of the photosphere and corona, thus allowing the properties of the solar wind measured in situ to be correlated with structures observed in the source regions at the Sun. During the perihelion segments of the orbit when the spacecraft is in quasi-corotation with the Sun, Solar Orbiter will determine the plasma parameters and compositional signatures of the solar wind, which can be compared directly with the spectroscopic signatures of coronal ions with differing charge-to-mass ratios and FIP. Solar Orbiter will determine magnetic connectivity by measuring energetic electrons and the associated x-rays and radio emissions and using these measurements to trace the magnetic field lines directly to the solar source regions. Photospheric magnetic field measurements, together with those made in situ, will allow the coronal magnetic field to be reconstructed by extrapolation with well-defined boundary conditions. Extreme ultraviolet imaging (EUV) imaging and spectroscopy will provide the images and plasma diagnostics needed to characterize the plasma state in the coronal loops, which can erupt and deliver material to solar wind streams in the outer corona. As Solar Orbiter observes different source regions, from active regions to quiet Sun to coronal holes, hovering for substantial amounts of time in each during the quasi-corotation periods, it will be able to answer the question of the origin of the solar wind.

EUV spectroscopy and imaging are needed to detect magnetic reconnection in the transition region and

corona—e.g., by the observation of plasma jets or of explosive events as seen in the heavy-ion Doppler motions believed to mark the reconnection-driven plasma outflow. These events appear to be associated with impulsive energetic particle bursts observed near 1 AU. The study of the time evolution of such events, and of their particle and radiation outputs, can reveal whether reconnection is quasi-steady or time-varying, and a comparison with magnetic field data will indicate the locations of the reconnection sites with respect to the overall magnetic field structure and topology. Solar Orbiter’s coronagraph and imager will construct global maps of the H and He outflow velocity and measure the degree of correlation of wind speed and He fraction.

Using the coronagraph to measure the velocity, acceleration, and mass density structures in the accelerating wind, Solar Orbiter will simultaneously provide images of solar structure from the chromosphere to the corona. Within the solar wind, the plasma and fields instrument suites will measure the radial, latitudinal, and longitudinal gradients of plasma and field parameters in the inner heliosphere, providing information fundamental to diagnosing the connection of the solar wind with the coronal structure. Combining Solar Orbiter data from the in-situ and remote-sensing instruments taken at different intervals will make it possible to determine the relative contributions of plumes, jets, and spicules to the fast wind.

2.1.2 What mechanisms heat and accelerate the solar wind?

Present state of knowledge. Despite more than a half-century of study, the basic physical processes responsible for heating the million-degree corona and accelerating the solar wind are still not known. Identification of these processes is important for understanding the origins and impacts of space weather and to make progress in fundamental stellar astrophysics.

Ultimately, the problem of solar wind acceleration is a question of the transfer, storage, and dissipation of the abundant energy present in the solar convective flows. The key question is to establish how a small fraction of that energy is transformed into magnetic and thermal energy above the photosphere. Both emerging magnetic flux and the constant convective shaking and tangling of magnetic field lines already threading the corona contribute to the processing of the energy in what is an extremely structured, highly dynamic region of the solar atmosphere, the route to dissipation involving cascading turbulence, current sheet collapse and reconnection, shocks, high-frequency waves, and wave-particle interactions. The advent of high-cadence high-resolution observations has demonstrated the extremely complex phenomenology of the energy flux in the lower atmosphere, including many types of transient events discovered and classified by Yohkoh, SOHO, TRACE, RHESSI, and Hinode.

Energy deposited in the corona is lost in the form of conduction, radiation (negligible in coronal holes), gravitational enthalpy, and kinetic energy fluxes into the accelerating solar wind plasma. Transition region pressures, coronal densities and temperatures, and the asymptotic solar wind speed are sensitive functions of the mode and location of energy deposition. The mass flux is not, however, as it depends only on the amplitude of the energy flux (Hansteen and Leer 1995). A relatively constant coronal energy flux therefore explains the small variations in mass flux between slow and fast solar wind found by Ulysses during its first two orbits, although the dramatic decrease in mass flux over the present cycle points also to a decreased efficiency of coronal heating and therefore to its dependence on the solar magnetic field (McComas et al. 2008; Schwadron and McComas 2008).

One of the fundamental experimental facts that has been difficult to account for theoretically is that the fast solar wind originates in regions where the electron temperature and densities are low, while the slow solar wind comes from hotter regions of the corona. The anticorrelation of solar wind speed with electron temperature is confirmed by the anti-correlation between wind speed and ‘freezing in’ temperature of the different ionisation states of heavy ions in the solar wind (Geiss et al. 1995) and implies that the electron pressure gradient does not play a major role in the acceleration of the fast wind. On the other hand, the speed of the solar wind is positively correlated with the in-situ proton temperature, and the fastest and least collisionally coupled wind streams also contain the largest distribution function anisotropies. Observations of the very high temperatures and anisotropies of coronal heavy ions suggest that other processes such as magnetic mirror and wave-particle interactions should also contribute strongly to the expansion of the fast wind (Li et al. 1998; Kohl et al. 1998; Kohl et al. 2006). In particular, either the direct generation of high-frequency waves close to the cyclotron resonance of ions or the turbulent cascade of energy to those frequencies should play an important role (**Figure 2.6**).

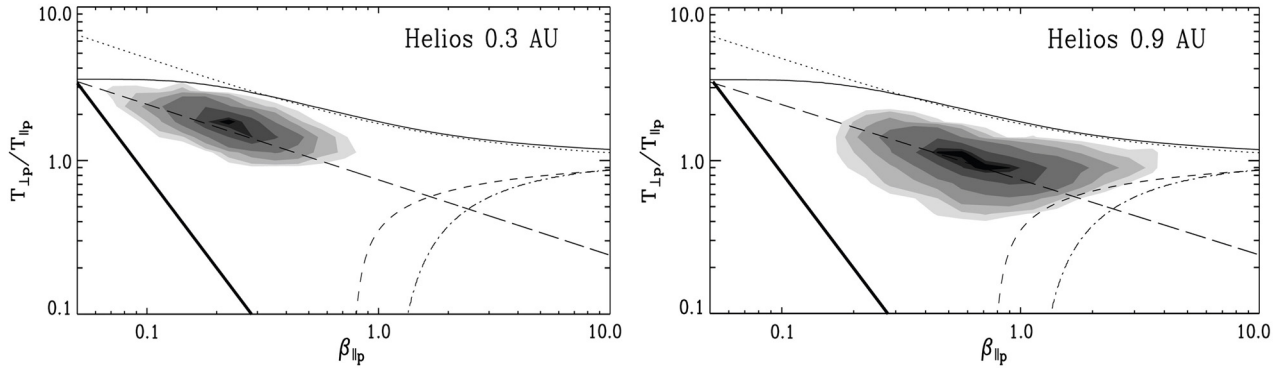


Figure 2.6. Histograms of the solar wind proton temperature anisotropy (ratio of perpendicular to parallel temperatures) versus the plasma pressure parallel to the field (parallel plasma beta) in the fast solar wind measured at two different radial distances by Helios. The dark line shows the decrease of anisotropy expected if the wind were expanding adiabatically without heating (dark continuous), and the actual distribution function contours with best fit of the run of anisotropy. Instability threshold conditions for the ion-cyclotron (solid), the mirror (dotted), the parallel (dashed) and oblique (dash-dotted) fire hose instabilities are also shown. Distribution functions display perpendicular heating and evolve towards marginal stability with distance from the Sun. Solar Orbiter will determine initial conditions for the perpendicular anisotropies, showing whether the heating drives the ions beyond the ion-cyclotron stability threshold inside 0.3 AU and help determine the nature of the plasma-wave interactions responsible for this heating. (From Matteini et al. 2007)

Theoretical attempts to develop self-consistent models of fast solar wind acceleration have followed two somewhat different paths. First, there are models in which the convection-driven jostling of magnetic flux tubes in the photosphere drives wave-like fluctuations that propagate up into the extended corona. The waves partially reflect back toward the Sun, develop into strong turbulence, and/or dissipate over a range of heights. These models also tend to attribute the differences between the fast and slow solar wind not to any major differences in the lower boundary conditions, but to the varying expansion factor of magnetic field lines in different areas of coronal holes (Cranmer et al. 2007, and references therein).

In the second class of models, the interchange reconnection models, the energy flux usually results from magnetic reconnection between closed, loop-like magnetic flux systems (which are in the process of emerging, fragmenting, and being otherwise jostled by convection) and the open flux tubes that connect to the solar wind. Here the differences between fast and slow solar wind result from qualitatively different rates of flux emergence, reconnection, and coronal heating in different regions on the Sun (Axford and McKenzie 1992; Fisk et al. 1999; Schwadron and McComas, 2003).

It has been difficult to evaluate competing models of fast wind acceleration and to assess observationally the relative contributions of locally emerging magnetic fields and waves to the heat input and pressure required to accelerate the wind largely because of the absence of measurements of the solar wind close to the Sun where they can be mapped with sufficient precision to a solar source region.

How Solar Orbiter will address the question. Solar Orbiter's combination of high-resolution measurements of the photospheric magnetic field together with images and spectra at unprecedented spatial resolution will make it possible to identify plasma processes such as reconnection/shock formation and wave dissipation in rapidly varying surface features, observe Doppler shifts of the generated upflows, and determine compositional signatures. Whatever the scale, magnetic reconnection leads to particle dissipative heating and acceleration and wave generation, which have the net effect of a local kinetic energy increase in the lower solar atmosphere that can be revealed through high-resolution extreme ultraviolet (EUV) imaging and spectroscopy. Wave propagation will be traced from the source site to the region of dissipation through observations of EUV-line broadening and Doppler shifts.

Global maps of the H and He outflow velocity, obtained by applying the Doppler dimming technique to the resonantly scattered component of the most intense emission lines of the outer corona (HI 121.6 and He II 30.4 nm), will provide the contours of the maximum coronal expansion velocity gradient for the two major components of the solar wind, and the role of high-frequency cyclotron waves will be comprehensively assessed by measuring the particle velocity distribution across the field and determining the height where the maximum gradient of outflow velocity occurs (Telloni et al. 2007).

Solar Orbiter's heliospheric imager will measure the velocity, acceleration, and mass density of structures

in the accelerating wind, allowing precise comparison with the different acceleration profiles of turbulence-driven and interchange reconnection-driven solar wind models.

As it is performing imaging and spectroscopic observations of the corona and photosphere, Solar Orbiter will simultaneously measure in situ the properties of the solar wind emanating from the source regions. The in-situ instrumentation will determine all of the properties predicted by solar wind acceleration models: speed, mass flux, composition, charge states, and wave amplitudes. Moving relative slowly over the solar surface near perihelion, Solar Orbiter will measure how properties of the solar wind vary depending on the changing properties of its source region, as a function of both space and time, distinguishing between competing models of solar wind generation.

2.1.3 What are the sources of turbulence in the solar wind and how does it evolve?

Present state of knowledge. The solar wind is filled with turbulence and instabilities. At large scales, the fast solar wind is dominated by antisunward propagating Alfvén waves thought to be generated by photospheric motions. At smaller scales, these waves decay and generate an active turbulent cascade, with a spectrum similar to the Kolmogorov hydrodynamic scaling of $f^{-5/3}$. In the slow solar wind, turbulence does not have a dominant Alfvénic component, and it is fully developed over all measured scales. There is strong evidence that the cascade to smaller scales is anisotropic, but it is not known how the anisotropy is generated or driven (Horbury et al. 2008). What do the differences between the turbulence observed in the fast wind and that observed in the slow wind reveal about the sources of the turbulence and of the wind itself?

Little is known about what drives the evolution of solar wind turbulence. Slow-fast wind shears, fine-scale structures, and gradients are all candidate mechanisms (Tu and Marsch 1990; Breech et al. 2008). To determine how the plasma environment affects the dynamical evolution of solar wind turbulence it is essential to measure the plasma and magnetic field fluctuations in the solar wind as close to the Sun as possible, before the effects of mechanisms such as velocity shear become significant, and then to observe how the turbulence evolves with heliocentric distance.

The dissipation of energy in a turbulent cascade contributes to the heating of the solar wind plasma. However, while measurements of the properties of solar wind turbulence in near-Earth orbit largely agree with observed heating rates (Smith et al. 2001; Marino et al. 2008), the details are controversial and dependent on precise models of turbulent dynamics. In order to establish a full energy budget for the solar wind, the heating rates as a function of distance and stream properties must be determined, including turbulence levels before the cascade develops significantly.

The statistical analysis of the fluctuating fields also reveals pervasive fine-scale structure (e.g., discontinuities and pressure balanced structures). The origin of these structures is uncertain: are they the remnant of complex coronal structuring in the form of strands of small-scale flux tubes advected by the solar wind flow (Borovsky 2008; Bruno et al. 2001), or are they generated locally by turbulent fluctuations?

At scales around the proton gyroradius and below, turbulent fluctuations interact directly with the solar wind ions. The precise nature of the turbulent cascade below the proton gyroradius is poorly understood and might even vary depending on local plasma conditions. Below the electron gyroradius, conditions are even less certain and the partitioning of turbulent energy into electron or ion heating is unknown at this time. In addition, solar wind expansion constantly drives distribution functions toward kinetic instabilities, where fluctuations with characteristic signatures are generated (e.g., Marsch 2006). What physical role do kinetic effects play with distance from the Sun? What role do wave-particle interactions play in accelerating the fast solar wind? What contribution do minor ions make to the turbulent energy density in near-Sun space?

How Solar Orbiter will address the question. Solar Orbiter will measure waves and turbulence in the solar wind over a wide range of latitudes and distances, including closer to the Sun than ever before, making it possible to study turbulence before it is significantly affected by stream-stream interactions. By travelling over a range of distances, the spacecraft will determine how the turbulence evolves and is driven as it is carried antisunward by the solar wind flow.

Detailed in-situ data will make it possible to distinguish between competing theories of turbulent dissipation and heating mechanisms in a range of plasma environments and are thus of critical importance for advancing

our understanding of coronal heating and of the role of turbulence in stellar winds.

By entering near-corotation close to the Sun, Solar Orbiter will be able to distinguish between the radial, longitudinal, and temporal scales of small-scale structures, determining whether they are the signatures of embedded flux tubes or are generated by local turbulence.

Solar Orbiter's magnetic and electric field measurements, combined with measurement of the full distribution functions of the protons and electrons will fully characterize plasma turbulence over all physically relevant time scales from very low frequencies to above the electron gyrofrequency. Because Solar Orbiter is a three-axis stabilized spacecraft, it can continuously view the solar wind beam with its proton instrument, measuring proton distributions at the gyroperiod and hence making it possible directly to diagnose wave-particle interactions in ways that are not possible on spinning spacecraft. By travelling closer to the Sun than ever before, it will measure wave-particle interactions before the particle distributions have fully thermalized, studying the same processes that occur in the corona. By measuring how the distributions and waves change with solar distance and between solar wind streams with different plasma properties, Solar Orbiter will make it possible to determine the relative effects of instabilities and turbulence in heating the plasma.

The solar wind is the only available plasma 'laboratory' where detailed studies of magnetohydrodynamic (MHD) turbulence can be carried out free from interference with spatial boundaries, and in the important domain of very large magnetic Reynolds numbers. Detailed comparison between experimental in-situ data and theoretical concepts will provide a more solid physical foundation for MHD turbulence theory, which will be of critical importance for understanding the solar (stellar) coronal heating mechanism and the role of turbulence in the solar (a stellar) wind.

2.2 How do solar transients drive heliospheric variability?

Significance of the question. The dynamic Sun exhibits many forms of transient phenomena, such as flares, CMEs, eruptive prominences, and shock waves. Many directly affect the structure and dynamics of the outflowing solar wind and thereby also eventually affect Earth's magnetosphere and upper atmosphere, with significant consequences for society through hazards to, for example, space-based technology systems and surface power systems. Understanding these impacts, with the ultimate aim of predicting them, has received much attention during the past decade and a half under the banner of 'space weather.' However, many fundamental questions remain about the physics underpinning these phenomena and their origins, and these questions must be answered before we can realistically expect to be able to predict the occurrence of solar transients and their effects on geospace and the heliosphere. These questions are also pertinent, within the framework of the 'solar-stellar connection,' to our understanding of other stellar systems that exhibit transient behaviour such as flaring (e.g., Getman et al. 2008).

Solar Orbiter will provide a critical step forward in understanding the origin of solar transient phenomena and their impact on the heliosphere. Located close to the solar sources of transients, Solar Orbiter will be able both to determine the inputs to the heliosphere and to measure directly the heliospheric consequences of eruptive events at distances close enough to sample the fields and plasmas in their pristine state, prior to significant processing during their propagation to 1 AU. Solar Orbiter will thus be a key augmentation to the chain of solar-terrestrial observatories in Earth orbit and at the libration points, providing a critical perspective from its orbit close to the Sun and out of the ecliptic.

Below we discuss in more detail three interrelated questions which flow down from this top-level question: How do CMEs evolve through the corona and inner heliosphere? How do CMEs contribute to solar magnetic flux and helicity balance? How and where do shocks form in the corona and inner heliosphere?

2.2.1 How do CMEs evolve through the corona and inner heliosphere?

Present state of knowledge. Following earlier observations by space-based white-light coronagraphs, considerable progress in understanding CMEs has been achieved using data from the ESA-NASA SOHO mission, which provides continuous coverage of the Sun and combines coronagraphs with an EUV imager and off-limb spectrometer. Other spacecraft, such as ACE, WIND and Ulysses, which carried comprehensive in-situ instrumentation, have contributed significantly to our understanding of the interplanetary manifestation

of these events. With a full solar cycle of CME observations, the basic features of CMEs are now understood. CMEs appear to originate from highly-sheared magnetic field regions on the Sun known as filament channels, which support colder plasma condensations known as prominences. Eruptions develop in the low corona within 10-15 minutes, while the associated shocks cross the solar disk within 1 hour. CMEs reach speeds of up to 3000 km s⁻¹ and carry energies (kinetic, thermal and magnetic) of $\sim 10^{32}$ ergs. They can also accelerate rapidly during the very early stages of their formation, with the CME velocity being closely tied, in time, to the associated flare's soft x-ray light profile (Zhang and Dere 2006). High-resolution SOHO coronagraph images (**Figure 2.7**) have provided evidence for a magnetic flux rope structure in some CMEs as well as for post-CME current sheets. Both features are predicted by CME initiation models (e.g., Lin & Forbes 2000; Lynch et al. 2004).

STEREO observations are making it possible to chart in three dimensions the trajectories of CMEs in the corona and heliosphere, thereby improving our understanding of CME evolution and propagation. STEREO data have supported detailed comparison both of in-situ measurements with remote-sensing observations and of MHD heliospheric simulations with observations. The combination of high-cadence coronagraphic and EUV imaging simplifies the separation of the CME proper from its effects in the surrounding corona (Patsourakos and Vourlidas 2009) and allows a more accurate determination of its dynamics.

Despite the advances in our understanding enabled by SOHO and STEREO, very basic questions remain unanswered. These concern the source and initiation of eruptions, their early evolution, and the heliospheric propagation of CMEs. All current CME models predict that the topology of ICMEs is that of a twisted flux

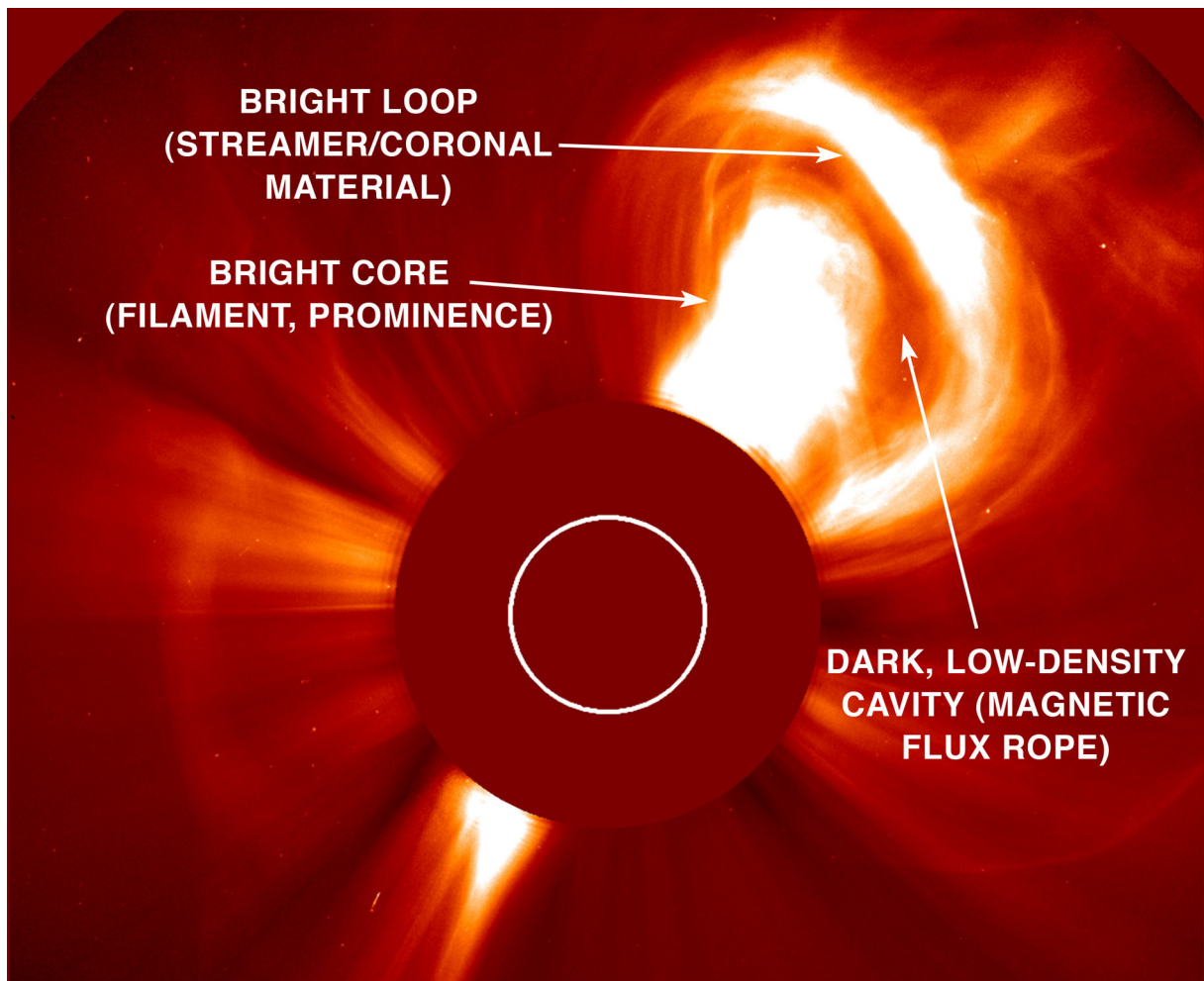


Figure 2.7. A limb CME as viewed by LASCO on SOHO in December, 2002. The dark, low-density region inside the structure formed by the bright loop of streamer material is thought to be the magnetic flux rope predicted by current CME initiation models. CMEs are believed to originate from prominence eruptions, yet in ICMEs observed at 1 AU prominence plasma (the bright core in this image) is very rarely detected. Solar Orbiter will, with its unique orbit, enable in-situ measurements of the ejecta and their radial (and out-of-the-ecliptic) evolution in much more detail than possible from Earth orbit, where many features have been washed out. (Adapted from the HELEX report)

rope as a result of the flare reconnection that occurs behind the ejection. Observations at 1 AU, however, find that less than half of all ICMEs, even those associated with strong flares, have a flux rope structure (Richardson and Cane 2004). Many ICMEs at 1 AU appear to have a complex magnetic structure with no clearly-defined topology. Moreover, for ICMEs that do contain flux ropes, the orientation is often significantly different from that expected on the basis of the orientation of the magnetic fields in the prospective source region. CMEs are believed to originate from prominence eruptions, yet in ICMEs observed at 1 AU prominence plasma is very rarely detected. These major disconnects between theoretical models (of prominence eruption and CME propagation) and observations (remote and in situ) need to be resolved if any understanding of the CME process is to be achieved.

How Solar Orbiter will address the question. To advance our understanding of the structure of ICMEs and its relation to CMEs at the Sun beyond what has been achieved with SOHO and STEREO requires a combination of remote-sensing and in-situ measurements made at close perihelion and in near-corotation with the Sun. Through combined observations with its magnetograph, imaging spectrograph, and soft x-ray imager, Solar Orbiter will provide the data required to establish the properties of CMEs at the Sun and to determine how coronal magnetic energy is released into CME kinetic energy, flare-associated thermal/non-thermal particle acceleration, and heating. Observations with the imaging spectrograph will be used to determine the composition of CMEs in the low corona and to establish how they expand and rotate and will also provide vital clues to the energy partition within a CME once it is released. Solar Orbiter will make comprehensive in-situ measurements of the fields and plasmas (particularly composition) of ICMEs following their release and, critically, prior to their processing during propagation in the heliosphere. These measurements will allow the properties of an ICME to be related to those of the CME at the Sun and to the conditions in the CME source region as observed by Solar Orbiter's remote-sensing instruments and will make it possible to examine the evolution of CMEs in the inner heliosphere. Solar Orbiter's combination of remote-sensing and in-situ observations will also establish unambiguously the magnetic connectivity of the ICME and reveal how the magnetic energy within flux ropes is dissipated to heat and accelerate the associated particles. Solar Orbiter data will also reveal how the structure of the magnetic field at the front of a CME evolves in the inner heliosphere—a critical link in understanding, and eventually predicting, how transient events on the Sun may determine the geoeffective potential of the event.

To fully understand the physical system surrounding CME ejection, the temporal evolution of active regions and CME-related shocks and current sheets must be tracked from their formation in the corona to their expulsion in the solar wind. During the mission phases when the spacecraft is in near-corotation with the Sun, Solar Orbiter will continuously observe individual active regions, free from projection complications, over longer periods than are possible from Earth orbit. Solar Orbiter will thus be able to monitor the development of sheared magnetic fields and neutral lines and to trace the flux of magnetic energy into the corona. Observations from the vantage point of near-corotation will make it possible to follow the evolution of the current sheet behind a CME with unprecedented detail and to clarify the varying distribution of energy in different forms (heating, particle acceleration, kinetic).

2.2.2 How do CMEs contribute to the solar magnetic flux and helicity balance?

Present state of knowledge. Magnetic flux is transported into the heliosphere both by the solar wind, in the form of open flux carried mostly by the fast wind from polar coronal holes, and by coronal mass ejections, which drag closed flux with them as they propagate into the heliosphere. At some point the closed flux introduced by CMEs must be opened to avoid an unsustainable buildup of magnetic flux in the heliosphere. Measurements of the magnetic flux content of the heliosphere from near the Earth (covering more than 40 years and 4 cycles) show that the total amount of magnetic flux in the solar system changes over the solar cycle (**Figure 2.8**). Longer-term variations are also known to occur. Proxies such as geomagnetic activity and cosmic ray fluxes provide evidence that the average IMF strength has increased substantially in the last 100 years, perhaps by as much as a factor of 2. Surprisingly, however, during the current solar minimum the IMF strength is lower than at any time since the beginning of the space age and is still decreasing.

The relative contribution of the solar wind and CMEs to the heliospheric magnetic flux budget is an unresolved question, as is the process by which the flux added by the CMEs is removed. Models to explain the solar cycle variation assume a background level of open flux, to which CMEs add extra flux during solar

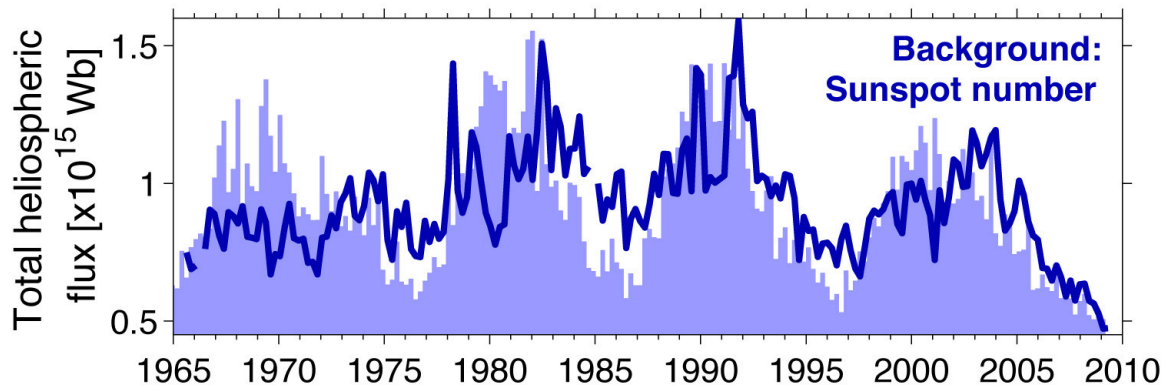


Figure 2.8. Near-Earth interplanetary magnetic field strength (thick line) for the last 45 years, with the sunspot number (background filled values). The magnetic field strength varies over the solar cycle, but is lower now than at any time since the beginning of the space age. This change was not predicted and is not understood. Solar Orbiter will investigate the evolving links between solar and interplanetary magnetic fields. (From M. Owens, Imperial College London)

maximum, increasing the intensity of the IMF. The exceptionally low intensity of the IMF during the current minimum has been attributed to the low rate of CME occurrence [Owens et al. 2008]. Alternatively, there may simply be no ‘background’ open flux level.

There is evidence that the flux introduced into the heliosphere by CMEs may be removed by magnetic reconnection within the trailing edges of CMEs, which disconnects the CME from the Sun or by interchange reconnection closer to the solar surface [e.g., Owens and Crooker 2006]. Recent observations show that the reconnection process occurs quite often in the solar wind, even when the magnetic field is not under compression. However, the rate and/or locations at which reconnection generally removes open flux are not at present known.

Together with magnetic flux, the solar wind and CMEs carry magnetic helicity away from the sun. Helicity is a fundamental property of magnetic fields in natural plasmas, where it plays a special role because it is conserved not only by the ideal dynamics, but also during the relaxation which follows instabilities and dissipation. Helicity is injected into the corona when sunspots and active regions emerge, via the twisting and braiding of magnetic flux. During the coronal heating process the overall helicity is conserved and tends to accumulate at the largest possible scales. It is natural to assume that critical helicity thresholds may be involved in the triggering of CMEs, but how solar eruptions depend on the relative amounts of energy and helicity injection during active region emergence and evolution is unknown. Yet this understanding could be a crucial element in the prediction of large solar events.

How Solar Orbiter will address the question. Fundamental to the question of contribution of CMEs to the heliospheric flux budget is the flux content of individual events. Encountering CMEs close to the Sun before interplanetary dynamics affects their structure, Solar Orbiter will measure their magnetic flux content directly; comparisons with remote-sensing measurements of their source regions will clarify the relation between CME flux and the eruption process. As Solar Orbiter moves through the inner heliosphere, it will encounter CMEs at different solar distances, making it possible to quantify the effect of interplanetary dynamics on their apparent flux content.

The flux carried outwards by CMEs must eventually disconnect completely from the Sun, or interchange reconnect with existing open field lines. Solar Orbiter will diagnose the magnetic connectivity of the solar wind and CME plasma using suprathermal electron and energetic particle measurements. These particles, which stream rapidly along the magnetic field from the Sun, indicate whether a magnetic flux tube is connected to the Sun at one end, at both ends, or not at all. These particles disappear when the field is completely disconnected, or may reverse their flow direction as a result of interchange reconnection. However, scattering and reflection due to curved, tangled, or compressed magnetic field lines act to smear out these signatures with increasing solar distance, leading to ambiguity in connectivity measurements. Solar Orbiter, by travelling close to the Sun before this scattering is significant, will determine the original level of magnetic connectivity; covering a wide range of distances in the inner heliosphere, the spacecraft will measure how the connectivity changes as field lines are carried away from the Sun.

Solar Orbiter will also directly sample reconnection regions in the solar wind as they pass the spacecraft,

determining their occurrence rates in the inner heliosphere as a function of distance and testing theories of CME disconnection by searching for reconnection signatures in the tails of CMEs.

The contribution to the heliospheric magnetic flux of small scale plasmoids, ejected from the tops of streamers following reconnection events, is unclear. Solar Orbiter, slowly moving above the solar surface during perihelion passes, will determine the magnetic structure, connectivity, and plasma properties including composition of these ejecta, using spectroscopic imaging observations to unambiguously link them to their source regions.

To assess the role of CMEs in maintaining the solar magnetic helicity balance, Solar Orbiter will compare the helicity content of active regions as determined from remote sensing of the photospheric magnetic field with that of magnetic clouds measured in situ. Such a comparison requires both extended remote-sensing observations of the same active region over the region's lifetime and in-situ measurements of magnetic clouds from a vantage point as close to the solar source as possible. During the near-corotation segments of its orbit, Solar Orbiter will 'dwell' over particular active regions and observe the emergent flux for a longer interval (up to 30 days) than is possible from 1 AU, where perspective effects complicate extended observations. The resulting data will be used to calculate the helicity content of an active region, track its temporal variation, and determine the change in helicity before and after the launch of any CMEs. Should a magnetic cloud result from an eruptive event in the active region over which Solar Orbiter is dwelling, the relatively small heliocentric distances between the solar source and the spacecraft will make it highly probable that Solar Orbiter will directly encounter the magnetic cloud soon after its release. Determination of the cloud's properties and connectivity through Solar Orbiter's in-situ particle-and-fields measurements will enable the first-ever comparison of a magnetic cloud in a relatively unevolved state with the properties of the solar source, an impossibility with measurements made at 1 AU. The comparison of the helicity change in the source region with the value measured in the magnetic cloud will provide insight into the role of CMEs in the helicity balance of the Sun.

2.2.3 How and where do shocks form in the corona and inner heliosphere?

Present state of knowledge. The rapid expulsion of material during CMEs can drive shock waves in the corona and heliosphere. Shocks in the lower corona can also be driven by flares, and in the case of CME/eruptive flare events it may be difficult to unambiguously identify the driver (Vršnak and Cliver 2008). CME-driven shocks are of particular interest because of the central role they play in accelerating coronal and solar wind particles to very high energies in SEP events (see Section 2.3).

Shocks form when the speed of the driver is super-Alfvénic. The formation and evolution of shocks in corona and the inner heliosphere thus depend (1) on the speed of the driving CME and (2) on the Alfvén speed of the ambient plasma and its spatial and temporal variations. According to one model of the radial distribution of the Alfvén speed in the corona near active regions, for example, shocks can form essentially in two locations, in the middle corona ($1.2\text{--}3 R_s$), where there is an Alfvén speed minimum, and distances beyond an Alfvén speed maximum at $\sim 4 R_s$ (Mann et al. 2003). A recent study of CMEs with and without type II radio bursts (indicative of shock formation) has shown that some of the fast and wide CMEs observed produced no shock or only a weak shock because they propagated through tenuous regions in the corona where the Alfvén velocity exceeded that of the CME (Gopalswamy et al. 2008). CME shock formation/evolution can also be affected by the interaction between an older, slower-moving CME and a faster CME that overtakes it. Depending on the Alfvén speed in the former, the interaction may result in the strengthening or weakening of an existing shock driven by the overtaking CME or, if there is no existing shock, the formation of one (Gopalswamy 2001; 2002).

Recent studies of LASCO images obtained during the rising phase of solar cycle 23 have demonstrated the feasibility of detecting CME-driven shocks from a few to $\sim 20 R_s$ and of measuring their density compression ratio and propagation direction (Vourlidas et al. 2003; Ontiveros and Vourlidas 2009) (**Figure 2.9**). This development has opened the way for the investigation of shock formation and evolution in the lower corona and heliosphere through Solar Orbiter's combination of remote-sensing observations and in-situ measurements.

How Solar Orbiter will address the question. Understanding shock generation and evolution in the inner heliosphere requires knowledge of the spatial distribution and temporal variation of plasma parameters (density, temperature, and magnetic field) throughout the corona. Solar Orbiter's remote-sensing measurements—in particular electron density maps derived from the polarized visible-light images and maps of the density and outflow velocity of coronal hydrogen and helium—will provide much improved basic plasma models of the

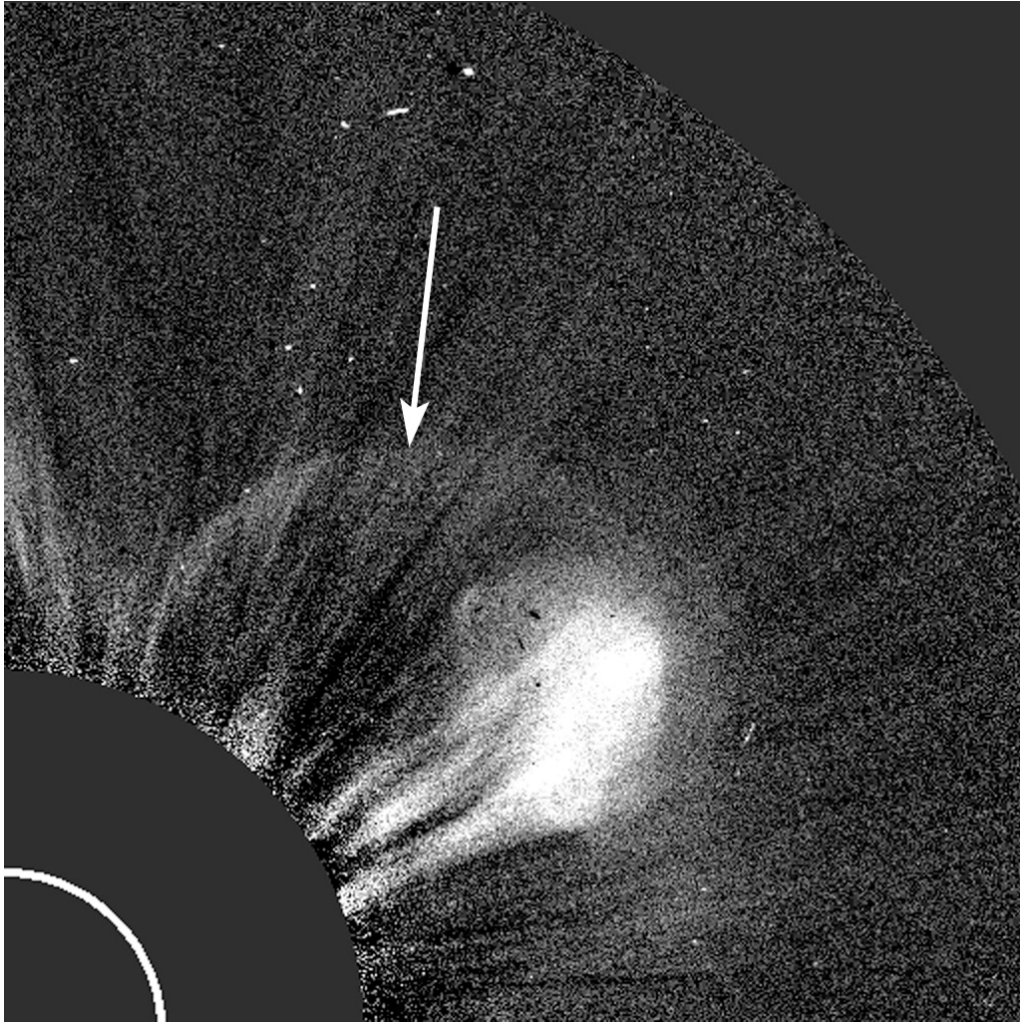


Figure 2.9. Example of a CME-driven shock signature in a coronagraph white light image. The image was taken by the LASCO/C2 coronagraph on 12/18/2000 at 02:06 UT. The CME is narrow and the shock appears as a parabolic front extending to the NW of the CME front. The occulter edge is at $2.2 R_s$ and the solar disk is marked by a white circle. With its remote-sensing instruments, Solar Orbiter will be able to observe the formation and evolution of shocks in the lower corona, and the in-situ instruments will measure the properties of the shock as it propagates through the inner heliosphere. This powerful combination of remote-sensing and in-situ measurements will help constrain models of shock formation and provide valuable insight into the role of CME-driven shocks in SEP acceleration. (From A. Vourlidas, NRL)

corona, so that the Alfvén speed and magnetic field direction can be reconstructed over the distance range from the Sun to the spacecraft. Remote sensing will also provide observations of shock drivers, such as flares (location, intensity, thermal/non-thermal electron populations, time-profiles), and manifestations of CMEs (waves, dimmings, etc.) in the low corona with spatial resolution of a few hundred kilometres and cadence of a few seconds. It will measure the acceleration profile of the latter and then track the CMEs through the crucial heights for shock formation ($2-10 R_s$) and provide speed, acceleration, and shock compression ratio measurements.

Type II bursts, detected by Solar Orbiter, will indicate shock-accelerated electron beams produced by the passage of a CME and thus provide warning of an approaching shock to the in-situ instruments. These in-situ plasma and magnetic field measurements will fully characterize the upstream and downstream plasma and magnetic field properties and quantify their microphysical properties, such as turbulence levels and transient electric fields (while also directly measuring any SEPs - cf. Section 2.3). Spacecraft potential measurements also allow for rapid determinations of the plasma density, and of electric and magnetic field fluctuations, on microphysical scales, comparable to the Doppler-shifted ion scales, which are characteristic of the spatial scales of shocks. The evolution of such parameters will provide insight into the processes dissipating shock fronts throughout the range of magnetic/velocity/density and pressure parameter space. Because of Solar Orbiter's

close proximity to the Sun, the measurements of the solar wind plasma, electric field, and magnetic field will be unspoiled by the dynamical wind interaction pressure effects due to solar rotation and will provide the first reliable data on the magnetosonic speed, the spatial variation of the plasma pressure and magnetic field in the inner heliosphere. A recent MHD modelling study has shown that interactions among recurring CMEs and their shocks occur typically in the distance range around 0.2-0.5 AU (Lugaz et al. 2005). Solar Orbiter will spend significant time in the regions of recurring CME interactions and so will be able to investigate the effects of such interactions on the evolution of CME-driven shocks.

2.3 How do solar eruptions produce energetic particle radiation that fills the heliosphere?

Significance of the Question. Astrophysical sites throughout the solar system and galaxy have the universal ability to accelerate ions and electrons to high speeds, forming energetic particle radiation. Detected remotely from radio and light emission around supernovae remnants, the Sun, and planets, or directly from particles that reach our detectors, this radiation arises from the explosive release of stored energy that can cause magnetic fields to rearrange, or can launch shock waves which accelerate particles by repeatedly imparting many small boosts to their speed. The nearly universal occurrence of energetic particle radiation, along with the effects it can have on planetary environments, evolution of life forms, and space systems has fostered a broad interest in this phenomenon that has long made it a high priority area of investigation in space science. Since remote sites in the galaxy cannot be studied directly, solar system sources of energetic particles give the best opportunity for studying all aspects of this complex problem.

The Sun is the most powerful particle accelerator in the solar system, routinely producing energetic particle radiation at speeds close to the speed of light, sufficiently energetic to be detected at ground level on Earth even under the protection of our magnetic field and atmosphere. SEP events can severely affect space hardware, disrupt radio communications, and cause re-routing of commercial air traffic away from polar regions. In addition to large events, which occur roughly monthly during periods of high sunspot count, more numerous, smaller solar events can occur by the thousands each year, providing multiple opportunities to understand the physical processes involved.

Below we discuss in more detail three interrelated questions that flow down from this top-level question: How and where are energetic particles accelerated at the Sun? How are energetic particles released from their sources and distributed in space and time? What are the seed populations for energetic particles?

2.3.1 How and where are energetic particles accelerated at the Sun?

Present state of knowledge. One of the two major physical mechanisms for energizing particles involves particles interacting with moving or turbulent magnetic fields, gaining small amounts of energy at each step and eventually reaching high energies. Called Fermi or stochastic acceleration, this mechanism is believed to operate in shock waves and in turbulent regions such as those associated with reconnecting magnetic fields or in heated coronal loops. The second major physical mechanism is a magnetic field whose strength or configuration changes in time, producing an electric field which can directly accelerate particles in a single step. At the Sun, such changes occur when large magnetic loop structures reconnect, or are explosively rearranged due to the stress from the motion of their footpoints on the solar surface (e.g., Aschwanden 2006; Giacalone and Kota 2006).

Multiple processes may take place in SEP events, and while it is not possible to cleanly separate them, they can be split into two broad classes, the first being events associated with shock waves. **Figure 2.10** shows a sketch wherein an instability in coronal magnetic loops has resulted in an eruption that launches a CME. As it moves into space, it drives a shock creating turbulence that accelerates SEPs from a seed population of ions filling the interplanetary medium (inset 2). Mixed into this may be particles from an associated solar flare (inset 1). CMEs often accelerate particles for hours as they move away from the Sun, and in some cases are still accelerating particles when they pass Earth orbit in a day or two (**Figure 2.11**). Since CMEs can be huge as shown in the LASCO image, it is easy to see how they can fill a large portion of the heliosphere with SEPs. However, the correlation of the observed radiation intensities with CME properties is poor, indicating that additional aspects of the mechanism such as seed populations or shock geometry must play important roles that

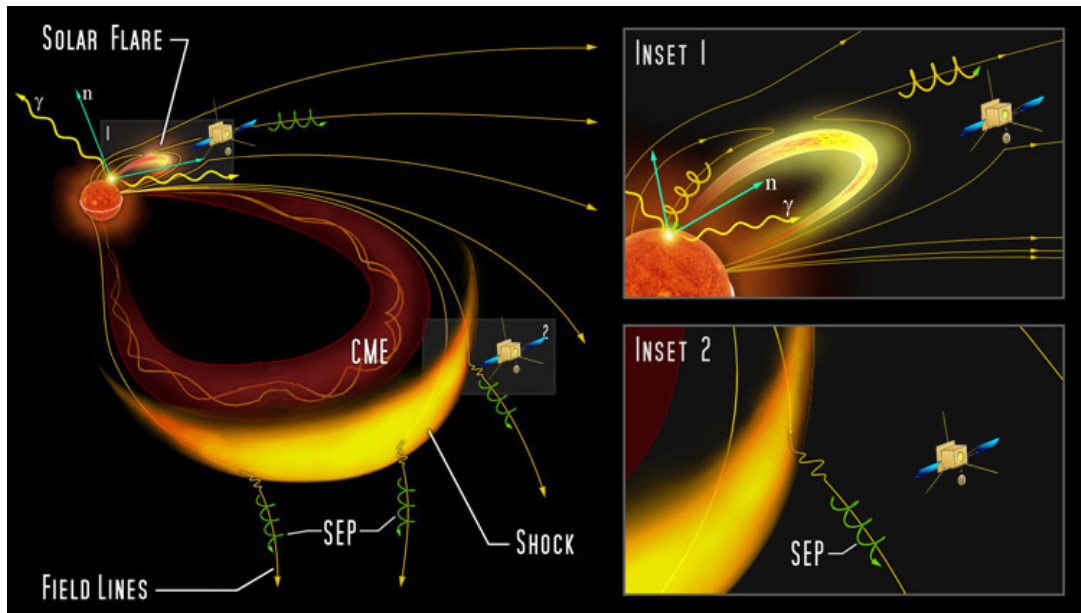


Figure 2.10. Sketch showing a solar flare and CME driving an interplanetary shock. Both the solar flare source and shock may contribute to the interplanetary energetic particle populations. However, the relative importance of acceleration processes due to flares and CME-driven shocks cannot be determined at 1 AU because of particle mixing. Solar Orbiter will allow tests of the relative importance of the different acceleration mechanisms because it goes close to the Sun. There, the shock will pass over Solar Orbiter while still in the early phases of particle acceleration, making it possible for the first time to directly compare the energetic particles with shock properties such as mach number, turbulence level, and with the local seed population. Simultaneous in-situ observations of magnetic field lines connecting back to flare sites and to shock fronts driven by CMEs, together with concurrent remote imaging of flares, wide field-of-view imaging of CMEs and spectroscopic identification of the CME-driven shocks from Solar Orbiter, will make it possible to determine the relative importance of the associated acceleration processes. (Adapted from NASA's Solar Sentinels STDT report)

are not yet well understood (Gopalswamy 2006; Desai et al. 2006; Mewaldt 2006).

The second class of events is associated with plasma and magnetic field processes in loops and active regions that accelerate particles. Reconnecting magnetic loops, and emerging magnetic flux regions provide sites for stochastic energetic particle acceleration or acceleration by electric fields. Because these regions are relatively small, the acceleration process is quick: on the order of seconds or minutes, but the resulting event is small and often difficult to observe. Since the energized particles are in the relatively high densities of the corona, they collide with coronal plasma, producing ultraviolet (UV) and x-ray signatures that make it possible to locate their acceleration sites and probe the local plasma density. Most of these particles remain trapped on their parent loops, travelling down the legs to the solar surface where they lose their energy to ambient material, producing x- and γ -rays. A few escape on magnetic field lines leading to interplanetary space, traceable by their ('type III') radio signatures, electrons, and highly fractionated ion abundances where the rare ^3He can be enhanced by 1000-10,000 times more than in solar material. **Figure 2.12** illustrates another site where reconnection can accelerate particles: in the current sheet behind a CME liftoff. In this case, particles can be accelerated for hours, and may 'leak' around the CME structure and become mixed with the shock accelerated particles. (Lin 2006; Cargill et al. 2006; Drake et al. 2009)

The energetic particles from these events reach our detectors at Earth orbit after spiralling around the IMF, which is an Archimedes spiral on average. But since the IMF meanders, and has many kinks, the length of the particle's path has a good deal of uncertainty, and the particles themselves scatter and mix, smearing and blurring signatures of the acceleration at the Sun. Although we can enumerate candidate mechanisms for producing SEPs, a critical question is: what actually happens in nature? Which processes dominate? How can shocks form fast enough to accelerate ions and electrons to relativistic energies in a matter of minutes, as happened in the January 20, 2005 SEP event?

How Solar Orbiter will address the question. Solar Orbiter will make decisive progress on the origins of SEPs by going close to Sun, thus enabling precise determination of the sequences of events, along with comprehensive in-situ determination of the field and plasma properties and the suprathermal ion pool in the inner heliosphere.

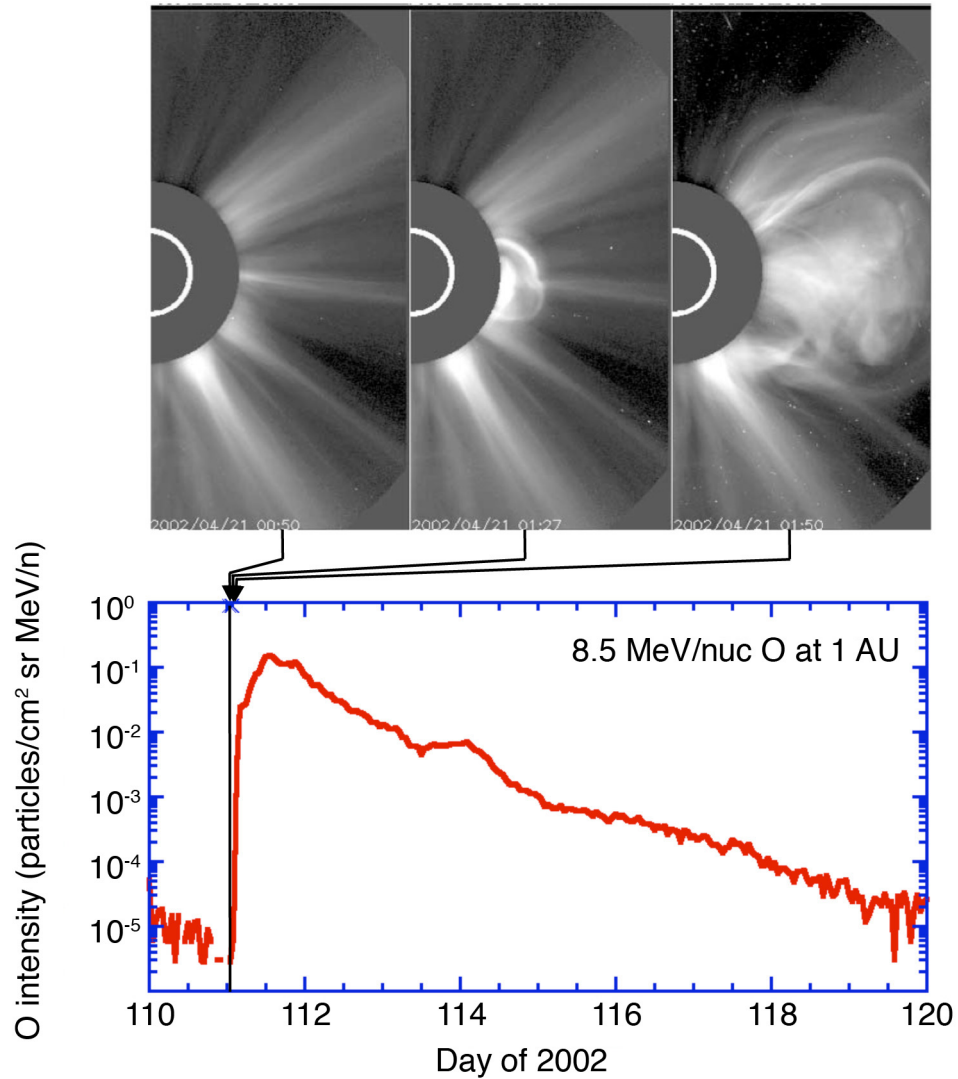


Figure 2.11. Upper panel: SOHO LASCO observations of a CME erupting from the Sun's western hemisphere, with exposure times at 00:50, 01:27, and 01:50. The CME reached a speed of 2700 km/s at 18 R_s , and the associated interplanetary shock passed Earth around ~0415 UT on April 23, about 51 hours after the liftoff. Lower panel: ACE observations of high energy SEP O nuclei showing an increase in intensity of nearly 5 orders of magnitude beginning shortly after the CME liftoff. Note that, while the CME photos are all taken near the intensity onset, the ACE intensities remained elevated for days, long after the shock had passed the Earth. Solar Orbiter will provide much more accurate timing and particle distribution measurements because of its much shorter magnetic connection to the acceleration sites. This will pinpoint the acceleration mechanisms and determine the importance of interplanetary transport processes. (Adapted from Emslie et al. 2004)

Recent progress at 1 AU has relied on combining remote and in-situ observations from different missions such as ACE, SOHO, Wind, RHESSI, Hinode, and TRACE — where using multiple spacecraft is possible since they are all at virtually the same vantage point. But to do this in close to the Sun, where there is an enormous observational advantage due to proximity, it is necessary to carry the whole suite on one spacecraft, since the probe's trajectory is not in synchronization with Earth. Almost the entire Solar Orbiter payload contributes to unravelling the question of SEP origins: visible, UV, and x-ray imaging of loops, flares, and CMEs with their location and timing; x-ray signatures of energetic particle interactions at loop footpoints, or on loops themselves; radio signatures of coronal shocks and escaping electrons; magnetic field, plasma wave and solar wind measurements to determine turbulence levels and identify shock passages; seed population specification from the heavy ion composition of solar wind and suprathermals in the inner heliosphere; finally, the accelerated energetic particles themselves: their timing, velocity distributions, scattering characteristics, and composition.

CME and shock associated SEPs. Moving from the lower corona to the interplanetary medium, shocks evolve rapidly since the sound speed drops as plasma density and magnetic field strength decline as $\sim 1/r^2$. Solar

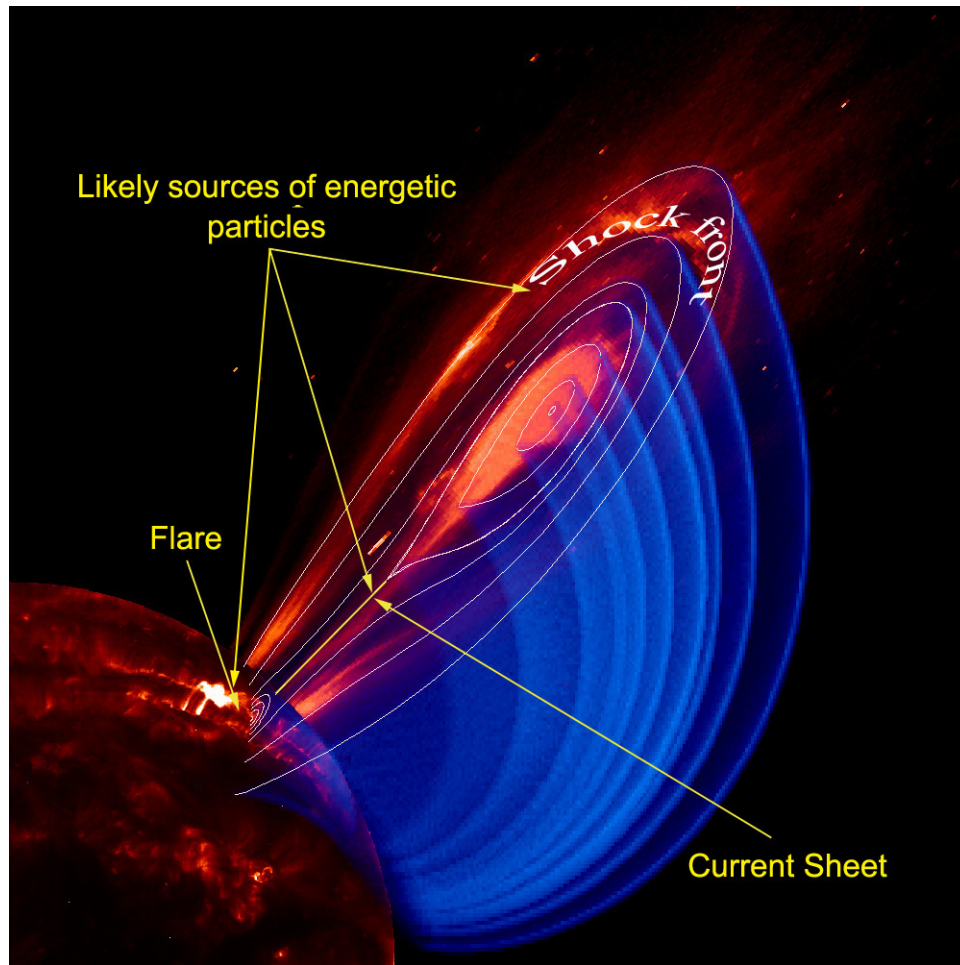


Figure 2.12. Composite illustration of a unified flare/CME system showing potential solar energetic particle source regions. The coronagraph image (red image off the limb) shows the CME with a trailing current sheet seen nearly head-on. A cutaway of the modeled magnetic field structure is shown by the blue overlap. Post flare loops are shown on the UV disk image. By going closer to the Sun, Solar Orbiter will be able to distinguish between the timing and release signatures from the shock front vs. the connection region at the current sheet. (Figure from NASA's Solar Sentinels STDT report)

Orbiter's coronagraphs will remotely identify shock front location, speed, and compression ratios through this critical region within $\sim 10 R_s$. Combining this information with local electron densities as well as coronal ion velocities given by Solar Orbiter radio and light polarization observations will provide critical constraints on shock evolution models in regions too close to the Sun for direct sampling.

In the regions explored by Solar Orbiter close to the Sun, the IMF is almost radial with much less variation (uncertainty) in length than is the case at 1 AU, so the knowledge of the actual path length improves by a factor of 3-5 as the length shortens. Having observed the CMEs and their radio signatures in the corona and the x-ray signatures of the energetic particles near the Sun, Solar Orbiter will then determine subsequent arrival time of the particles in situ that can be accurately compared to CME position. As the shock then rolls past the spacecraft, Solar Orbiter will measure the shock speed and strength as well as the associated plasma turbulence, electric, and magnetic field fluctuations. This will give a complete description of the acceleration parameters in the inner heliosphere where much of the particle acceleration takes place. Indirect evidence from 1 AU indicates that shock acceleration properties depend on the longitude of the shock compared to the observer; close to the Sun, Solar Orbiter can cleanly test this property since the IMF is nearly radial, the CME liftoff site is known, and the accelerated particles will have little chance to mix. In the high-latitude phase of the mission, Solar Orbiter will be able to look down on the longitudinal extent of CMEs in visible, UV, and hard x-rays, allowing first direct observations of the longitudinal size of the acceleration region. This will make it possible to test currently unconstrained acceleration and transport models by using measured CME size, speed, and shape to specify the accelerating shock.

SEPs associated with coronal loops and reconnection regions. As Solar Orbiter approaches the Sun, the

photon and particle signatures from small events will increase by $1/r^2$, making it possible to observe events 15-20 times smaller than ever before, in effect opening a new window for SEP processes. We may detect for the first time energetic particle populations from x-ray microflares, a candidate mechanism for coronal heating that cannot be studied further away from the Sun due to background problems. For the small flares that produce x-ray, electron, and ^3He -enrichments we will observe with great accuracy events that at 1 AU are not far above the level of detection: the timing of particle and radio signatures, the composition and spectra, etc., providing strong new constraints on the process operating in these events. Particle acceleration on coronal loops will have new insights since the $1/r^2$ sensitivity advantage and viewing geometry will make it possible to view the x-ray emission from the tops of loops in numerous cases where the much stronger footpoint sources are occulted behind the solar limb. These studies of faint coronal sources that are only rarely observable from 1 AU will give crucial information about the location and plasma properties of suspected electron acceleration sites in the high corona.

2.3.2 How are energetic particles released from their sources and distributed in space and time?

Present state of knowledge. SEPs associated with CME driven shocks have been long known to often arrive at Earth orbit hours later than would be expected based on their velocities. There are two alternate processes that might cause this. (1) The acceleration may require significant time to energize the particles since they must repeatedly collide with the shock to gain energy in many small steps, so the process may continue for many hours as the shock moves well into the inner solar system. Or (2) the particle intensities near the shock may create strong turbulence that traps the particles in the vicinity of the shock, and their intensity observed at earth orbit depends on the physics of the particles escaping from the trapping region. Once free of the vicinity of the shock, SEPs may spiral relatively freely on their way to earth orbit, or more usually will be scattered repeatedly from kinks in the IMF, delaying their arrival further. The amount of scattering in the interplanetary space varies depending on other activity such as recent passage of other shocks or solar wind stream interactions. By the time the particles reach Earth orbit, they are so thoroughly mixed that these effects cannot be untangled. (Gopalswamy et al. 2006; Cohen et al. 2007)

Particles accelerated on magnetic loops can reach very high energies in seconds after the onset of flaring activity, and then collide with the solar surface where they emit gamma radiation. There is a poor correlation between the intensity of the gamma radiation and the SEP intensities observed at earth orbit, so most particles from this powerful acceleration process do not escape. Much more common are flare events observed in UV and x-rays that produce sudden acceleration of electrons, sketched in **Figure 2.13**. The electrons can escape from the corona, producing nonthermal radio emission as they interact with the local plasma. Moving from higher to lower frequencies as the local plasma density decreases with altitude, the (type III) radio emission makes it possible to track the energetic electron burst into interplanetary space where it may pass by the observer. Energetic ions, greatly enriched in ^3He and heavy nuclei, accompany these electron bursts (Lin 2006; Mason 2007).

Key open questions in shock associated events are whether particle arrival delays at 1 AU are due to the length of time needed to accelerate the particles, or due to trapping in the turbulence near an accelerating shock, or a combination of both? For particles accelerated on loops, are the electrons and ions accelerated from sites low in the corona or at higher altitudes, and how are they related to the x- and gamma ray signatures?

How Solar Orbiter will address the question. Solar Orbiter will revolutionize our understanding of SEP acceleration associated with CME driven shocks by probing the inner heliospheric sites where particle acceleration and release take place. Solar Orbiter will observe how shocks evolve, and whether they are still accelerating particles as they pass by the spacecraft. If particle arrivals are controlled by the time it takes the shock to accelerate them, then the highest energy particles will be delayed since they require many more interactions with the shock. If trapping and release controls the timing, then as the shock moves by the faster and slower particles will have similar intensity changes. Since Solar Orbiter will simultaneously measure the turbulence properties in the shock acceleration region, it will be possible to construct a complete theory and models of the acceleration process, and its radial dependence in the inner heliosphere.

For SEPs accelerated on loops or in reconnection regions, Solar Orbiter will see the coronal location from UV and x-rays, and then trace the progress of released electrons by radio emission that will drift to the plasma

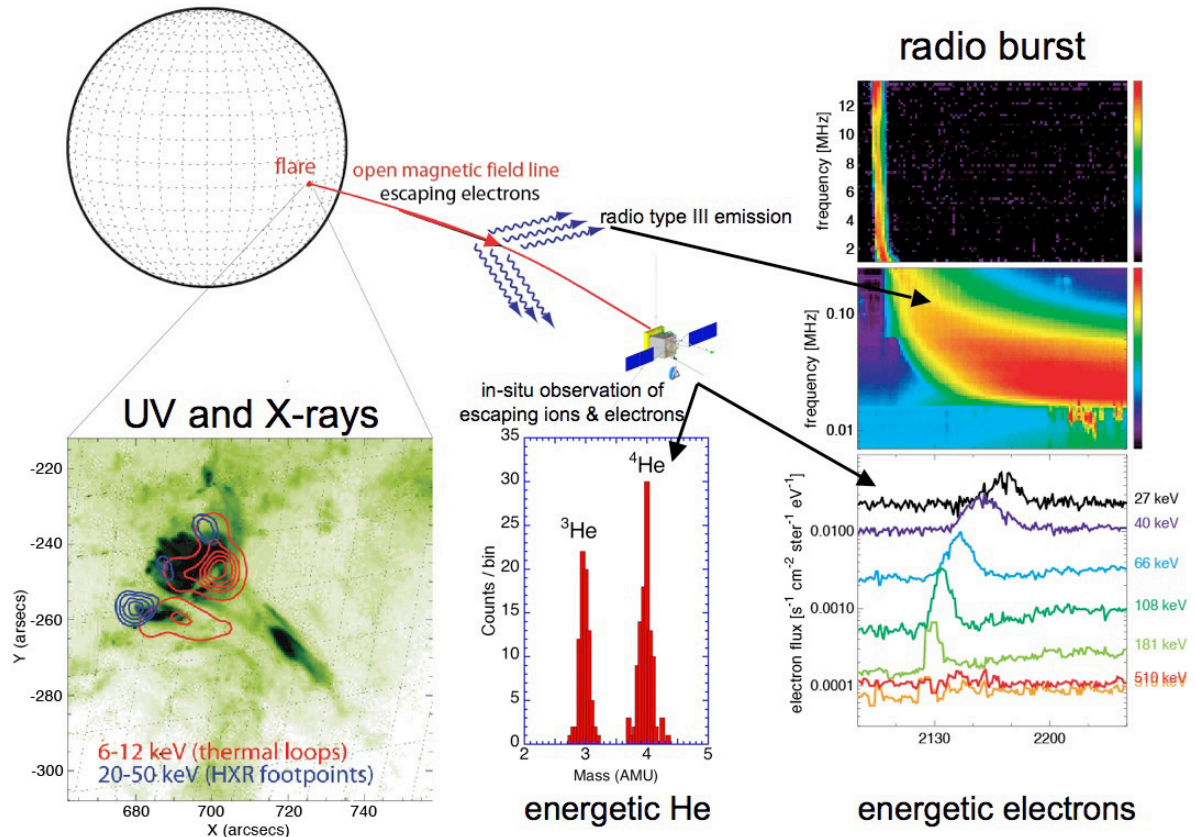


Figure 2.13. Coordinated remote and in-situ observations of a flare source (lower left) producing a jet seen in UV and x-rays which outline the loops and interactions at loop footpoints (blue). Escaping electrons produce a radio burst (upper right) whose frequency depends on coronal height of the emitting particles. At the Solar Orbiter spacecraft, prompt arrival of energetic electrons time the arrival of escaping particles, and energetic ions provide signatures of extreme fractionation produced by the acceleration mechanism. The prompt arrival of the particles establishes that Solar Orbiter is magnetically connected to the x-ray source, allowing comparison with coronal magnetic field models in the region of the active region. (Figure adapted from A. Benz, 3rd Solar Orbiter Workshop, Sorrento)

frequency at the spacecraft for those bursts that pass by. This unambiguously establishes that the magnetic field line at Solar Orbiter connects to the coronal UV and x-ray emission site. Since Solar Orbiter can be connected to active regions for periods of days, this will provide multiple tracings between the heliospheric magnetic field and its origin in the corona. The corotation phase of Solar Orbiter will considerably lengthen the periods of connection to active regions, greatly increasing the number of field line origin sites that can be determined from a single active region. X-ray emission from the flaring sites can be used to derive the energetic electron spectrum at the flare site, which in turn can be compared with the escaping population to see if most of the accelerated electrons are released (usually most do not escape). Thanks to the $1/r^2$ intensity advantage, Solar Orbiter will observe thousands of these cases and thereby permit detailed mapping of coronal sources and the trapping properties of the acceleration sites.

2.3.3 What are the seed populations for energetic particles?

Present state of knowledge. The low-energy particles accelerated by CME-driven shocks to SEP energies are called the seed population. The observed ionization states of SEP ions show temperatures typical of the corona, ruling out hot material on flare loops as the seeds. But SEPs also show significant abundances of ions such as ^3He and singly ionized He, which are virtually absent from the solar wind. The observed energetic particle abundances indicate that the suprathermal ion pool, composed of ions from a few to a few 10s the speed of the solar wind, is the likely source. At 1 AU the suprathermal ion pool is ~ 100 times more variable in intensity than the solar wind, and varies in composition depending on solar and interplanetary activity. The suprathermal ions are continuously present at 1 AU (**Figure 2.14**), but it is not known if there is a continuous solar source, or if

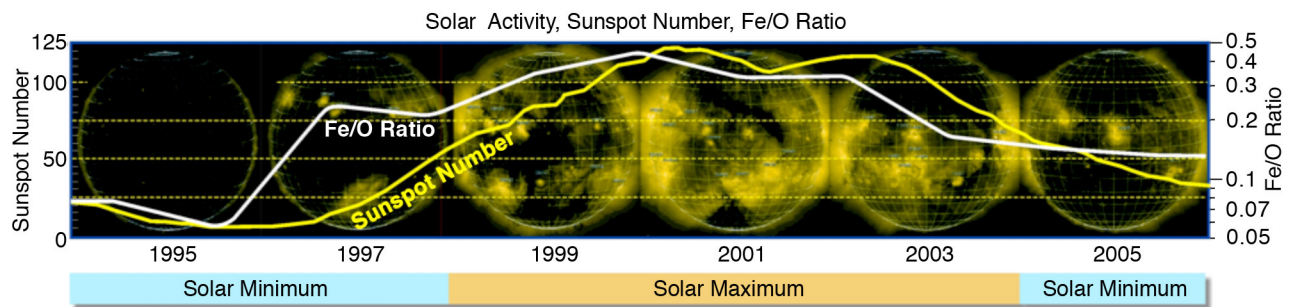


Figure 2.14. The seed population for SEP shock accelerated particles is the suprathermal ion pool. At 1 AU this pool has large variations over the solar cycle as shown above for the Fe/O ratio: the average pool composition goes from domination by flare activity at solar maximum (high Fe/O), to interplanetary sources at solar minimum (low Fe/O). Day-to-day variations in the pool's composition can be larger than shown here because of other transient activity such as interplanetary shock passages. Inside 1 AU, where almost all shock acceleration of particles takes place, the suprathermal ion pool is completely unexplored, and will be mapped for the first time by Solar Orbiter. (Figure from M. Desai, 2nd Solar Orbiter Workshop, Athens)

these ions are from other activities such as acceleration in association with fast- and slow-solar wind streams. Inside 1 AU, the suprathermal ion pool is expected to show significant radial dependence due to the different processes that contribute to the mixture, but it is unexplored (Desai et al. 2006; Mewaldt et al. 2007; Lee 2007; Fisk and Gloeckler 2007).

For SEPs accelerated on loops or in reconnection regions that give rise to electron and type-III radio bursts, ionization states are coronal-like at lower energies and change over to much hotter flare-like at high energies. This may be evidence for a complex source, or, more likely, of energetic particle stripping as the ions escape from a low coronal source. For SEPs accelerated at reconnection sites behind CMEs (Figure 2.12) abundances and ionization states would be coronal (Klecker et al. 2006).

Critical questions in this area are: what is the suprathermal ion pool in the inner heliosphere, including its composition and temporal and spatial variations? What turbulence or stochastic mechanisms in the inner heliosphere accelerate particles to suprathermal energies? Are the source locations and arrival times of electrons from SEPs on loops or reconnection regions consistent with a low or high coronal source?

How Solar Orbiter will address the question. By systematically mapping the suprathermal ion pool in the inner heliosphere with spectroscopic and in-situ data, Solar Orbiter will provide the missing seed particle data for models of SEP acceleration associated with shocks. Together with the shock and turbulence parameters also measured on Solar Orbiter there will be the first well-constrained models. Since the suprathermal ion pool composition varies, different shock events will be expected to produce correspondingly different energetic particle populations that can be examined on a case-by-case basis. The *high-latitude phase* of the mission will add an important third dimension to the suprathermal pool mapping, since it will be more heavily influenced by, e.g., mid-latitude streamer belts, making it possible to probe the solar and interplanetary origins of the seed particle populations. Taken together, these observations will make it possible to construct the first complete physics-based theory and models of particle acceleration close to the Sun.

For SEPs accelerated on loops or in reconnection regions the $1/r^2$ advantage of Solar Orbiter will again provide a decisive advantage since particle properties will be accurately measured and comparable with much more precise information on the coronal location. This will permit distinguishing between low coronal sources that result in stripping of escaping particles, vs. higher sources which could mimic stripping properties. SEPs accelerated from reconnection regions in back of CME liftoffs will be identified by comparing energetic particle timing with the location of the CME, and energetic particle composition with that determined spectroscopically for the remote coronal source.

2.4. How does the solar dynamo work and drive the connections between the Sun and heliosphere?

Significance of the question. The Sun's magnetic field dominates the solar atmosphere. It structures the

coronal plasma, drives much of the coronal dynamics, and produces all the observed energetic phenomena. One of the most striking features of solar magnetism is its ~ 11 -year activity cycle, which is manifest in all the associated solar and heliospheric phenomena. Similar activity cycles are also observed in a broad range of stars in the right half of the Hertzsprung-Russell diagram, and the Sun is an important test case for dynamo models of stellar activity.

The Sun's global magnetic field is generated by a dynamo generally believed to be seated in the tachocline, the shear layer at the base of the convection zone. According to flux-transport dynamo models (e.g., Dikpati and Gilman 2008), meridional circulation, and other near-surface flows transport magnetic flux from decaying active regions to the poles. There subduction carries it to the tachocline to be reprocessed for the next cycle. This 'conveyor belt' scenario provides a natural explanation for the sunspot cycle, and characterizing the flows that drive it will provide a crucial test of our models and may also allow us to predict the length and amplitude of future cycles. However, current models fail miserably at predicting actual global solar behaviour. For example, the current sunspot minimum has been far deeper and longer than predicted by any solar modelling group, indicating that crucial elements are missing from current understanding.

A major weakness of current global dynamo models is poor constraint of the meridional circulation at high latitudes. The exact profile and nature of the turnover from poleward flow to subduction strongly affects behaviour of the resulting global dynamo (e.g., Dikpati and Charbonneau 1999), but detecting and characterizing the solar flow is essentially impossible at shallow viewing angles in the ecliptic plane.

In addition to the global dynamo, turbulent convection may drive a local dynamo that could be responsible for generating the observed weak, small-scale internetwork field, which is ubiquitous across the surface and appears to dominate the emergent unsigned flux there.

A key objective of the Solar Orbiter mission is to measure and characterize the flows that transport the solar magnetic fields: complex near-surface flows, the meridional flow, and the differential rotation at all latitudes and radii. Of particular and perhaps paramount importance for advancing our understanding of the solar dynamo and the polarity reversal of the global magnetic field is a detailed knowledge of magnetic flux transport near the poles. Hinode, peering over the Sun's limb from a heliographic latitude of 7° , has provided a tantalizing glimpse of the Sun's high-latitude region above 70° ; however, observations from near the ecliptic lack the detail, coverage, and unambiguous interpretation needed to understand the properties and dynamics of the polar region. Thus, Solar Orbiter's imaging of the properties and dynamics of the polar region during the out-of-the-ecliptic phase of the mission (reaching heliographic latitudes of 25° during the nominal mission and as high as 34° during the extended mission) will provide badly needed constraints on our models of the solar dynamo.

Most of the open magnetic flux that extends into the heliosphere originates from the Sun's polar regions, from polar coronal holes. The current solar minimum activity period, which is deeper and more extended than previously measured minima, demonstrates the importance of this polar field to the solar wind and heliosphere. There is evidence that the solar wind dynamic pressure, composition and turbulence levels, as well as the strength of the heliospheric magnetic field, have all changed in the last few years in ways that are unprecedented in the space age. None of these changes were predicted, and current solar conditions present a challenge to our understanding of the solar dynamo and its effects on the solar system at large and the Earth in particular.

Below we discuss in more detail three interrelated questions that flow down from this top-level question: How is magnetic flux transported to and reprocessed at high solar latitudes? What are the properties of the magnetic field at high solar latitudes? Are there separate dynamo processes in the Sun?

2.4.1. How is magnetic flux transported to and reprocessed at high solar latitudes?

Present state of knowledge. In the last decade, the mapping of surface and subsurface flow fields at low and middle latitudes has seen major advances, largely due to the availability of high-quality data from the SOHO's Michelson Doppler Imager (MDI) instrument. These data have provided accurate knowledge of differential rotation, the low latitude, near-surface part of the meridional flows, and the near-surface torsional oscillations, which are rhythmic changes in the rotation speed that travel from mid-latitudes both equatorward and poleward (Howe et al. 2006). Local helioseismic techniques have also reached a level of maturity that allows the three-dimensional structure of the shallow velocity field beneath the solar surface to be determined.

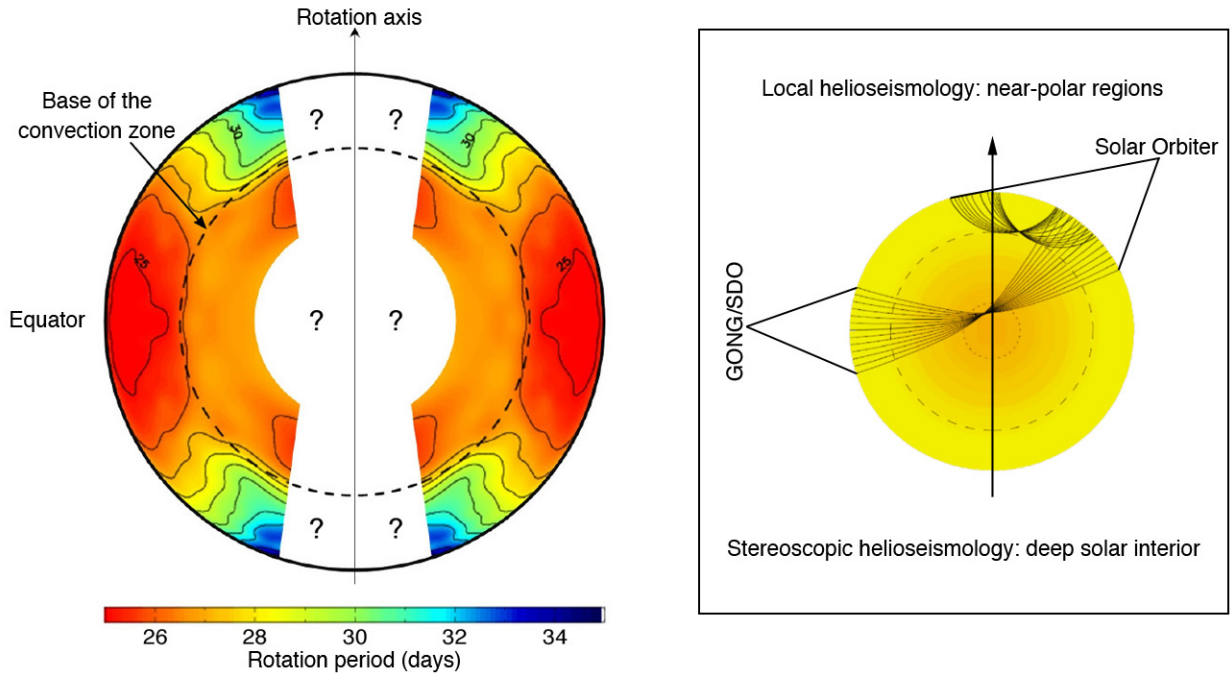


Figure 2.15. Left: Rotation profile in the solar interior as derived from GONG and MDI data. By traveling to high latitudes, Solar Orbiter will use local helioseismology to determine the currently unknown properties of the solar interior below the poles (Corbard 1998). Right: Solar Orbiter's helioseismology capabilities: (i) probing near polar regions with local helioseismology and (ii) probing the deep solar interior with stereoscopic helioseismology in combination with near-Earth observations (e.g., GONG or SDO).

Despite these advances, progress in understanding the operation of the solar dynamo depends on how well we understand differential rotation and the meridional flows near the poles of the Sun. However, because of the lack of out-of-the ecliptic observations, the near-polar flow fields remain poorly mapped, as does the differential rotation at high latitudes (see Beck 2000; Thompson et al. 2003; and **Figure 2.15**). The meridional flow in particular, the very foundation of the flux transport dynamo, is not well characterized above $\sim 50^\circ$ latitude; it is not even certain that it consists of only one cell in each hemisphere. The return flow, believed to occur at the base of the convection zone, is entirely undetermined save for the requirement of mass conservation. All these flows must be better constrained observationally in order to help solve the puzzle of the solar cycle and to advance our understanding of the operation of the solar dynamo (and, more broadly, of stellar dynamos generally).

How Solar Orbiter will address this question. Solar Orbiter will measure or infer local and convective flows, rotation, and meridional circulation in the photosphere and in the subsurface convection zone at all heliographic latitudes including, during the later stages of the nominal mission, at the critical near-polar latitudes. Solar Orbiter will reveal the patterns of differential rotation, the geometry of the meridional flow, the structure of subduction areas around the poles where the solar plasma dives back into the Sun, and the properties of convection cells below the solar surface. This will be achieved through correlation tracking of small features, direct imaging of Doppler shifts, and helioseismological observations (including the first from a high-latitude vantage point). By monitoring the temporal variations over the course of the mission, it will be possible to deduce solar cycle variations in the flows.

Solar Orbiter will resolve small-scale magnetic features near the poles, even within the nominal mission phase (**Figure 2.16**), and right up to the poles during the extended mission. It will determine the detailed surface flow field through tracking algorithms. Such algorithms provide only inconclusive results when applied to polar data obtained from near-Earth orbit due to the foreshortening. Doppler maps of the line-of-sight velocity component will complement the correlation tracking measurements and will also reveal convection, rotation, and meridional circulation flows.

Time series of Doppler and intensity maps will be used to probe the three-dimensional mass flows in the

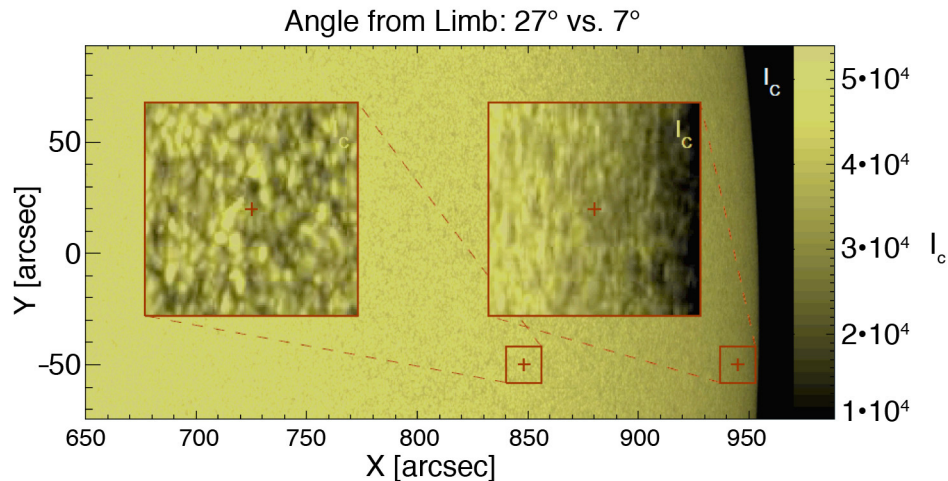


Figure 2.16. Comparison of solar granulation at the poles as viewed from 27° where the fine scale structure can be resolved with much higher fidelity than is obtained in the ecliptic plane twice a year (7°). The latter is the perspective used by the Hinode satellite to offer the first vector magnetic field imaging of the solar pole. Solar Orbiter will characterize the properties and dynamics of the polar regions for the first time, including magnetic fields, plasma flows, and temperatures.

upper layers of the convection zone, at high heliographic latitudes. The flows will be inferred using the methods of local helioseismology (e.g., Gizon and Birch 2005): time-distance helioseismology, ring diagram analysis, helioseismic holography, and direct modelling. Using SOHO/MDI Dopplergrams, it was demonstrated that even complex velocity fields can be derived with a single day of data (e.g., Jackiewicz et al. 2008).

The deeper layers of the convection zone will be studied using both local and the global methods of helioseismology. Moreover, Solar Orbiter will provide the first opportunity to implement the novel technique of stereoscopic helioseismology to probe flows and structural heterogeneities deep in the convection zone, even reaching down to the tachocline. Combining Solar Orbiter observations with ground- or space-based helioseismological observations from 1 AU (e.g., GONG or SDO) will open new windows into the Sun. Looking at the Sun from two distinct viewing angles will increase the observed fraction of the Sun's surface and will benefit global helioseismology because the modes of oscillation will be easier to disentangle (reduction of spatial leaks). With stereoscopic helioseismology, new acoustic ray paths can be taken into account to probe deeper layers in the interior (**Figure 2.15**), including the bottom of the convection zone.

2.4.2. What are the properties of the magnetic field at high solar latitudes?

Present state of knowledge. Meridional circulation transports the surface magnetic flux toward the poles, where a concentration of magnetic flux is expected to occur. However, because of the directional sensitivity of the Zeeman effect and magnetic polarity cancellation resulting from geometric foreshortening, present-day observations from the ecliptic at 1 AU can provide only a poor representation of the polar magnetic field. The high resolution of Hinode's Solar Optical Telescope (SOT) can partly overcome the second disadvantage (Tsuneta et al. 2008), but not the first. Consequently, an accurate quantitative estimate of the polar magnetic field remains a major and as yet unattained goal.

The polar field is directly related to the dynamo process, presumably as a source of poloidal field that is wound up by the differential rotation in the shear layer at the base of the convection zone. The distribution of the magnetic field at the poles drives the formation and evolution of polar coronal holes, polar plumes, x-ray jets, and other events and structures that characterize the polar corona. Polar coronal holes have been intensively studied from the non-ideal vantage point offered by the ecliptic, but never imaged from outside the ecliptic. Consequently the distribution of the polar field and the origin of polar structures are only poorly determined. The fast solar wind is associated with open field lines inside coronal holes, whereas at least parts of the slow solar wind are thought to emanate from the coronal hole boundaries. Understanding the interaction of open and closed field lines across these boundaries is of paramount importance for elucidating the connection between the solar magnetic field and the heliosphere.

The magnetic flux in the heliosphere varies with the solar cycle (Owens et al. 2008 and **Figure 2.8**). There is evidence that the heliospheric magnetic flux has increased substantially in the last hundred years, perhaps by as much as a factor of two (Lockwood et al. 1999; Rouillard et al. 2007), possibly due to a long-term change in the Sun's dynamo action. As noted earlier, however, the interplanetary magnetic field is dramatically lower than expected during the current solar minimum. Models based on the injection of flux into the heliosphere by coronal mass ejections (cf. Section 2.2.2) cannot explain this reduction, and it is becoming clear that the processes by which flux is added to and removed from the heliosphere are more complex than previously thought.

How Solar Orbiter will address this question. Solar Orbiter's comprehensive imaging instruments will characterize the properties and dynamics of the polar regions for the first time, including magnetic fields, plasma flows, and temperatures (**Figure 2.16**). Solar Orbiter will make the first reliable measurements of the amount of polar magnetic flux, its spatial distribution and its evolution (by comparing results from different orbits), providing an independent constraint on the strength and direction of the meridional flow near the pole. The evolution of Solar Orbiter's orbit to higher heliographic latitudes will make it possible to study the transport of magnetic flux from the activity belts toward the poles, which drives the polarity reversal of the global magnetic field (see Wang et al. 1989; Sheeley 1991; Makarov et al. 2003). From its viewpoint outside the ecliptic, Solar Orbiter will probe the cancellation processes that take place when flux elements of opposite polarity meet as part of the polarity reversal process. Joint observations from Solar Orbiter and spacecraft in the ecliptic will determine, with high accuracy, the transversal magnetic field, which is notoriously difficult to measure, along with derived quantities such as the electric current density.

Solar Orbiter will measure the photospheric magnetic field at the poles, while simultaneously imaging the coronal and heliospheric structure at visible and EUV wavelengths. In addition, as the spacecraft passes through the mid-latitude slow/fast wind boundary at around 0.5 AU, the field and plasma properties of the solar wind will be measured. With the help of magnetic field extrapolation methods these observations will, for the first time, allow the photospheric and coronal magnetic field in polar coronal holes to be studied simultaneously and the evolution of polar coronal hole boundaries and other coronal structures to be investigated. The images are complementary to those from low-latitude instruments (see **Figure 2.17** for a simulated EUV image).

Solar Orbiter's observations from progressively higher heliographic latitudes (25° by the end of the nominal mission) will enable the first coordinated investigation (jointly with spacecraft in the ecliptic) of the three-dimensional structure of the inner heliosphere. These observations will reveal the links between the Sun's polar regions and the properties of the solar wind and interplanetary magnetic field, in particular the heliospheric current sheet, which is used as a proxy for the tilt of the solar magnetic dipole. In addition, Solar Orbiter will pass both north and south of the solar equatorial plane in each orbit, with repeated transits through the equatorial streamer belt and through the slow/fast wind boundary at mid-latitudes into the polar wind, making it possible to follow the evolution of the solar wind and interplanetary magnetic field as well as of the sources in the polar coronal holes. Ulysses has shown that poleward of the edge of coronal holes the properties of the solar wind are relatively uniform, so that Solar Orbiter only needs to reach heliographic latitudes just above the coronal hole edge to enter the high-speed solar wind. The orbital inclination of 25° reached during the nominal mission is sufficiently high to satisfy this constraint.

2.4.3. Are there separate dynamo processes acting in the Sun?

Present state of knowledge. MHD simulations indicate that a local turbulent dynamo should be acting in the Sun's turbulent convection zone (Brun et al. 2004) and even in the near-surface layers (Vögler and Schüssler 2007). Hinode/SOT has detected ubiquitous horizontal magnetic fields in quiet regions of the Sun (Lites et al. 2007), which are possibly generated by local dynamo action (Pietarila Graham et al. 2009). These small, weak features (inter-network fields; Zirin 1987) bring 100 times more magnetic flux to the solar surface than the stronger features that are known to be the product of the global dynamo, and have themselves shown to be in cross-scale turbulent equilibrium (Schrijver et al. 1997). Even the smallest observable features have been shown to be formed primarily by aggregation of yet smaller, yet more prevalent features too small to resolve with current instrumentation (Lamb et al. 2008, 2009). It is, however, still uncertain whether a separate local, turbulent dynamo really is acting on the Sun and how strongly it contributes to the Sun's magnetic flux (and magnetic energy). In particular, all solar magnetic features, from the smallest observable intergranular flux concentrations to the largest active regions, have been shown (Parnell et al. 2009) to have a power law (scale

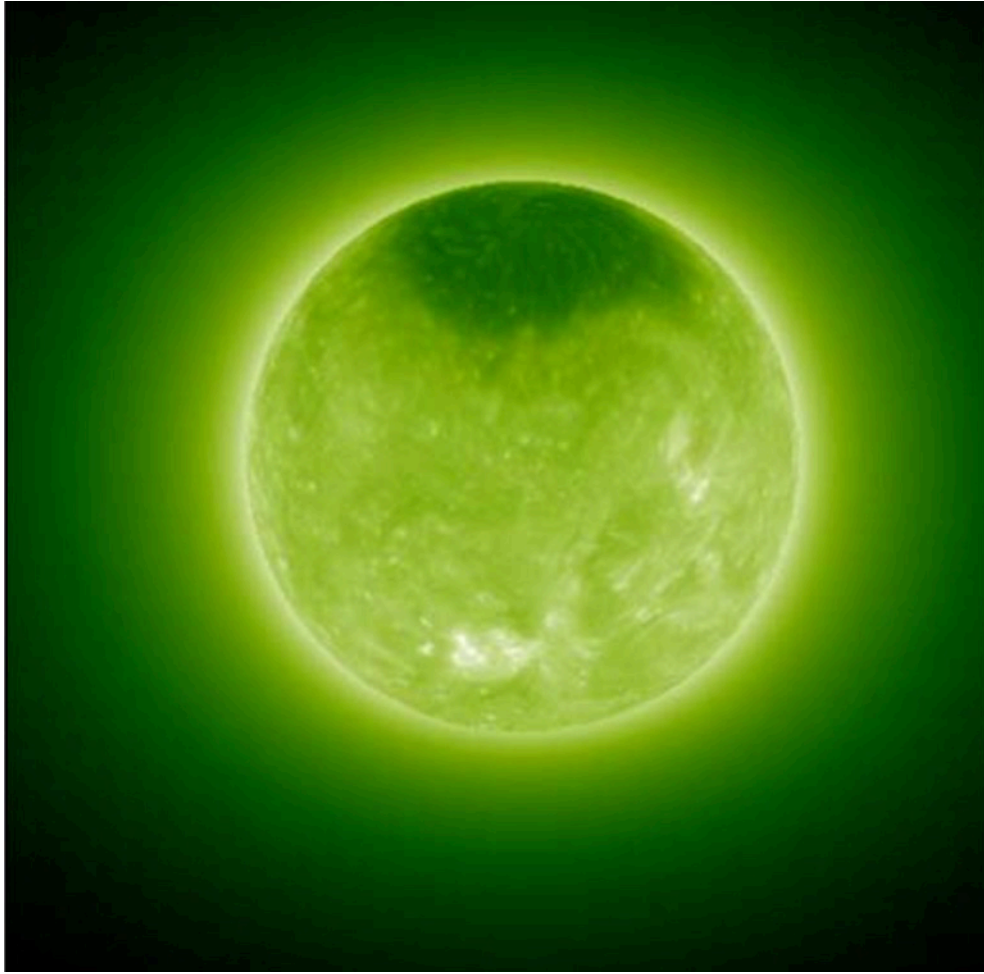


Figure 2.17. Simulated EUV view of the ultraviolet corona from 35° heliolatitude. Solar Orbiter's remote-sensing instruments and unique high-latitude vantage point will enable the first-ever simultaneous measurements of the polar magnetic field and the associated structures in a polar coronal magnetic hole.

free) probability distribution function, suggesting that a single turbulent mechanism may be responsible for all observable scales of magnetic activity.

How Solar Orbiter will address this question. One way to distinguish between the products of a global and a local dynamo is to study the distribution of small elements of freshly emerging magnetic flux over heliographic latitude. The global dynamo, presumably owing to the structure of the differential rotation and the meridional flow near the base of the convection zone, leads to the emergence of large bipolar magnetic regions (active regions) at the solar surface at latitudes between 5° and 30° and of smaller ephemeral active regions over a larger range of latitudes, but concentrated also at low latitudes. In contrast, a local turbulent dynamo is expected to enhance field more uniformly across the surface.

Observations carried out from the ecliptic cannot quantitatively determine the latitudinal distribution of magnetic flux and in particular the emergence of small-scale magnetic features (inter-network fields) due to foreshortening and the different sensitivity of the Zeeman effect to longitudinal and transversal fields. Solar Orbiter, by flying to latitudes of 25° and higher above the ecliptic, will be able to measure weak magnetic features equally well at low and high latitudes (Martínez Pillet 2006). If the number and size (i.e., magnetic flux) distributions of such features are significantly different at high latitudes, then even the weak features are probably due to the global dynamo. If, however, they are evenly distributed, then the evidence for a significant role of a local dynamo will be greatly strengthened. Current work is confounded by viewing angle restrictions near the poles, by the ubiquitous seething horizontal field (e.g., Harvey et al. 2007), and by small deflections in near-vertical fields, which dominate observed feature distributions near the limb of the Sun.

3.0 Science Implementation: Scientific Requirements and Payload

This chapter describes how the Solar Orbiter science investigations will be implemented and places special emphasis on demonstrating traceability: the flowdown from the science objectives discussed in the previous chapter to the observations and measurements required to meet those objectives, to the instrumentation needed to provide the required measurements, and to the requirements placed by the science objectives on the design of the orbit. **Tables 3.1-3.4** map the science questions to the required observations and instrumentation. **Table 3.5** then traces in detail the flowdown from required observations to specific measurement requirements to the capabilities of the selected payload. The first section of this chapter concludes with a brief discussion of the implications of the observational requirements and orbit design for the design of the spacecraft.

The instruments that have been selected for Solar Orbiter are described in Section 3.2, with **Tables 3.6** and **3.7** providing an overview of the payload and the payload resource requirements, respectively. For more detailed information on the payload, see the Solar Orbiter Engineering Interface Documents, Part B (EID-Bs). Telemetry rates and inter-instrument communication are discussed in the section on science planning and operations. The last two sections of the chapter discuss supporting observations and the role of theory and modelling in achieving scientific closure.

3.1. Observations, Measurements, and Orbital Characteristics

The overarching objective of the Solar Orbiter mission is to address the central question of heliophysics: ***How does the Sun create and control the heliosphere?*** Achieving this objective is the next critical step in an overall strategy to address one of the fundamental questions in the Cosmic Vision theme: ***How does the Solar System work?*** To this end, Solar Orbiter will use a carefully selected combination of in-situ and remote-sensing instrumentation, a unique orbit and mission design, and a well-planned observational strategy to explore systematically the region where the solar wind is born and heliospheric structures are formed.

As discussed in Chapter 2, the broad question that defines the overarching objective of the Solar Orbiter mission is broken down into four interrelated scientific questions:

1. How and where do the solar wind plasma and magnetic field originate in the corona?
2. How do transients drive heliospheric variability?
3. How do solar eruptions produce energetic particle radiation that fills the heliosphere?
4. How does the solar dynamo work and drive connections between the Sun and heliosphere?

Common to all of these questions is the requirement that Solar Orbiter make in-situ measurements of the solar wind plasma, fields, waves, and energetic particles close enough to the Sun that they are still relatively pristine and have not had their properties modified by dynamical evolution during their propagation. Solar Orbiter must also relate these in-situ measurements back to their source regions and structures on the Sun through simultaneous, high-resolution imaging and spectroscopic observations both in and out of the ecliptic plane.

3.1.1 Measurement Requirements and Instrument Capabilities

The measurement requirements for Solar Orbiter have been defined by two independent science definition teams. The Solar Orbiter Science Definition Team provided the input for the Solar Orbiter Science Requirements Document, taking into account the Payload Definition Document and the reports from the Payload Working Groups. The Joint ESA-NASA HELEX Science and Technology Definition Team subsequently refined Solar Orbiter's observation and measurement requirements in the context of the joint HELEX mission. These studies formed the basis for the competitive announcements of opportunity released by ESA and NASA and the initial instrument selection (see Section 3.2 below).

Tables 3.1-3.4 specify the observations required to address the science objectives and the science questions detailed in Chapter 2. The required observations are repeated in the first column of **Table 3.5**, which maps them

to instruments and measurements in the second column. The third column gives the detailed measurement requirements for each of the observations, and fourth column gives the corresponding capabilities of the selected instruments.

Table 3.1 Required observations and instrumentation for Solar Orbiter Objective 2.1.

Objective 2.1 How and where do the solar wind plasma and magnetic field originate in the corona?
2.1.1 What are the source regions of the solar wind and heliospheric magnetic field?
<ul style="list-style-type: none"> • Composition of source regions from remote (SPICE) and in-situ (SWA) observations • Magnetic connectivity (STIX, SWA, RPW, EPD) • Full disk photospheric magnetic fields (PHI) • In-situ magnetic field (MAG) • Full Sun, high-resolution and spectral images of corona and chromosphere (EUI, SPICE, METIS) • Global maps of H and He flow velocities and He fractions (METIS, SoloHI)
2.1.2 What mechanisms heat and accelerate the solar wind?
<ul style="list-style-type: none"> • High-resolution images of the photospheric magnetic field (PHI) • High-resolution images of coronal loops and evolving structures (EUI, SPICE) • Wave propagation and heating (SPICE, SWA, MAG, RPW) • H and He flow velocities (SPICE, METIS) • H and He flow velocities (SPICE, METIS) • Velocities and mass density of evolving structures (SoloHI, METIS) • Composition and plasma properties of associated wind (SWA, MAG, RPW) • Distribution of smallest flares and solar particle events (STIX, EPD)
2.1.3 What are the sources of solar wind turbulence and how does it evolve?
<ul style="list-style-type: none"> • High-cadence measurements of the plasma microstate across a wide band of heliolatitudes for all relevant solar wind regimes and heliocentric distances (MAG, SWA, RPW) • Images of source regions in Doppler-broadened lines (SPICE) • Identification of dropouts and measurement of SEP scattering by turbulence (EPD) • Time history of velocity and brightness of solar wind features and turbulence (METIS, SoloHI) • High-resolution, high-cadence maps of photospheric magnetic field (PHI)

Table 3.2 Required observations and instrumentation for Solar Orbiter Objective 2.2.

Objective 2.2 How do solar transients drive heliospheric variability?
2.2.1 How do CMEs evolve through the corona and inner heliosphere?
<ul style="list-style-type: none"> • High-resolution maps of photospheric magnetic field (PHI) • CME source location, expansion, rotation, and composition through corona (EUI, SPICE, STIX) • CME to in-situ properties (MAG, RPW, SWA) • Evolution of CME properties in the corona mapped to those measured in situ (SoloHI, METIS, MAG, RPW, SWA) • Distribution of energy into heat, particle acceleration, and bulk kinetic energy (SWA, MAG, EPD)
2.2.2 How do CMEs contribute to solar magnetic flux and helicity balance?
<ul style="list-style-type: none"> • In-situ properties of ejecta (SWA, MAG, RPW) • Full-disk maps of photospheric magnetic field to determine source region helicity (PHI) • Map source regions to in-situ properties magnetic connectivity, polarity, and helicity (EUI, METIS, SPICE, SoloHI, SWA, MAG, EPD)
2.2.3 How and where do shocks form in the corona and inner heliosphere?
<ul style="list-style-type: none"> • Global maps of electron density, H & He flow velocities (METIS) • Position and speed of shocks (SPICE, METIS, SoloHI, EUI, RPW, SWA) • Full-sun and high-resolution coronal and chromospheric images (EUI, STIX, METIS, SPICE) • Location, intensity, thermal/non-thermal distribution of erupting regions (SoloHI, RPW) • Timing of eruptions and coronal manifestations (EUI, SoloHI) • Plasma, electric and magnetic fields in situ (SWA, MAG, RPW, EPD)

3.1.2 Orbit Requirements

The science objectives discussed in Chapter 2 specifically identify a set of orbit characteristics and mission design parameters that define the Solar Orbiter mission. In summary, the requirements on the orbit are to: 1) go close to the Sun (within 0.25 AU); 2) have periods of extended near co-rotation with the solar surface (keeping in sight individual solar surface features for one solar rotation); 3) achieve moderate out-of-ecliptic viewing

Table 3.3 Required observations and instrumentation for Solar Orbiter Objective 2.3.

Objective 2.3 How do solar eruptions produce energetic particle radiation that fills the heliosphere?
2.3.1 How and where are energetic particles accelerated at the Sun?
<ul style="list-style-type: none"> • UV and x-ray imaging of loops, flares, and CMEs (EUI, SPICE, STIX, METIS, SoloHI) • Global maps of electron densities, H, He flow velocities (METIS) • Imaging of coronal suprathermal seed population (SPICE) • Location, timing, and motion of CMEs and shocks (EUI, SoloHI) • X-ray signatures of energetic particle interactions at loop footpoints, or on loops themselves (STIX) • Radio signatures of coronal shocks and escaping electrons (RPW) • Magnetic field, plasma wave and solar wind measurements to determine turbulence levels and identify shock passages (MAG, RPW, SWA) • Seed population specification from the heavy ion composition of solar wind and suprathermals in the inner heliosphere timing (SWA) • Velocity distributions, scattering characteristics, spectra and composition of energetic particles (EPD) • Timing and properties of small events (STIX, EPD, RPW, EUI) • Images of longitudinal extent of CMEs in visible, UV, and hard x-rays (SoloHI, METIS, EUI, SPICE, STIX)
2.3.2 How are energetic particles released from their sources and distributed in space and time?
<ul style="list-style-type: none"> • Timing, location, and intensity profiles of EUV, radio, and x-ray emissions in relation to energetic-particle intensities at a wide range of energies (EUI, SPICE, RPW, STIX, EPD) • X-ray spectral images of flaring regions (STIX) • High-resolution, high-cadence maps of photospheric magnetic field (PHI) • Turbulence properties throughout the inner heliosphere and corona (MAG, SWA, RPW, SPICE) • Magnetic connectivity (SWA, MAG, EPD)
2.3.3 What are the seed populations for energetic particles?
<ul style="list-style-type: none"> • Map coronal suprathermal ion pool (SPICE) • Map inner-heliosphere suprathermal ions (EPD, SWA) • Shock and turbulence parameters (MAG, SWA, RPW)

Table 3.4 Required observations and instrumentation for Solar Orbiter Objective 2.4.

Objective 2.4 How does the solar dynamo work and drive connections between the Sun and the heliosphere?
2.4.1 How is magnetic flux transported to and reprocessed at high solar latitudes?
<ul style="list-style-type: none"> • Full-disk & high-resolution maps of the photospheric magnetic field and local and convective flows, maps of rotation, differential rotation, and meridional circulation, structure of subduction areas, properties of sub-surface convection cells (PHI) • High-resolution images of small-scale magnetic features at the poles (EUI, SPICE, PHI)
2.4.2 What are the properties of the magnetic field at high solar latitudes?
<ul style="list-style-type: none"> • Amount, distribution, and evolution of polar photospheric magnetic flux transversal magnetic field (PHI) • Magnetic fields, plasma flows, and temperatures in polar regions (PHI, EUI, SPICE) • Images of coronal and heliospheric structure in visible and EUV (EUI, METIS, SoloHI) • Properties of bulk solar wind (SWA, MAG) • Magnetic connectivity (SWA, MAG, EPD, EUI)
2.4.3 Are there separate dynamo processes acting in the Sun?
<ul style="list-style-type: none"> • Latitudinal distribution of small-scale, emerging magnetic flux (PHI)

Table 3.5 Measurement and instrument requirements.

Required Observations (cf. Tables 3.1 – 3.4)	Instrument: Measurement	Measurement Requirements and Coordinated Observation Plans	Selected Payload Capability
Global maps of H and He flow velocities and He fractions	METIS: visible, H I and He II Ly-alpha lines, polarization brightness	<p><u>Polarized visible-light imaging:</u> Physical quantity: electron density FOV: ~ 1.2 to $3.5 R_{\odot}$ (at 0.23 AU); $3 - 15 R_{\odot}$ (at 1 AU) Spatial res: $< 8 \text{ arcsec}$ (10^3 km at 0.23 AU) Spectral coverage: $450\text{-}650 \text{ nm}$ Stray-light rejection: $10^{-11} \text{ B/B}_{\odot}$ Polarization S/N: $> 10^2$ Cadence: 5 min. (CMEs obs.); 10 min. (synoptic)</p> <p><u>UV & EUV imaging:</u> Physical quantities: hydrogen and singly-ionized helium densities, and outflow velocities FOV: $\sim 1.2 - 3.5 R_{\odot}$ (Solar Orbiter at 0.23 AU); extendable to $3 - 15 R_{\odot}$ (1 AU) Spatial resolution: $< 8 \text{ arcsec}$ Spectral coverage: H I Ly-α, 121.6 nm; He II Ly-α, 30.4 nm Spectral Resolution: $\Delta\lambda/\lambda \leq 10^{-1}$ Cadence: $< 15 \text{ min.}$</p>	$1.2 - 3.0 R_{\odot}$ @ 0.23 AU at $13''$ at $10 \text{ s} / 20 \text{ min} / 1 \text{ hr}$ cadence (vis/UV/EUV)
Mapping of coronal features to inner heliosphere, evolution of velocities and mass densities of coronal structures	SoloHI: White light, polarization brightness	<p><u>Visible-light (VL) imaging:</u> Physical quantity: electron distribution Spatial res: $\sim \text{arcmin}$ Stray-light rejection: $10^{-14} \text{ B/B}_{\odot}$ Cadence: 60 min.</p>	$40^{\circ} \times 40^{\circ}$ at better than $1''$ / pixel

Table 3.5 Measurement and instrument requirements (cont'd).

Required Observations (cf. Tables 3.1 – 3.4)	Instrument: Measurement	Measurement Requirements and Coordinated Observation Plans	Selected Payload Capability
Composition of coronal source region	SPICE: imaging EUV spectroscopy in two channels (plus one 2 nd order band)	<p>On disk:</p> <ul style="list-style-type: none"> - Best spatial resolution 1 arcsec - Instantaneous FOV = 16 arcmin x 1 arcsec - Rastered FOV = 16 arcmin x 4 arcmin - Two lines per temperature decade - Exposure time 5 s - Spectral cadence of 20 min - Compositional signatures <p>Off disk:</p> <ul style="list-style-type: none"> - Spatial resolution 1 arcmin - Stare (no raster) - Spectral cadence of 10 min - Radial coverage out to 2 R_s - Compositional signatures and outflow 	<p>(1, 2, and 6)'' x 17' slits 1''/pixel and 76 mA/pixel</p> <p>cadence 16 min per raster</p> <p>4 arcsec resolution rastered 5 min cadence 1.0 – 3.0 R_s</p>
Composition of solar wind and compositional changes at solar wind boundaries	SWA: mass, charge, energy of ions	Many heavy ion 1-dim energy spectra (0.5 – 60 keV/q, 5% energy resolution); FOV = ±25°; cadence: up to 1 min at 0.3 AU	SWA-HIS: 3D VDFs, FOV = (-33°–+63°) x (±18°), 0.5 – 100 keV/e, 5.6% resolution, 5 min cadence, 30 s burst mode (heavy ions) 3 s (alpha particles) sensitivity ~ 2 x 10 ⁻⁵
Full-disk and high-resolution EUV images of chromosphere and corona	EUI: 174 and 304 Å and HI Ly-alpha	<p>(a) FSI: 2 passbands (cool/hot), 5.5° FOV, 7.2 arcsec/pixel, 1 min maximum cadence, SNR>2 in QS (dimmings) and off limb (CME ejecta).</p> <p>(b) HRI: 2 passbands, 17 arcmin FOV, >1 k format, 5 s cadence in burst mode, SNR>5 on AR loops (nanoflares).</p>	<p>FSI: 5.2° x 5.2° at 9'' resolution, cool and hot passbands (He II 304 Å) and Fe IX/X 174 Å)</p> <p>HRI: 1000'' at 1'' resolution Ly-α (1216 Å), Fe IX/X (174 Å), FeXVI (335 Å)</p>
In-situ magnetic field properties	MAG: magnetic field vector	±1000 nT, 0.5nT absolute precision; 0-20 Hz	Ranges: from ±32 nT to ±2048 nT at ~ 4 pT resolution, up to 128 vectors/sec

Table 3.5 Measurement and instrument requirements (cont'd).

Required Observations (cf. Tables 3.1 – 3.4)	Instrument: Measurement	Measurement Requirements and Coordinated Observation Plans	Selected Payload Capability
High-cadence plasma properties	SWA: proton and electron E/q spectra MAG: magnetic field vectors	Solar wind protons: Detailed 3D velocity distribution functions at 10-s time resolution; FOV: $\pm 45^\circ$ to Sun, $\pm 15^\circ$ north/south, angular resolution of 2° Solar wind electrons: 3D velocity distribution functions (about 5 -5000 eV, 10% energy resolution); 10-s resolution MAG: already covered by previous requirements (see above in table) (MAG vectors will be used to derive reduced high-cadence VDFs by SWA)	SWA: up to 1/10s (in burst mode), FOV = $(-17.5^\circ$ to $+47.5^\circ) \times (\pm 22.5^\circ)$, resolution $< 2^\circ$ SWA/EAS: FOV = $(360^\circ \times (\pm 45^\circ))$, 1 eV-5 kV, 10-12% resolution, 3 s / 10 s cadence, 0.125 s in burst mode
Full-disk and high-resolution images of photospheric magnetic field	PHI: Stokes parameters of FeI 617.3 nm line	High-Res Mode: Vector magnetic field with accuracy of 0.1 G (longitudinal), 20 G (transverse); $15' \times 15'$ FOV; resolution ~ 1 arcsec (0.5 arcsec pixel size) Cadence: 1 min over selected periods of time; Low-Res (full disk) Mode: (a) Vector magnetic field with accuracy of 0.1 G (longitudinal), 2 G (transverse); Pixel size: ~ 5 arcsec; Capability: Cadence of 1 min. over selected period of times on the whole orbit FOV: > 150 arcmin (full apparent Sun) (b) Continuum imaging, Doppler measurements on the whole orbit, cadence of 1 min	PHI/HRT: accuracy: 0.1 G/14 G $16.8' \times 16.8'$ at 150 km (at 0.23 AU) plus full disk ~ 1 arcsec at 617.3 nm; 45-60 sec cadence PHI/FDT: accuracy same as for HRT cadence: 45-60 s FOV > 156 arcmin
High-resolution images of loops	EUI: high-resolution EUV images	EUI: already covered by previous requirements (see above in table)	See EUI/HRI resolution above
Wave propagation and heating	SPICE: Doppler broadening of lines; RPW: spectra and waveforms;	SPICE: already covered by previous requirements (see above in table), plus motions to ± 5 km/s Radio waves: 3-axis electric and magnetic spectra and correlations; frequency range: 100 kHz to 20 MHz	SPICE: see above in table; RPW: range from $\mu\text{V/m}$ to V/m, down to near-DC

Table 3.5 Measurement and instrument requirements (cont'd).

Required Observations (cf. Tables 3.1 – 3.4)	Instrument: Measurement	Measurement Requirements and Coordinated Observation Plans	Selected Payload Capability
Magnetic connectivity	MAG: local field direction SWA: halo/strahl electron pitch-angle distribution	MAG: already covered by previous requirements (see above in table) SWA: electrons FOV at least 2π solid angle, ideally $\pm 180^\circ$ to Sun, $\pm 45^\circ$ north/south, angular resolution 10° , core-halo electron pitch-angle distributions with strahl population; While MAG provides B vector, strahl electrons and pitch-angle distributions give connectivity.	MAG: see above in table SWA/EAS: two orthogonal sensor heads, each with 32 azimuthal angle bins and 16 elevation angle bins to provide a combined coverage close to 4π steradian
X-ray imaging of loops, flares	STIX: high-resolution energy-resolved x-ray images of loops and footpoints	Energy range: 3 to 150 keV; Energy resolution: $\Delta E/E \sim 0.2$ FWHM; Angular Resolution: $< \sim 7$ arcsec; FOV for imaging: $> \sim 20$ arcmin; FOV for source centroid location: Full Sun at 0.23 AU, i.e. ~ 150 arcmin; Effective area ~ 15 cm ² ; time resolution (for flares) $< \sim 5$ s, ~ 1 s in burst mode	STIX: range: 4–150 keV, resolution: 1 keV @ 6 keV, 15 keV @ 150 keV; 7" to 8.8" at > 0.1 s exposure time, > 0.1 s time resolution
Timing of radio emissions	RPW: magnetic/electric fields	3-axis electric and magnetic spectra and correlations; frequency range: 100 kHz to 20 MHz	From DC to 20 MHz/500 kHz (electric/magnetic) at up to 500 kS/s*
Timing of EUV emission	EUI: high-cadence imaging	5 s or better cadence	EUI: up to 2 s typical for EUV, sub-second in high-cadence mode for Ly- α
Timing of energetic particles	EPD: proton/electron measurements: particle intensities in various energy ranges, velocity dispersion, different species	Electrons: Energy range: ~ 2 keV to ~ 1 MeV, energy resolution: $\Delta E/E \sim 0.2$; geometry factor $> \sim 0.1$ – 1 cm ² sr; time resolution 10 s at < 0.5 AU, 1 min > 0.5 AU Protons: Energy range: 0.005 to > 100 MeV; energy resolution: $\Delta E/E \sim 0.2$; geometry factor $> \sim 0.1$ – 1 cm ² sr; time resolution 20 s below 10 MeV at < 0.5 AU, 1 min > 0.5 AU	EPD/EPT: time resolution up to 1 s in burst mode, electrons 2 keV – 30 MeV ions: 3 keV – 100 MeV/nuc

* kS/s = kilosamples per second

Table 3.5 Measurement and instrument requirements (cont'd).

Required Observations (cf. Tables 3.1 – 3.4)	Instrument: Measurement	Measurement Requirements and Coordinated Observation Plans	Selected Payload Capability
Turbulence levels	MAG: high-cadence magnetic field RPW: high-cadence electric and magnetic field, power spectral densities	MAG: already covered by previous requirements (see above in table) Plasma wave electric spectra for thermal-noise spectroscopy; sensitivity: $3 \text{ nV/Hz}^{1/2}$; frequency range: 10-800 kHz. Electric and magnetic spectra and waveforms in an internal burst mode (triggered internally or on input), frequency range: near DC to 1 MHz; AC magnetic fields: 10Hz – 10kHz; waveform capture already covered by previous requirement (see above in table)	MAG: see above in table RPW: see above in table up to 500 kS/s*
	SWA: high-cadence bulk ion and electron properties, EPD: electron and proton anisotropies		SWA: see above in table
Suprathermal seed population	EPD: suprathermal particle composition	electrons: angular resolution 30° over 60° FOV as close to Sun as possible; protons: two angular sectors from $0-90^\circ$ as close to the Sun as possible up to 10 MeV Heavy Ions: He – Fe, energy range: 0.02 – 10 MeV/nucleon (species dependent) Composition: separate ^3He , ^4He , C, N, O and Fe as a minimum; energy resolution: $\Delta E/E \sim 0.2$; geometry factor $> \sim 0.1-1 \text{ cm}^2 \text{ sr}$; time resolution 30 s $< 0.5 \text{ AU}$, 1 min $> 0.5 \text{ AU}$	EPD: up to 1s (burst mode), all sensors cover 1st-order anisotropy, EPT has 4 FOVs, LET 6 FOVs, see Fig. 3.5 EPD/SIS: $0.24 \text{ cm}^2 \text{ sr geom. factor}$; ^3He , major species He-Fe, $\Delta E/E < 0.1$; range 0.01 - 10 MeV/nuc
Solar wind bulk properties	SWA: electron, proton, alpha-particle velocities, temperatures, densities	SWA: already covered by previous requirements (see above in table)	SWA: $\sim 3 \text{ s cadence}$
Distribution of smallest flares and solar particle events	EPD: small flux events STIX: low x-ray intensity	EPD: already covered by previous requirement (see above in table) STIX: already covered by previous requirements (see above in table) While STIX can observe microflares on the disk via x-ray emissions, EPD will measure the properties of the escaping particles to determine energy deposition in the corona.	EPD: Low-noise detectors & FEE, large geometric factors SIS: $0.24 \text{ cm}^2 \text{ sr}$, LET up to $1.7 \text{ cm}^2 \text{ sr}$ in single-detector mode STIX: 12 cm^2 effective area

*kS/s = kilosamples per second

Table 3.5 Measurement and instrument requirements (cont'd).

Required Observations (cf. Tables 3.1 – 3.4)	Instrument: Measurement	Measurement Requirements and Coordinated Observation Plans	Selected Payload Capability
High-cadence measurements of the plasma micro state across a wide band of helio-latitudes for all relevant solar wind regimes and heliocentric distances	MAG: high-cadence magnetic field SWA: high-cadence 2-d electron/proton VDFs, composition RPW: high-cadence electric and magnetic field spectra, wave forms	MAG: already covered by previous requirements (see above in table) SWA: already covered by previous requirements (see above in table) RPW: already covered by previous requirements (see above in table) Accurate timing between the three instruments is ensured by SpaceWire time signal to in-situ payload. Occasional burst modes chosen such as to cover all solar wind regimes at all distances and latitudes. This is controlled by the MAG DPU. Composition will be used to determine coronal origin of solar wind.	MAG: see above in table SWA: 0.125 s e ⁻ , 0.1 s protons, 3 s alpha articles, 30 s heavy ions RPW: low frequency (near DC up to local plasma frequency) and time-domain sampling, at up to 500 kS/s*
Images of source regions in Doppler-broadened lines	SPICE: on-disk and limb imaging spectroscopy in UV	SPICE: already covered by previous requirements (see above in table)	SPICE: see above in table
Identify dropouts and measure scattering of SEPs by turbulence	EPD: intensities and anisotropies of low-energy ions, protons and electrons MAG: B-vectors SWA: bulk solar wind	EPD: already covered by previous requirements (see above in table) at least 1st-order anisotropies (forward-backward) Use velocity dispersion plots in conjunction with pitch-angle distributions and correlate with solar wind turbulence levels and variations at the coronal source.	EPD/STEIN: few keV – 40 keV e ⁻ /p, 1 st order anisotropy EPD/EPT: 20 – 700 keV electrons, 20 – 9 MeV protons, 4 FOVs EPD/LET: low-energy protons in 6 FOVs
Time history of velocity and brightness of solar wind features and turbulence	METIS: high-cadence visible, H I and He II Ly-alpha lines; SoloHI: white-light and pB	METIS: already covered by previous requirements (see above in table) SoloHI: already covered by previous requirements (see above in table) Derive acceleration and heating properties from time-height and time-brightness plots.	METIS: see above in table at 20 min cadence SoloHI: see above in table at 30 min cadence
High-resolution, high-cadence maps of photospheric magnetic field	PHI: Stokes parameters	PHI: already covered by previous requirements (see above in table)	PHI: see above in table at 1 hr cadence

* kS/s = kilosamples per second

Table 3.5 Measurement and instrument requirements (cont'd).

Required Observations (cf. Tables 3.1 – 3.4)	Instrument: Measurement	Measurement Requirements and Coordinated Observation Plans	Selected Payload Capability
Map CME source location, expansion, rotation, and composition through corona	STIX: x-ray emission for location of associated flare	STIX: already covered by previous requirements (see above in table)	STIX: see above in table
	EUI: high-resolution images of source region	EUI: already covered by previous requirements (see above in table)	EUI: see above in table
	SPICE: on-disk and limb imaging spectroscopy	SPICE: already covered by previous requirements (see above in table)	SPICE: see above in table
	METIS: H and He flow velocities, electron densities	METIS: already covered by previous requirements (see above in table)	METIS: see above in table
	SoloHI: track to inner heliosphere	SoloHI: already covered by previous requirements (see above in table)	SoloHI: see above in table
	RPW: radio emission	RPW: already covered by previous requirements (see above in table)	RPW: up to 20 MHz
		Coordinated observations focusing on promising active region. STIX/EUI measure associated flare, SPICE/METIS flow velocities, expansion of different ions, SoloHI tracks to interplanetary space, while RPW measures radio emission from accelerated electrons at local plasma frequency (compare with METIS e^- density)	
Map CME to in-situ properties	PHI: high-resolution photospheric magnetic field	PHI: already covered by previous requirements (see above in table)	PHI: see above in table
	EUI: high-resolution images of source region	EUI: already covered by previous requirements (see above in table)	EUI: see above in table
	SPICE: composition of source region	SPICE: already covered by previous requirements (see above in table)	SPICE: see above in table
	SWA: composition of in-situ CME	SWA: already covered by previous requirements (see above in table)	SWA: elemental and charge-state composition
	RPW: time history of (type II) radio emission	RPW: already covered by previous requirements (see above in table)	RPW: up to 20 MHz
	MAG: in-situ magnetic field rotation	MAG: already covered by previous requirements (see above in table) While EUI&STIX provide context and timing, SPICE gives composition, for comparison with SWA composition. Compare PHI and MAG field data, track evolution with RPW.	MAG: see above in table

Table 3.5 Measurement and instrument requirements (cont'd).

Required Observations (cf. Tables 3.1 – 3.4)	Instrument: Measurement	Measurement Requirements and Coordinated Observation Plans	Selected Payload Capability
Link evolution of CME properties to those measured in situ	SoloHI: measure evolution of morphology out to Solar Orbiter orbit	SoloHI: already covered by previous requirements (see above in table) Use statistical properties of CMEs to link them to in-situ properties. When Solar Probe Plus is appropriately located, compare with in-situ data.	SoloHI: very low background/stray light ($< 5 \times 10^{-13}$ B/B _{sun} at 0.88 AU), FOV $5^\circ - 45^\circ$
Distribution of energy into heat, particle acceleration, and bulk kinetic energy	SWA: 3D velocity distribution functions, bulk speed MAG: magnetic pressure EPD: particle spectra	SWA: already covered by previous requirements (see above in table) MAG: already covered by previous requirements (see above in table) EPD: already covered by previous requirements (see above in table) Measure directly, in situ, the energy content in the various forms and acquire distribution as statistics build up.	SWA: normal operation mode MAG: normal operation mode EPD: normal operation mode
Energetic particle timing	EPD: particle intensities in different energy ranges and for different species	EPD: already covered by previous requirements (see above in table)	EPD: burst mode intervals
Image coronal suprathermal population	SPICE: imaging UV spectroscopy	SPICE: already covered by previous requirements (see above in table) excellent signal to noise ratio, low background Use intensity differences in highly Doppler-broadened lines	SPICE: see above in table
x-ray signatures of energetic particle interactions at loop footpoints or on loops themselves	STIX: high-cadence, energy resolved images	STIX: already covered by previous requirements (see above in table)	STIX: see above in table
Radio signatures of coronal shocks and escaping electrons	RPW: Type II and III radio	RPW: already covered by previous requirements (see above in table)	RPW: see above in table

Table 3.5 Measurement and instrument requirements (cont'd).

Required Observations (cf. Tables 3.1 – 3.4)	Instrument: Measurement	Measurement Requirements and Coordinated Observation Plans	Selected Payload Capability
Magnetic field, plasma wave, and solar wind measurements to determine turbulence levels and shock passage	MAG: high-cadence magnetic field RPW: high-cadence electric/magnetic field SWA: high-cadence bulk plasma properties, 2D VDFs,	MAG: already covered by previous requirements (see above in table) RPW: already covered by previous requirements (see above in table) SWA: already covered by previous requirements (see above in table) Use RPW of MAG to trigger in-situ suite. MAG and SWA data provide Alfvén velocity and turbulence parameters such as Elsässer variables; RPW measures electric field properties which influence solar wind electron and proton VDFs.	MAG: burst mode (128 vectors/s) RPW: burst mode SWA: burst mode
Seed population specification from the heavy ion composition of solar wind and suprathermals in the heliosphere	SWA: heavy ion composition and long-term velocity distribution functions EPD: suprathermal particle population	SWA: already covered by previous requirements (see above in table) This drives upper range of HIS energy band (100 keV/e) EPD: already covered by previous requirements (see above in table) Cross calibrated SWA and EPD/SIS fluences over a wide range in latitudes and distance	SWA: normal operation mode EPD/SIS: normal operation mode high latitudes and full radial coverage
Timing, velocity distributions, scattering characteristics, spectra and composition of energetic particles, continuous spectra of multiple heavy ion species in energy range 0.1–100 MeV/n	EPD: full composition, anisotropies, energy coverage, occasional high-cadence studies; Resolution of ^3He and multiple heavy ion species	EPD: already covered by previous requirements (see above in table)	EPD: 2 keV–20 MeV e^- , 3 keV – 100 MeV p ; 8 keV/n – 200 MeV/n ions continuous coverage with geometric factors $> 0.1 \text{ cm}^2\text{sr}$ 3 – 40 keV neutrals, normal operation, occasional burst mode

Table 3.5 Measurement and instrument requirements (cont'd).

Required Observations (cf. Tables 3.1 – 3.4)	Instrument: Measurement	Measurement Requirements and Coordinated Observation Plans	Selected payload capability
Timing of EUV, radio, and x-ray emissions in relation to energetic particle intensities at a wide range of energies	EUI, STIX: high-cadence images of active region, trigger to EPD RPW: type II and type III radio emission EPD: staggered high-cadence measurements of particle intensities	EUI: already covered by previous requirements (see above in table) STIX: already covered by previous requirements (see above in table) RPW: already covered by previous requirements (see above in table) EPD: already covered by previous requirements (see above in table) EUI/STIX provide trigger to EPD. RPW gives shock location (if present) from radio emission, and EPD determines particle properties. HET and EPT (for electrons) are triggered first, lower energy LET later (velocity dispersion)	EUI: see above in table STIX: see above in table RPW: see above in table EPD: see above in table
Full-disk & high-resolution maps of the photospheric magnetic field and local and convective flows, maps of rotation, differential rotation, and meridional circulation, structure of subduction areas, properties of sub-surface convection cells;	PHI: full-disk and high-resolution Stokes parameters, Doppler shifts, intensity variations	PHI: already covered by previous requirements (see above in table)	PHI: see above in table, normal operation mode
High-resolution images of small-scale magnetic features at the poles	EUI: high-resolution EUV images SPICE: high-resolution spectroscopy PHI: high-resolution Stokes parameters	EUI: already covered by previous requirements (see above in table) SPICE: already covered by previous requirements (see above in table) PHI: already covered by previous requirements (see above in table) coordinated high-resolution FOVs	EUI: normal operation mode SPICE: normal operation mode PHI: normal operation mode

Table 3.5 Measurement and instrument requirements. (cont'd)

Required Observations (cf. Tables 3.1 – 3.4)	Instrument: Measurement	Measurement Requirements and Coordinated Observation Plans	Selected Payload Capability
Amount, distribution, and evolution of polar photospheric magnetic flux	PHI: full-disk and high-resolution Stokes parameters	PHI: already covered by previous requirements (see above in table)	PHI: normal operation mode
Transversal magnetic field in the photosphere	PHI: high-resolution Stokes parameters other remote-sensing observations (e.g. SDO/HMI)	PHI: already covered by previous requirements (see above in table)	PHI: normal operation mode
Latitudinal distribution of small-scale, emerging magnetic flux in the photosphere	PHI: high-resolution Stokes parameters	PHI: already covered by previous requirements (see above in table)	PHI: normal operation mode
Position and speed of shocks	METIS: flow velocities, electron densities SoloHI: white-light coronagraphy SPICE: temperatures from Doppler-broadened lines RPW: radio emissions	METIS: already covered by previous requirements (see above in table) SoloHI: already covered by previous requirements (see above in table) SPICE: already covered by previous requirements (see above in table) RPW: already covered by previous requirements (see above in table) Use METIS electro-density maps to pin-point radio emission and compare with RPW type-II radio bursts. Compare speeds of features in METIS/SPICE with derived velocities, use temperatures and magnetic field extrapolations to determine magnetosonic speed and compare with shock speed	METIS: see above in table SoloHI: see above in table SPICE: see above in table RPW: see above in table
High-cadence microphysics of plasma	SWA: burst mode 2-d velocity distribution functions MAG: burst mode EPD: burst mode RPW: burst mode trigger to in-situ	SWA: already covered by previous requirements (see above in table) MAG: already covered by previous requirements (see above in table) EPD: already covered by previous requirements (see above in table) RPW: already covered by previous requirements (see above in table), trigger in-situ payload via SpaceWire	SWA: see above in table MAG: see above in table EPD: see above in table RPW: see above in table

Table 3.5 Measurement and instrument requirements. (cont'd)

Required Observations (cf. Tables 3.1 – 3.4)	Instrument: Measurement	Measurement Requirements and Coordinated Observation Plans	Selected Payload Capability
Timing and properties of small events	STIX: high-cadence, high-resolution EUI: high-cadence, high-resolution images EPD: energy spectra of electrons and protons RPW: high-cadence	STIX: already covered by previous requirements (see above in table) EUI: already covered by previous requirements (see above in table) EPD: already covered by previous requirements (see above in table) RPW: already covered by previous requirements (see above in table), low background, low noise	STIX: see above in table EUI: see above in table EPD: see above in table RPW: see above in table
Images of longitudinal extent of CMEs in visible and UV	METIS: flow velocities SoloHI: white light EUI: UV images	METIS: already covered by previous requirements (see above in table) SoloHI: already covered by previous requirements (see above in table) EUI: already covered by previous requirements (see above in table)	METIS: see above in table SoloHI: see above in table EUI: see above in table
Magnetic fields, plasma flows, and temperatures of polar regions	PHI: high-resolution photospheric magnetic field EUI: high-resolution EUV images SPICE: high-resolution images, Doppler-broadened lines	PHI: already covered by previous requirements (see above in table) EUI: already covered by previous requirements (see above in table) SPICE: already covered by previous requirements (see above in table)	PHI: see above in table EUI: see above in table SPICE: see above in table
Images of coronal and heliospheric structure in visible and EUV	METIS: electron density, H, He flows SoloHI: white-light images of corona EUI: coronal images	METIS: already covered by previous requirements (see above in table) SoloHI: already covered by previous requirements (see above in table) EUI: already covered by previous requirements (see above in table)	METIS: see above in table SoloHI: see above in table EUI: see above in table
Images of evolution of coronal hole boundaries	EUI: full-disk images in EUV	EUI: already covered by previous requirements (see above in table) Make available as data product for comparison with in-situ data and observations from near-Earth assets.	EUI: see above in table

($\sim 25^\circ$) and latitudinal coverage; and 4) comprehensively characterize conditions in the inner heliosphere as a function of distance and latitude. The science definition teams and the payload working groups, representing the scientific community, have worked closely with ESTEC engineers to design a mission that is both feasible from an engineering point of view and will achieve the science objectives discussed in the preceding chapter. One critical factor that drives the mission and spacecraft design is the perihelion distance, while a second is the trade between perihelion distance and near-corotation with the solar surface; and a third is inclination of the orbit. The detailed scientific rationale for these requirements is reviewed below.

Perihelion Distance Requirement. The Helios mission, which reached a perihelion distance of 0.29 AU, demonstrated that stream-stream interactions, solar wind acceleration and wave-particle interactions are still active at this distance. In order to measure the less processed, pristine solar wind streams and the ongoing interaction at their interfaces as well as the kinetic processes that accelerate and heat the wind, Solar Orbiter must spend sufficient time within 0.3 AU to cover 180° in solar longitude in order to guarantee multiple observations of the fast-slow stream interface. This drives the requirement on the amount of time (at least 90 days, i.e., three solar rotations) that Solar Orbiter spends within 0.3 AU; in practice this requires that the perihelion distance lie within 0.25 AU.

Another driver to go close to the Sun is the measurement of energetic particles, which should be made within one or two scattering mean free paths (typically 0.2 AU; Palmer 1982) of their source in order to minimize propagation effects. Solar Orbiter must therefore spend several solar rotations, sufficient to pass over several active regions, while within 0.4 AU.

Co-Rotation Requirement. The ability to achieve corotation is intimately linked, through orbital mechanics, with Solar Orbiter's perihelion distance. The main drivers for near-corotation are the need to observe solar features or source regions, while at the same time sampling in situ the solar wind and energetic particles emanating from them on time scales which are comparable to their growth and evolution. From Earth orbit, no region can be observed for more than 14 days, observations being further restricted by line-of-sight effects when the regions are near the solar limb. In order to determine the evolution of solar features, Solar Orbiter must travel sufficiently slowly above the solar surface to observe a feature within $\pm 30^\circ$ of the disk centre for at least ten days (this is twice as long as can be achieved from Earth orbit and is comparable to active region growth times). Furthermore, Solar Orbiter must also maintain an uninterrupted view of solar features for an entire solar rotation (around 27 days), which is comparable to the total lifetime of a small active region.

Latitude Requirement. The principal driver for attaining an out-of-ecliptic vantage point is to resolve outstanding questions about the dynamics of the solar dynamo and to measure directly the fast/slow solar wind boundary emanating from the edges of high latitude coronal holes. The inclination of the heliospheric current sheet (HCS) means that this boundary must be sampled at a range of latitudes, comparable to the HCS inclination, resulting in a requirement to measure from $\pm 15^\circ$ solar latitude within 0.5 AU. In order to accurately measure the polar magnetic field and its dynamics and meridional transport, at least five consecutive days of observations above 25° are required. As is clearly visible in **Figure 2.16**, the 25° solar latitude reached at the end of the nominal science mission is sufficient to perform those crucial measurements.

Comprehensive Characterization of the Inner Heliosphere. Many of Solar Orbiter's science objectives require a comprehensive characterization of the properties of the inner heliosphere at a level of sophistication never previously achieved. The only other mission to explore the inner heliosphere between 0.3 and 1 AU, Helios, had a payload limited in many ways (measurements, cadence) compared to modern instrumentation and lacked several critical elements such as remote-sensing (imaging and spectroscopy) observations and composition measurements. Helios was also restricted to measurements in the ecliptic plane. Solar Orbiter will make critical, previously unavailable measurements that are essential to fully characterize the inner heliosphere and relate these properties out to near-Earth measurements at 1 AU.

3.1.3 Summary of Requirements on the Solar Orbiter Spacecraft

The scientific measurement requirements detailed above place the following requirements on the spacecraft:

1. Solar Orbiter must be a three-axis stabilized spacecraft with a pointing accuracy sufficient to achieve the scientific objectives
2. Solar Orbiter must satisfy electromagnetic cleanliness such that the magnetometer and radio and plasma waves instruments can accurately measure relevant physical parameters.

- For each operational orbit, the Solar Orbiter spacecraft must allow full operations of the complete payload for a minimum of three continuous periods of 10 days each.

3.2 Selected Payload Summary

The Solar Orbiter payload was selected from proposals submitted in response to the ESA AO for the Solar Orbiter Payload (released on 18 October 2007) and to the NASA SMEX/FOSO AO (released on 22 October 2007). Following a review of the 14 proposals submitted to ESA, the PRC issued a final report on 24 May 2008 recommending a payload for selection. ESA subsequently called for an independent review of the PRC's recommended payload in the context of a joint scientific programme with NASA's high-priority Solar Probe Plus mission.² The joint ESA-NASA review panel confirmed the validity of the recommended payload in its report of March 2009. As a result, the instrument selections as recommended by the PRC in 2008 were formally announced on 20 March 2009 (selection to be confirmed after mission approval). In parallel, NASA announced the results of the FOSO selection, and selected 2 instruments and portions of 2 instruments to be included in the Solar Orbiter payload.

The selected payload is described in the sections that follow, and **Figure 3.1** illustrates the accommodation of the instruments on the spacecraft. An overview of the payload is shown in **Table 3.6**, and a summary of the payload resource requirements is shown in **Table 3.7**. The available payload resource envelope is 180 kg of mass and 180 W of power, and includes resources for several payload support elements. A summary of the overall payload resources can be found in **Table 3.8**. Complete, detailed information about the selected payload can be found in the individual EID-Bs for each instrument.

3.2.1 In-Situ Instruments

Solar Wind Analyzer (SWA). The Solar Wind Analyser (SWA) instrument suite (**Figure 3.2**) comprises 3 sensors and a shared data processing unit (DPU), and will completely characterize the solar wind between 0.23–1.4 AU. The overarching objective of SWA is to provide comprehensive in-situ measurements of the solar wind to establish the fundamental physical links between the Sun's highly dynamic magnetized atmosphere and the solar wind in all its quiet and disturbed states. These measurements are vital to Solar Orbiter

² The PRC's original payload recommendation was made in the context of the HELEX programme, a joint ESA-NASA programme involving both Solar Orbiter and the NASA Sentinels mission. During the course of 2008, however, NASA assigned higher priority to a re-designed Solar Probe mission, Solar Probe Plus, which is planned to be operating at the same time as Solar Orbiter and whose science objectives are strongly synergistic with those of Solar Orbiter (cf. Section 3.4.1).

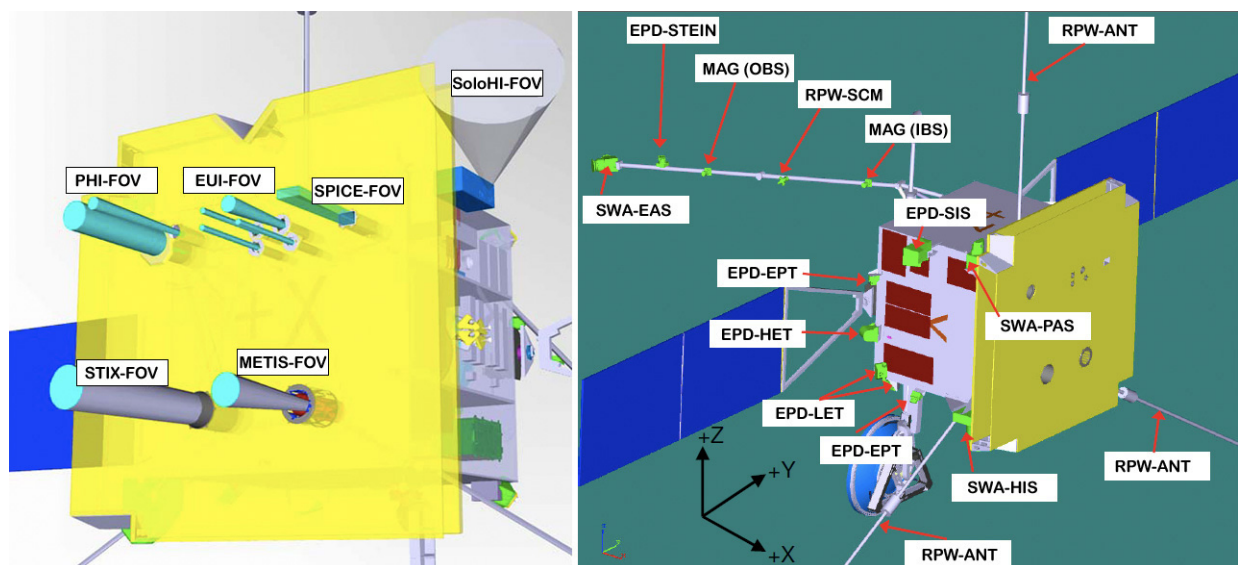


Figure 3.1. Drawings illustrating the accommodation of Solar Orbiter's remote-sensing instruments (left) and in-situ instruments (right).

Table 3.6 Overview of the selected Solar Orbiter payload.

Investigation	Principal Investigator	Collaborating countries	Measurement	Technique
Solar Wind Analyzer (SWA)	C. Owen, MSSL, UK	UK, I, F, Japan, D, CH, USA	Solar wind ion and electron bulk properties, ion composition (1 eV- 5 keV electrons; 0.2 - 100 keV/q ions)	Multiple sensors (electrons, proton/alpha, heavy ions); electrostatic deflection, time-of-flight measurement, solid state detectors
Energetic Particle Detector (EPD)	J. Rodriguez-Pacheco, Univ. of Alcalá, E	E, D, FI, GR, CH, F, Slovakia, USA	Composition, timing, and distribution functions of suprathermal and energetic particles (8 keV/n - 200 MeV/n ions; 20-700 keV electrons)	Multiple solid-state dE/dx vs E detector telescopes, time-of-flight measurement
Magnetometer (MAG)	T. Horbury, ICSTM, London, UK	UK, A, I, H, D, F, E, DK, USA	DC vector magnetic fields (0 - 64 Hz)	Dual fluxgate sensors
Radio & Plasma Waves (RPW)	M. Maksimovic, Obs de Meudon, Paris, F	F, SE, CZ, NO, UK, A, D, GR, AU, I, H, FI, Russia, USA	AC electric and magnetic fields (~DC - 20 MHz)	Electric antennas, Search Coil Magnetometer; Low-frequency and Thermal Noise/High-frequency receivers, Time-domain sampling
Polarimetric and Helioseismic Imager (PHI)	S. Solanki, MPS, Lindau, D	D, E, F, SE, NO, CH, AU, USA	Vector magnetic field and line-of-sight velocity in the photosphere	High-resolution telescope: off-axis Ritchey-Chrétien, Full-disk telescope: refractor, Fabry-Perot filtergraph
EUV Imager (EUI)	P. Rochus, CSL, Liege, B	B, UK, F, D, USA	Full-disk EUV and high-resolution EUV and Lyman- α imaging of the solar atmosphere	Full-Sun Imager: dual-band EUV off-axis Herschelian, 2 High-res.. Imagers: dual-band EUV + Ly- α off-axis Ritchey-Chrétien
Spectral Imaging of the Coronal Environment (SPICE)	D. Hassler, SwRI, Boulder, USA	USA, UK, D, F, N	EUV spectroscopy of the solar disk and corona	Off-axis paraboloid telescope, TVLS grating spectrograph
X-ray Spectrometer Telescope (STIX)	A. Benz, ETH Zürich, CH	CH, PL, D, CZ, IRE, A, UK, F, USA	Solar thermal and non-thermal x-ray emission (4 - 150 keV)	Fourier transform imaging, CZT detectors
Coronagraph (METIS/COR)	E. Antonucci, Univ. of Turin, I	I, UK, F, D, GR, USA	Visible, UV and EUV imaging of the solar corona	Externally-occulted coronagraph
Heliospheric Imager (SolOHI)	R. Howard, NRL, Washington DC, USA	USA	White-light imaging of the extended corona	Wide-angle lens with aperture stop

Table 3.7 *Solar Orbiter selected payload resource summary:*

Investigation	Total Mass (kg)	Margin (%)	Power (W)	Margin (%)	Dimensions	Telemetry (kbps)	FOV	Heritage
Solar Wind Analyzer (SWA)	15.9	15.0	14.2	~15	EAS: 11.6 cm x dia. 13.6 cm PAS: 30 x 20 x 20 cm HIS: 31 x 28 x 25 cm	14	EAS: 360° x ±45° x 2 orthogonal sensors to provide 4- π ster FOV PAS: -17.5° to +47.5° Azimuth-22.5° to +22.5° Elevation HIS: -33° to +63° Azimuth -17° to +17° Elevation	Ulysses, ACE, STEREO
Energetic Particle Detector (EPD)	13.8	15.0	16.1	20.0	EPT1,2: 11 x 7 x 12 cm SIS1,2: 35 x 13 x 11 cm LET1,2: 22 x 15 x 11 cm HET: 13.6 x 17 x 16.2 cm STEIN: 10 x 13 x 13 cm CDPU/LVPS: 15 x 15 x 10 cm	3.1	EPT 1,2: 30° cones SIS: 22° cone (2x) LET1,2: 40° cone (3x) HET: 50° cone (x2) STEIN: 60° x 70° (2x)	STEREO, SOHO, ACE
Magnetometer (MAG)	2.1	10.0	1.9	25.0	Fluxgate sensor (2x): 9.75 x 4.9 x 6.7 cm Electronics: 15.9 x 16.2 x 9.8 cm	0.9 (normal) 6.8 (burst mode)	N/A	VEX, Themis, Rosette Lander, Double Star
Radio & Plasma Waves (RPW)	13.6	15.0	11.5	20.0	Antenna (3x): 650 cm long SCM: 13.6 x dia. 10.4 cm Electronics: 24 x 21 x 15 cm	5	N/A	STEREO
Polarimetric and Helioseismic Imager (PHI)	29.1	25.0	31.0	25.0	Optical unit: 79.5 x 40 x 29 cm Electronics: 20 x 40 x 29 cm	20	HRT: 16.8 x 16.8 arcmin FDT: 2.6° cone	SUNRISE/IMaX
EUV Imager (EUI)	18.1	20.0	24	25.0	Optical bench: 83 x 54.5 x 22.8 cm Electronics: 120x300x250 mm	20	FSI: 5.2 x 5.2 arcdeg HRI: 1000 x 1000 arcsec	SOHO, STEREO, TRACE, PROBA2
Spectral Imaging of Coronal Environment (SPICE)	18.4	18.0	28.8	25.0	Optical bench: 91.1 x 34.9 x 17.7 cm Electronics: 20 x 18.6 x 12.4 cm	17	1 arcsec x 17 arcmin slit	SOHO, SUMER, CDS, HINODE
X-ray Spectrometer Telescope (STIX)	4.4	10.0	4.4	10.0	Imager Module: 55 x dia. 18 cm Spectrometer: 18 x 20 x 22 cm Electronics: 16 x 20 x 22 cm	0.2	2.5° for spectroscopy 1.5° for imaging	RHESSI
Coronagraph (METIS/COR)	20.6	25.0	26.0	25.0	Optical Bench: 90 x 44 x 25 cm Electronics: 22 x 25 x 10 cm	10	1.3°-3° annular, off-limb corona	SCORE/ HERSCHEL
Heliospheric Imager (SoloHI)	11.2	20.0	10.0	10.0	Optical unit: 425x140x180 mm Electronics: 100x100x50 mm	20	40° x 40°, offset 5° from Sun centre	STEREO

Table 3.8 Overall payload resource summary.

Payload Element	Total Mass (kg)	Power (W)
In-Situ Instruments	45.3	43.7
Remote Sensing Instruments	101.9	124.2
Payload Support Elements		
Instrument Doors	14	4
PHI Filters	3.6	
Instrument Boom	9.9	
Margin	5	5
TOTAL	179.7	176.8

key properties for all ions: mass in the range 2–56 amu/q, charge (q), energy in the range 0.5–100 keV/q (for azimuth) and 0.5–16 keV/q (for elevation), $\Delta E/E \sim 6\%$ and direction of incidence (θ , ϕ) with $6^\circ \times 6^\circ$ pixel resolution. The time resolution for 3D distribution measurements is 5 minutes for a full scan in normal mode and 30 s for heavy ions or 3 s for alphas in burst mode.

The HIS and PAS sensors require fields of view containing the Sun-direction and therefore require apertures in the spacecraft heat shield or (preferably) mounting at the edge of the heat shield in such a way that they can protrude beyond its edge.

The SWA plasma sensors are integrated into a suite, and serviced by a common DPU, which provides a single power, telemetry, and control interface to the spacecraft as well as power, switching, commanding, data handling and data compression functions for all of the sensors (see electrical block diagram, **Figure 3.2 bottom panel**).

Energetic Particle Detector (EPD). The Energetic Particle Detector (EPD) experiment will measure the composition, timing, and distribution functions of suprathermal and energetic particles. Scientific topics to be addressed include the sources, acceleration mechanisms, and transport processes of solar energetic particles; magnetic connectivity through the use of suprathermal particles as field-line tracers; the radial dependence of CME-driven shocks and associated particle populations. EPD covers the energy range from just above the solar wind (a few keV/n) to relativistic electrons and high-energy ions (100 MeV/n protons, 200 MeV/n heavy ions). The overall energy coverage achieved with the EPD sensors is 0.002 MeV to 20 MeV for electrons, 0.003 MeV to 100 MeV for protons, 0.008 MeV/n to 200 MeV/n for heavy ions (species-dependent).

EPD consists of 5 separate sensors sharing a common data processing unit and low voltage power supply (CDPU/LVPS). Each sensor has specific measurement tasks to cover the required range of particles and energies. Multiple sensor heads at different locations on the spacecraft and/or multiple view directions relative to the magnetic field direction are required for measuring pitch angle distributions of particles. The sensors apply solid state charged particle detectors of various types, electrostatic deflection and time-of-flight systems, microchannel plates, thin foils, and magnets. The sensors and their measured particle species and energies are:

a) The SupraThermal Electrons Ions and Neutrals Telescope (STEIN). STEIN is a double-ended telescope, utilizing passively cooled silicon semiconductor detectors (SSDs) to measure suprathermal particles from ~ 3 –100 keV. STEIN utilizes an electrostatic deflection system to separate electrons and ions up to ~ 40 keV, and neutrals up to ~ 10 keV. STEIN is mounted on the magnetometer boom, with back-to-back $70^\circ \times 60^\circ$ fields of view covering both directions along the Parker spiral.

b) The Electron Proton Telescope (EPT). EPT (see **Figure 3.3 upper left**) measures electrons (20 keV to 700 keV) and protons (20 keV to 9 MeV) as well as their anisotropies. It consists of two dual double-ended telescopes. EPT1 points in the ecliptic plane along the Parker spiral in both the solar and anti-solar directions; EPT2 points 45° out of the ecliptic plane. The fields of view may be adjusted during the definition phase in the event of accommodation issues. EPT combines the dE/dx -E method with the magnet/foil technique in order to separate electrons from protons and heavier ions, and has extensive heritage from the successful instruments STEREO/SEPT and SOHO/EPHIN.

c) The Suprathermal Ion Spectrograph (SIS). SIS measures the composition of heavy ions (He–Fe) over the energy range ~ 8 keV/n–10 MeV/n. Ultra-heavy ions in ^3He -rich solar flare events will also be measured

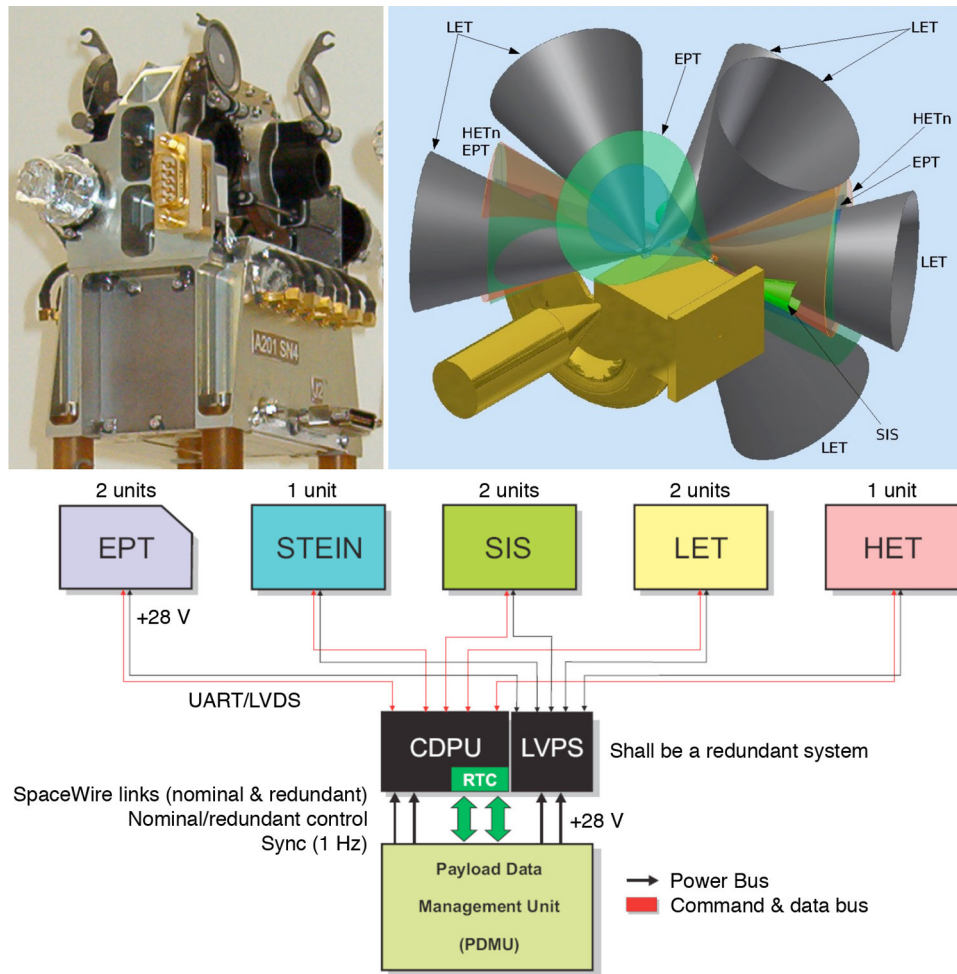


Figure 3.3. Solar Orbiter's Energetic Particle Detector. Upper left: the Electron Proton Telescope; upper right: the fields-of-view for each of the EPD sensors; bottom: EPD block diagram.

over a limited energy range below 1 MeV/n. SIS has two telescopes, each with 22° FOV pointing in the sunward and anti-sunward hemispheres and each with large ($>12 \text{ cm}^2$) detector areas required to characterize the previously unexplored ambient suprathermal ion pool in the inner heliosphere. SIS's high mass resolution ($m/\delta m \sim 50$) will allow detection of trace amounts of ^3He , and detailed abundant determination of multiple heavy ion species over the range He-Fe. SIS heritage is from the ACE/ULEIS instrument.

d) The Low Energy Telescope (LET). LET measures the species H-Ni over the energy range $\sim 1.5\text{--}60$ MeV/n. LET telescopes each have a 40° full angle FOV for high resolution of the different species, with 6 FOVs both in-ecliptic and out-of-ecliptic to provide particle anisotropies. LET covers the energy range where SEP energy spectral indices steepen ('break'). It can resolve ^3He and multiple heavy ion species in order to identify particle sources as well as the dependence of particle charge to mass ratio on the acceleration and transport processes. LET heritage is from SOHO/ERNE.

e) The High Energy Telescope (HET). HET covers the high-energy particle range for protons (up to 100 MeV) and heavier ions (200 MeV/nuc for O and heavier species), thus providing information on the largest SEP events, which can produce high energy, damaging interplanetary radiation levels. HET has two oppositely directed FOVs with 50° full angle and resolves ^3He and multiple heavy ion species. HET's large collecting power allows fast cadence for high-energy heavy ions. During the study phase, the possibility of obtaining limited information on the neutron flux intensity from HET will be investigated.

The FOVs of each of the EPD sensors is shown in **Figure 3.3 (upper right)**. An electrical block diagram showing the 5 separate EPD sensors, common data processing unit and low voltage power supply (CDPU/LVPS) is shown in the bottom panel of **Figure 3.3**.

Magnetometer (MAG). The magnetometer (MAG) experiment (**Figure 3.4**) will provide in-situ

measurements of the heliospheric magnetic field with high precision. In addition to studies of the near-Sun heliospheric plasma and fields, MAG will address how the magnetic field links into space and evolves over the solar cycle; how waves and turbulence are generated and dissipated, and how heliospheric structures develop in the inner solar system.

The magnetometer instrument comprises two digital fluxgate sensors operated in the dual-magnetometer mode (both in shadow and mounted on the instrument boom behind the spacecraft body) and an electronics box located inside the spacecraft structure. In-board to out-board sensor separation on the boom will be ~2 m. The fluxgate sensor design is highly suited to the Solar Orbiter mission, since it exhibits excellent stability, both with respect to time and changing temperature. A photograph of one of the sensors (cover removed) is shown in **Figure 3.4**. This sensor design has solid space heritage, having flown successfully on Cassini and Double Star. The dual-magnetometer technique allows background fields induced by the spacecraft to be subtracted from the true heliospheric magnetic field.

In addition to the fluxgate sensors with their own dedicated front-end electronics, the main functional elements of the instrument are an instrument controller unit (ICU) to control the instrument and manage communications with the spacecraft, and a power converter unit (PCU) for provision of secondary voltages to the sensor electronics, ICU and sensor heaters. The instrument block diagram is shown in **Figure 3.4 (left)**. The MAG instrument is largely autonomous in operation, requiring only a minimum of commanding for selecting from a set of science operations modes and corresponding telemetry bit-rates.

Preliminary thermal modelling shows that each sensor will require a 1-W heater (operated by the spacecraft) to maintain the sensors within the operating temperature range. The power of the required heaters will be confirmed once a boom design is selected and more detailed studies of the thermal environment have been completed.

Radio and Plasma Waves (RPW). The Radio and Plasma Waves (RPW) experiment (**Figure 3.5**) is unique amongst the Solar Orbiter instruments in that it makes both in-situ and remote-sensing measurements. RPW will measure magnetic and electric fields at high time resolution using a number of sensors/antennas, and it will determine the characteristics of electromagnetic and electrostatic waves in the solar wind from almost DC to 20 MHz. RPW has heritage from STEREO and BepiColombo Mercury Magnetospheric Orbiter (MMO) and consists of:

a) The Low Frequency Receiver (LFR). LFR covers both in-situ electric and magnetic measurements from DC to about 10 kHz and will provide both waveform and power spectra in this frequency range. High-level processed data (polarization and propagation properties of the observed waves), with various data rate possibilities (continuous or cyclic transmission, adaptable frequency bandwidth, as well as adaptable frequency and time resolutions) will also be provided by LFR.

b) The Thermal Noise and High Frequency receiver (TNR-HFR). TNR-HFR will determine properties

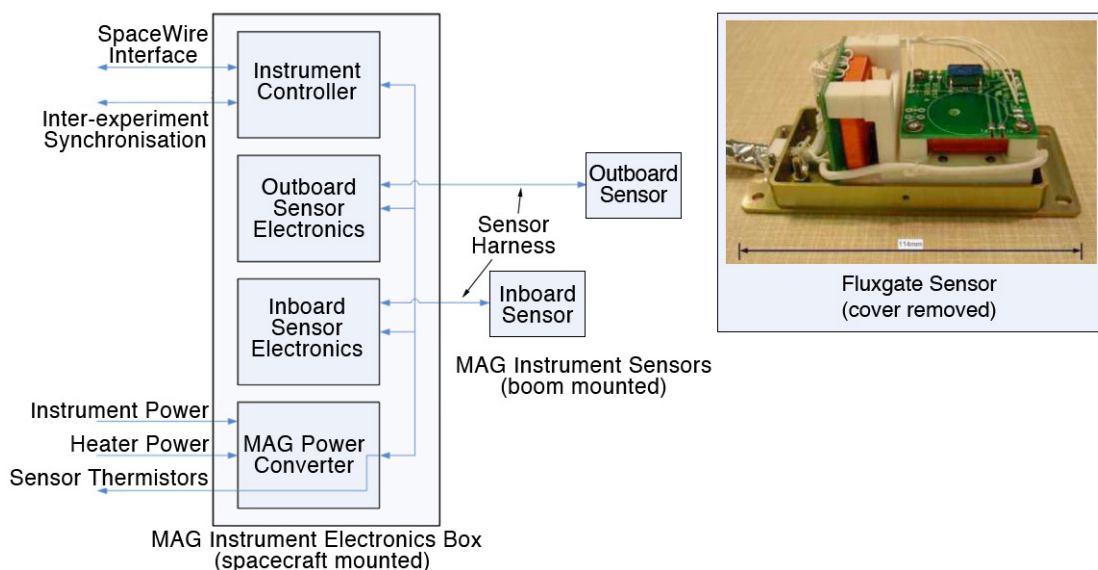


Figure 3.4. Solar Orbiter's Magnetometer. One of the sensors (with the cover removed) is shown on the right.

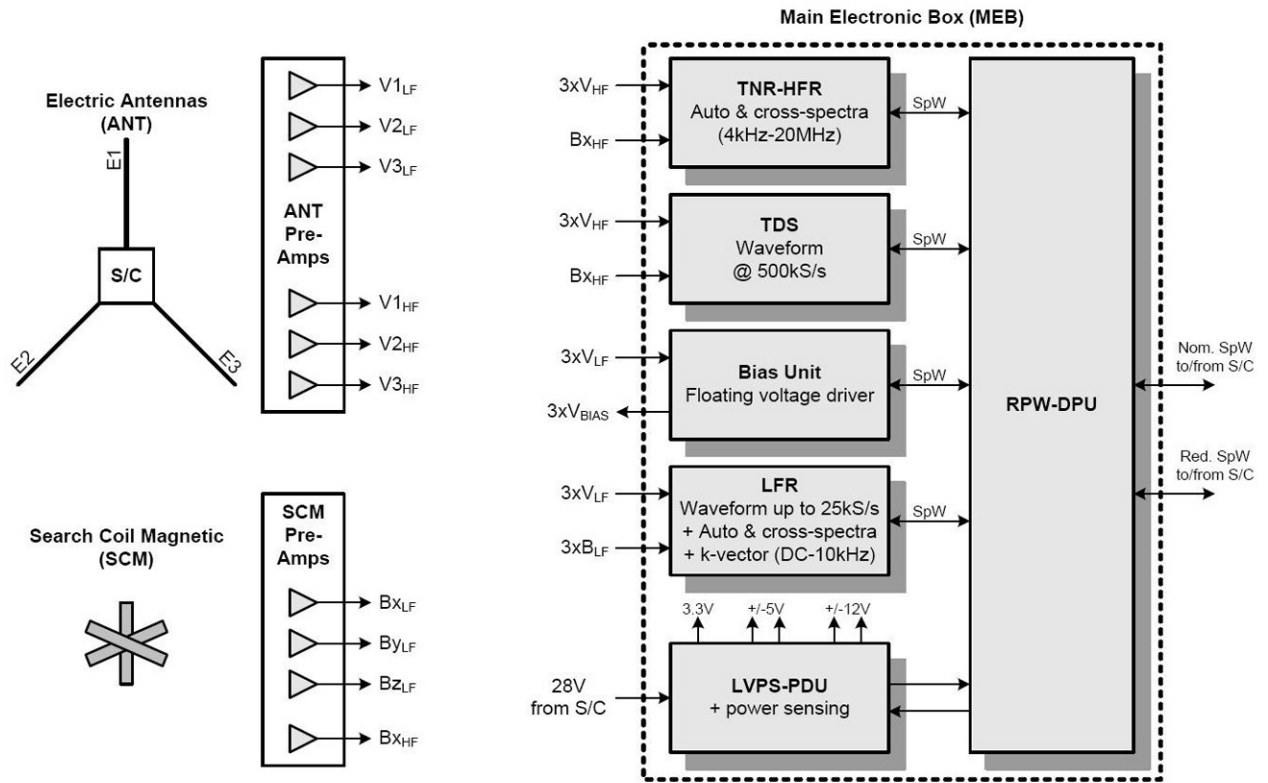


Figure 3.5. Block diagram of Solar Orbiter's Radio and Plasma Waves experiment. The placement of the antennas and the search coil magnetometer is illustrated in Figure 3.1 (right panel).

of the ambient electron population from measurements of the local thermal noise around the plasma frequency and remotely detect solar radio emissions. It will provide, at various temporal resolutions, electric power spectra from 4 kHz up to 20 MHz and magnetic power spectral densities from 4 kHz up to 500 kHz.

c) The Time Domain Sampler (TDS). TDS will perform digitization of the electric and magnetic field waveforms in the frequency range from 100 Hz to 250 kHz. These will be pre-processed and a selection of potentially interesting events will be stored in internal memory and later transmitted to the ground.

These three sub-systems (LFR, TNR-HFR, TDS) are connected to two different sensor units: a set of electric antennas (ANT) and a search coil magnetometer (SCM), both of which will be optimized to perform correctly for DC as well as high frequency measurements. The ANT sensor design is optimised to measure both DC/low frequency electric fields and higher frequency radio and thermal noise emissions. A biasing unit (BIAS, as described below) will allow DC electric measurements. ANT consists of a set of three identical antenna monopoles deployed from two corners and one side of the spacecraft (see **Figure 3.1, right panel**). After deployment, the three monopoles are 120° apart, in a plane perpendicular to the spacecraft-Sun axis. Each monopole consists of a rigid deployable boom and a deployable antenna sensor. The rigid deployable boom provides a larger spacing of the antenna sensor from the spacecraft and ensures that the antenna sensor will be fully illuminated and therefore well coupled to the local plasma potential through a photoelectron sheath. This is required for good DC/LF measurements.

The BIAS will drive a constant current to the electric antennas allowing reliable DC/LF electric field and satellite potential measurements by minimizing the impedance in the coupling to the plasma.

The SCM is an inductive magnetic sensor consisting of a core of a high permeability material (ferrite or permalloy) around which a main coil with several thousand turns and a secondary coil with a few turns are wound. The SCM is located on the instrument boom.

These subsystems have a common DPU that handles commands, data and communication with the spacecraft. Together with an LVPS, the four sub-systems will be integrated in a main electronic box (MEB) that will be located inside the spacecraft (**Figure 3.5**).

3.2.2 Remote-Sensing Instruments

Polarimetric and Helioseismic Imager (PHI). PHI will provide high-resolution and full-disk measurements of the photospheric vector magnetic field and line-of-sight (LOS) velocity, as well as the continuum intensity in the visible wavelength range at a cadence of one set of observables per minute. The LOS velocity maps will have the accuracy and stability to allow detailed helioseismic investigations of the solar interior, in particular of the solar convection zone.

The PHI instrument consists of two telescopes (**Figure 3.6**), a High Resolution Telescope (HRT) that will image a fraction of the solar disk at a resolution reaching ~ 150 km at perihelion, and a Full Disk Telescope (FDT) to image the full solar disk at all phases of the orbit. PHI will carry out measurements with a narrow-band filtergraph at several wavelength positions in a Zeeman-sensitive photospheric spectral line, and in the nearby continuum. At each spectral position, the polarization state of the incoming light will be analyzed. From the observables (the four Stokes parameters that fully describe an electromagnetic wave), a number of solar physical quantities will be retrieved: the LOS flow velocity (v_{LOS}) and the three components of the vector magnetic field (field strength, inclination, and azimuth). From these quantities, the LOS component and the transverse component of the magnetic field vector (B_{LOS} and B_{Trans}) can be derived. Together with the continuum intensity I_c (a proxy for the plasma temperature, which also provides the image context for the other variables), spatial maps of these variables constitute the main data products of the instrument.

The off-axis Ritchey-Chrétien HRT will image a fraction of the solar disk at a resolution reaching ~ 150 km at minimum perihelion distance (0.23 AU). The FDT provides a FOV of 2.6° with a pixel size of ~ 730 km (at 0.23 AU), giving a complete view of the solar disk during all orbital phases. An off-pointing mechanism allows the FDT to continue observing the whole solar disk while the spacecraft, including the HRT, is pointing off the solar disk centre. Continuous observations of the full solar disk by the FDT are needed to allow precise sensing of the solar limb and provide stable pointing. PHI will have its own image stabilization system (ISS) that compensates spacecraft jitter and other disturbances. This system is composed of a limb sensor and separate rapid tip-tilt mirrors for the FDT and the HRT.

In order to limit the amount of light entering the instrument, two entrance windows, one for each telescope, are mounted on the spacecraft's heat shield. These windows act as heat rejection filters with a transmission band of about 30nm width centred on the science wavelength, such that the total transmittance does not exceed 4% of the total incident energy. The feasibility of such a filter has been demonstrated during the ESA Technology Development Activity (TDA) [SO-OP-01].

Each telescope has its own polarization modulation package (PMP), located early in the optical path to minimize polarisation cross-talk effects. Each PMP consists of two liquid crystal variable retarders (LCVRs) followed by a linear polarizer. Spectral analysis is performed by a Fabry Perot filtergraph system (FG) consisting

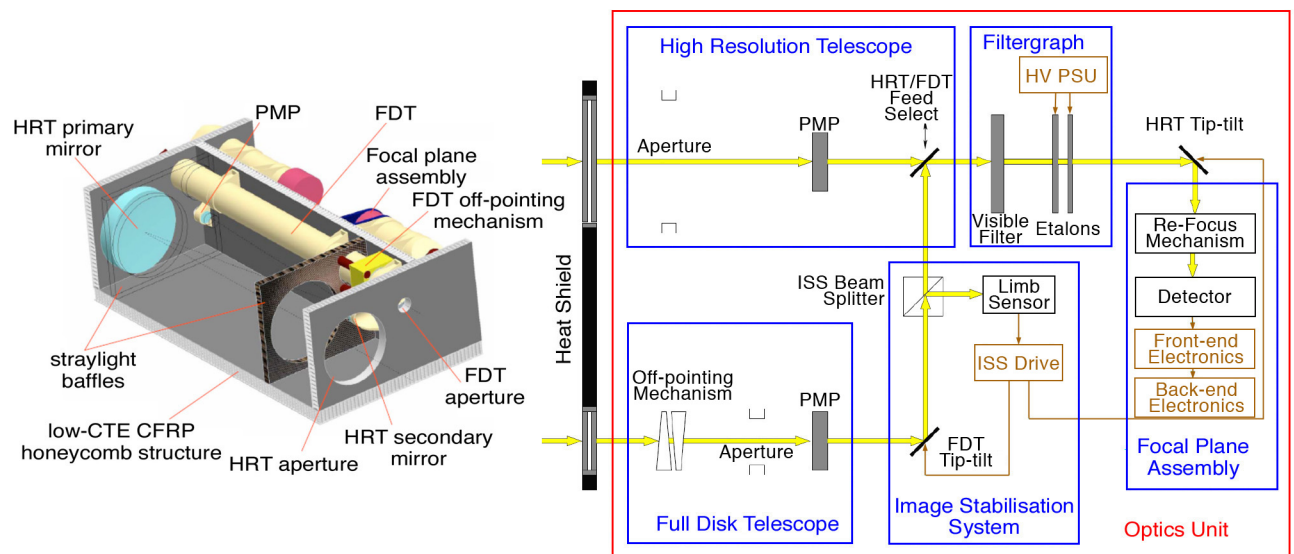


Figure 3.6. Left: 3D view of Solar Orbiter's Polarimetric and Helioseismic Imager, showing the High Resolution and Full Disk telescopes. Right: PHI block diagram.

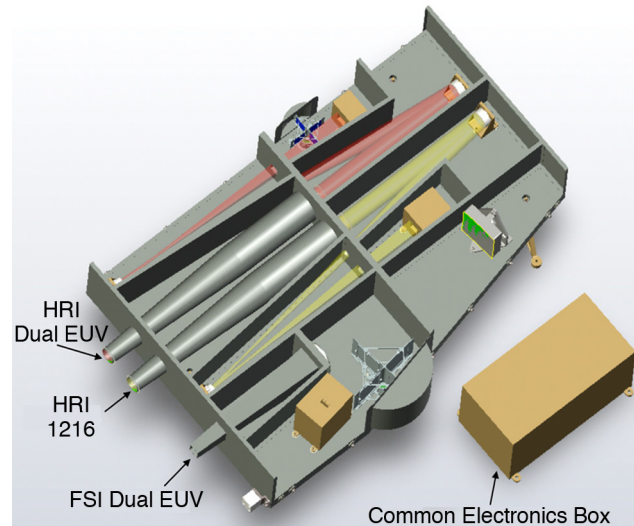


Figure 3.7. 3D cutaway view of the Extreme Ultraviolet Imager. EUI comprises three imagers, two high-resolution imagers (HRI) and a single full-disk imager (FSI).

of two lithium niobate (LiNbO₃) etalons which extract a spectral portion of the FeI 6173 Å absorption line and at a nearby continuum point. The FG provides a tuning range of ± 0.6 Å, which is required for compensating the spacecraft radial velocity of ± 30 km/s plus the range required to scan the spectral line (~ 400 mÅ, depending on the observing mode).

A digital processing unit (DPU) performs image accumulation, pre-processing, and calculation of physical variables (Stokes inversion and data compression), and controls the instrument interfaces with the spacecraft. A functional block diagram of PHI is also shown in **Figure 3.6**.

Extreme Ultraviolet Imager (EUI). The Extreme Ultraviolet Imager EUI (**Figure 3.7**) will provide image sequences of the solar atmospheric layers above the photosphere, thereby providing an indispensable link between the solar surface and outer corona that ultimately shapes the characteristics of the interplanetary medium. Scientific topics to be addressed include monitoring the low atmosphere counterparts of large-scale solar eruptive events such as CMEs and the study of fine-scale processes in the solar atmosphere. EUI will also provide the first-ever images of the Sun from an out-of-ecliptic viewpoint (up to 34° of solar latitude during the extended mission phase). The EUI instrument suite is composed of two high resolution imagers (HRI), one at Lyman- α and one dual band in the extreme UV alternatively at 174 and 335 Å, and one dual band full-Sun imager (FSI) working alternatively at the 174 and 304 Å EUV passbands, in addition to a common electronics

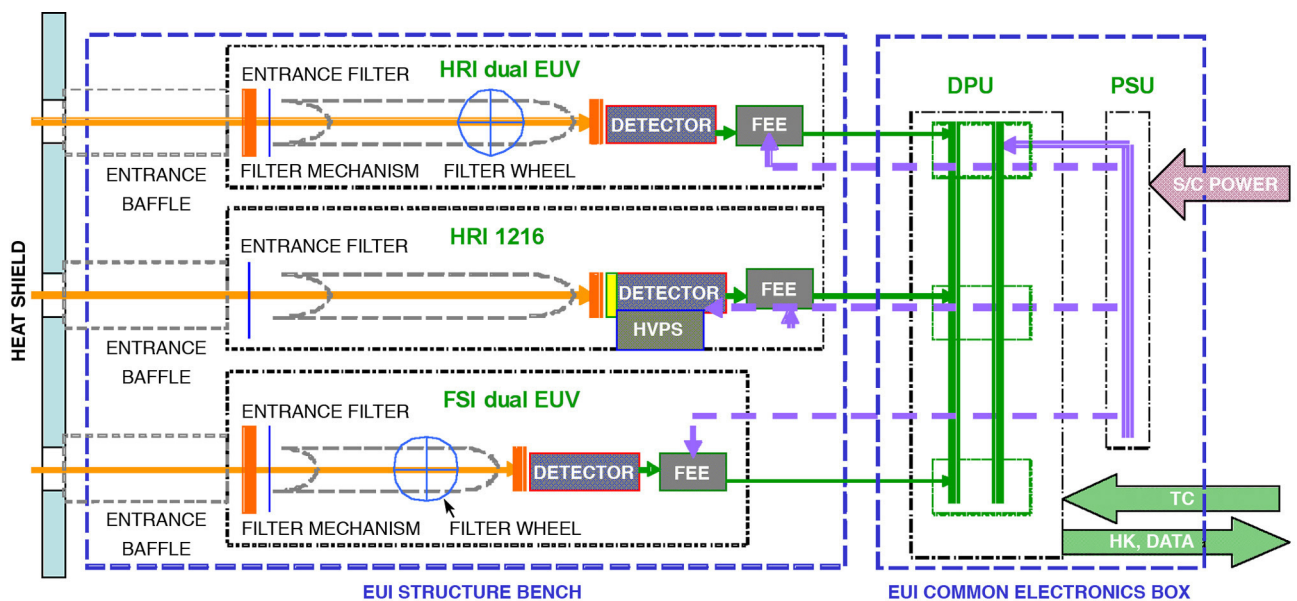


Figure 3.8. EUI functional block diagram.

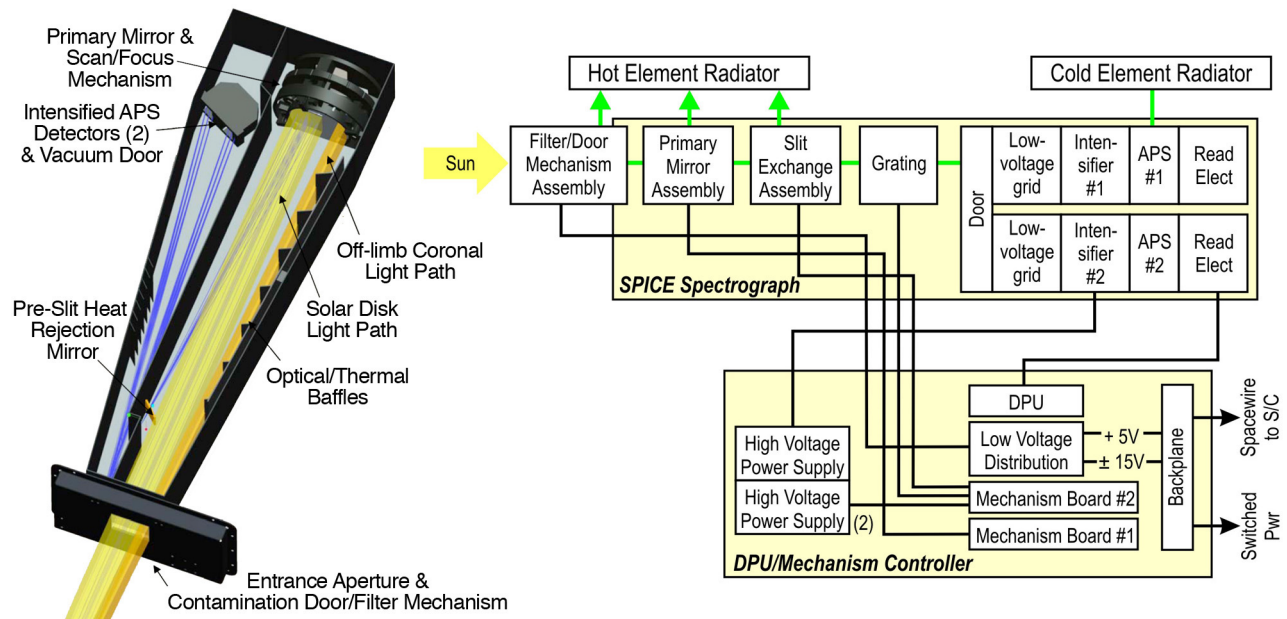


Figure 3.9. The optical layout and functional block diagram of the SPICE instrument.

box containing the data processing unit and power supply as shown in **Figures 3.7** and **3.8**.

The technology for building the EUI instrument under the challenging constraints of the Solar Orbiter mission is at a high level of maturity and builds on heritage from past missions (SOHO/EIT, TRACE, STEREO SECCHI/EUVI, PROBA-2 SWAP). In the Solar Orbiter EUI units, the image is produced by a mirror-telescope, working in nearly normal incidence. The EUV reflectivity of the optical surfaces is obtained with specific EUV multilayered coatings, providing the spectral selection of the EUV units (2 HRI and 1 FSI). The spectral selection is complemented with filters rejecting the visible and IR radiation. The UV photons reach detectors (back-thinned active pixel sensor [APS] detectors of 2k x 2k format for the HRI channels and 4k x 4k format for the FSI channel) where they are converted, amplified, and digitized by an A/D converter. For each detector pixel, the resulting signal in DN is proportional to the exposure time and to the solar flux corresponding to the small viewing angle of the pixel in the given band pass.

HRI and FSI have spatial resolutions of 1 arcsec and 9 arcsec, respectively. The temporal cadence of HRI depends on the target and can reach sub-second values to observe the fast dynamics of small-scale features. The FSI cadence will typically be of the order of 10 minutes in each passband, but can occasionally reach 10 s. Owing to its high-cadence imaging characteristics, EUI is capable of producing a much higher data volume than can be down-linked within the available telemetry. Two solutions will be implemented. First, state-of-the-art compression algorithms will be developed; a compression factor up to 50 will be carefully selected for each EUI passband so as to ensure that the compression algorithm does not compromise the targeted features. Second, fully autonomous onboard software will be created to perform an intelligent selection of the most interesting data (e.g., observations of an eruptive event) for transmission to the ground.

Spectral Imaging of the Coronal Environment (SPICE). The Spectral Imaging of the Coronal Environment (SPICE) instrument is an EUV imaging spectrograph designed to observe both on the solar disk and out in the corona to remotely characterize plasma properties at and near the Sun. Specific scientific topics to be addressed by SPICE include studies of solar wind origin by matching in-situ composition signatures in solar wind streams to surface feature composition; studies of the physical processes that inject material from closed structures into solar wind streams; studies of SEP source regions by imaging remotely the suprathermal ions thought to be seed populations of SEPs.

The SPICE instrument consists of a single element off-axis parabolic telescope and a toroidal variable line spaced (TVLS) grating spectrograph with two intensified active pixel sensor (IAPS) detectors. SPICE also includes a DPU to control each of the mechanisms, perform data compression and provide the SpaceWire interface to the spacecraft. The optical layout and functional block diagram of the SPICE are shown in **Figure 3.9**. The off-axis parabola mirror forms an image of the Sun onto the entrance slit assembly containing three interchangeable slits of differing widths. The slit selects a portion of the solar image and passes it to a concave

TVLS grating which re-images the spectrally dispersed radiation onto two array detectors. Beyond 0.35 AU, off-limb observations are made by inserting a quartz filter to reduce UV scattered light in the instrument and allow observations of the outer corona beyond $>0.30 R_{\odot}$. The two spectral passbands cover the same spatial field of view simultaneously with no scanning of the detectors or grating. The detectors are solar blind, IAPS sensors, and require no visible light rejection filters. The stigmatic spectra produced are magnified, yet maintain high spectral resolution in one dimension and high spatial resolution in the other. The SPICE observing strategy is to produce 2D spectro-heliograms (spectral images) of selected line profiles and line intensities only. The wavelengths covered by SPICE are 702-792 Å (Band 1), 972-1050 Å (Band 2) and 485-525 Å (2nd order). The selected lines represent the full range of temperatures and heights in the solar atmosphere, from the chromosphere to the flaring corona. SPICE derives heritage from SOHO/CDS, SOHO/SUMER, as well as the RAISE and EUNIS sounding rocket programs.

Spectrometer/Telescope for Imaging x-rays (STIX). The Spectrometer/Telescope for Imaging X-rays (STIX) (**Figure 3.10**) provides imaging spectroscopy of solar thermal and non-thermal x-ray emission from ~ 4 to 150 keV. STIX will provide quantitative information on the timing, location, intensity, and spectra of accelerated electrons as well as of high temperature thermal plasmas, mostly associated with flares and/or microflares.

STIX is based on a Fourier-transform imaging technique essentially identical to that used successfully by the Hard X-ray Telescope (HXT) on the Japanese Yohkoh mission, and very similar to that used for RHESSI. As shown in the figure, the STIX instrument comprises three mechanically-decoupled modules:

a) The Sun shades. The Sun shades required by STIX play two roles. First, they are a prime element of the thermal control system, limiting the incident optical and infrared solar flux seen by the instrument. Second, they preferentially absorb the intense flux of low energy x-rays produced during large flares that would otherwise contribute to pulse pile-up and life time issues for the detectors. The top sunshade has a central 5 mm diameter circular opening (transmitting 0.54 W at 0.23 AU) for use by the STIX aspect system, and the bottom shade has a corresponding 35 mm diameter opening.

b) The Imager. The STIX imager uses a set of 64 subcollimators, each of which consists of a pair of widely separated grids. X-ray transmission through the grid pairs is a very sensitive function of the direction of incidence, so that the relative count rates of the detectors behind the different subcollimators encode the spatial information. This can be subsequently decoded on the ground to reconstruct images of the source region at different x-ray energies. The grid parameters are chosen to provide imaging information in the form of spatial Fourier components of the source (visibilities) in analogy with the imaging information provided by

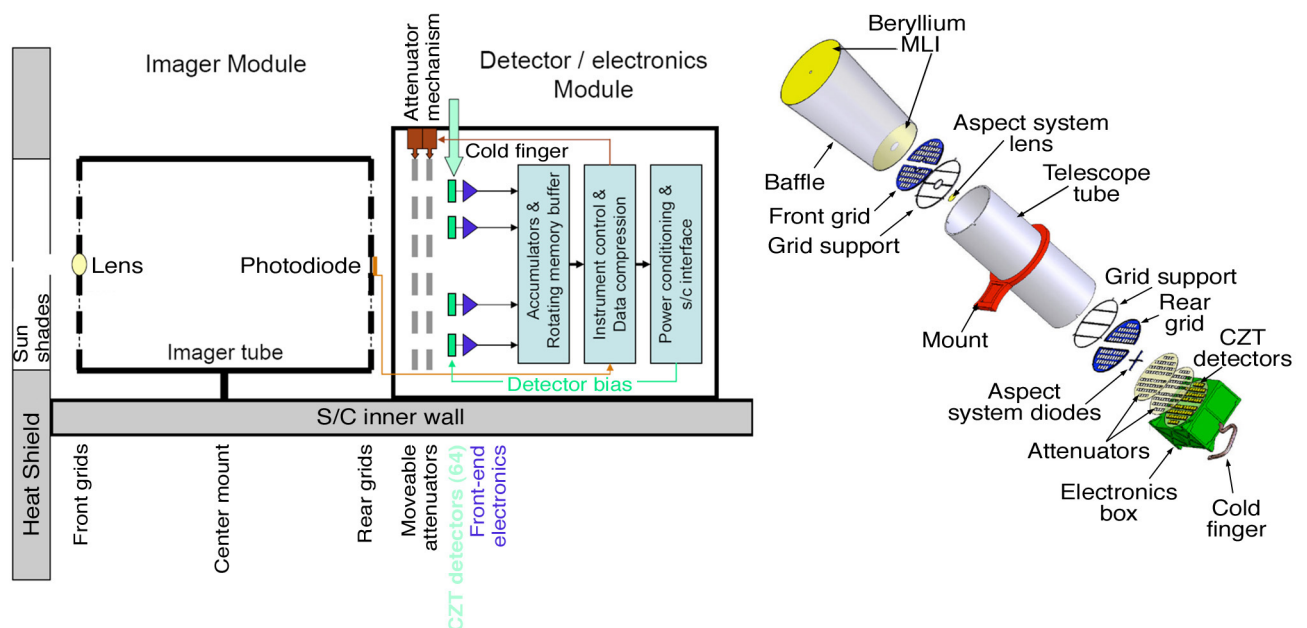


Figure 3.10. The Solar Orbiter Spectrometer Telescope for Imaging X-Rays. Left: STIX functional block diagram; Right: 3D exploded view of the instrument.

antenna pairs in a radio interferometer. The tungsten grids are fabricated with the same etch-and-stack process successfully used to make the finer RHESSI grids.

c) The Spectrometer. STIX uses 64 discrete Cadmium-Zinc-Telluride (CZT) planar detectors, one behind each subcollimator, to provide good energy resolution while operating at room temperature. CZT detectors have been flown in space, for example, on NASA's SWIFT mission where 32,768 such detectors are used. A cold finger is required to maintain detectors and electronics at 25° C or less. Moveable attenuators enable STIX to be responsive to the entire expected intensity range of x-ray flux. Such attenuators, based on temperature-sensitive shape memory alloy actuators, have proven to be effective and very reliable on RHESSI.

Telemetered STIX data corresponds to the rates of individual detectors. Data selection, time and energy binning are done on board, so that a telemetry rate of 0.2 kbps can transmit an average of ~2000 images per hour for image reconstruction on the ground. A flare flag with source location can be made available on board in real time.

Multi Element Telescope for Imaging and Spectroscopy (METIS/COR). The Multi Element Telescope for Imaging and Spectroscopy (METIS/COR) (**Figure 3.11**) will employ broad-band, polarized imaging of the visible K-corona and narrow-band imaging of the UV (HI Ly α , 121.6 nm) and EUV (He II Ly α , 30.4 nm) corona to study the structure and dynamics of the full corona with unprecedented temporal coverage and spatial resolution. METIS is an externally occulted coronagraph having an annular FOV between 1.2 and 3.0 R_s at a solar distance of 0.23 AU (1.8 to 5.3 R_s at a distance of 0.3 AU). This region of the corona is crucial in linking the solar atmospheric phenomena to their evolution in the inner heliosphere.

The unique capability of imaging the solar corona in three different wavelength bands by means of a single telescope is achieved by a combination of multilayer coatings of the mirrors, optimised to enhance reflectivity in the He II line, and spectral band-pass filters. Coronal light enters METIS through the external occulter aperture that provides occultation of the solar disk for both thermal protection and stray light rejection. An annular sector shaped Sun-disk rejection mirror reflects the light from the solar disk back through the front aperture. The hole in the heat rejection mirror is the aperture stop through which the coronal light enters the telescope. The telescope consists of aspherical primary and secondary mirrors in an off-axis Gregorian mount. A door that is part of the spacecraft heat shield closes the instrument when it is not operating to protect it and to reduce the thermal load on the spacecraft.

A filter wheel accommodates two filters: a narrow band interference filter (HF) optimized to transmit the HI 121.6 nm line and to reflect visible light, and an aluminium low pass filter (HeF) to block the wavelengths above the He II 30.4 nm line. With HF, the UV HI 121.6 nm corona and the VL K-corona are imaged simultaneously. With HeF, only the EUV He II 30.4 nm is imaged on the UV detector. The visible light channel includes a polarimeter assembly to observe the linearly polarized component of the K-corona. The polarimeter assembly uses a nematic liquid crystal variable retarder plates (LCVR) and a colour filter to select the spectral operation band. METIS has two detectors: one optimised for observations in visible light (450 – 650 nm), the other dedicated to UV (121.6 nm) and EUV(30.4 nm) detection. Both detectors have 20 μm pixels and an array size of 2048 \times 2048 pixels. An APS is baselined for the visible light detector, while the baseline for the UV detector

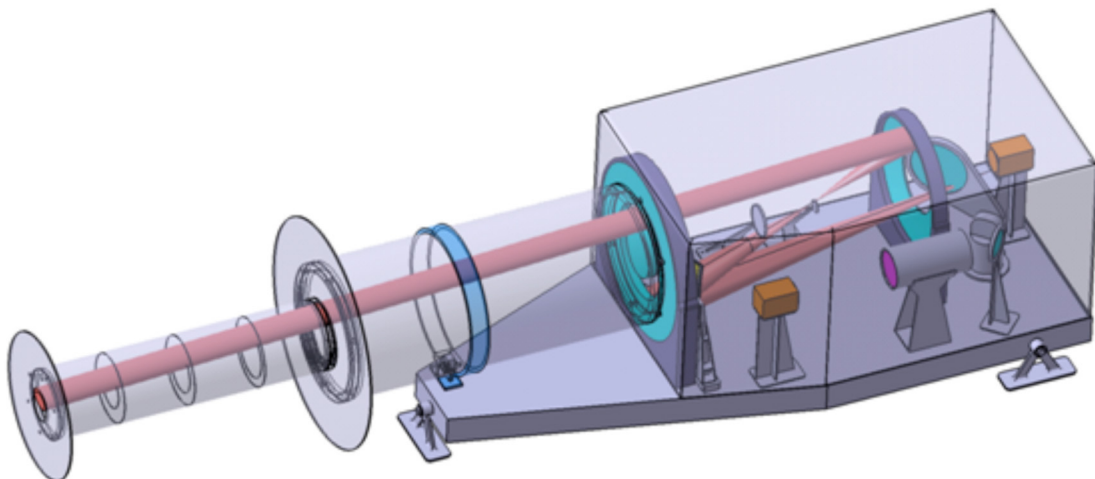


Figure 3.11. 3D view of the Multi Element Telescope for Imaging and Spectroscopy (METIS).

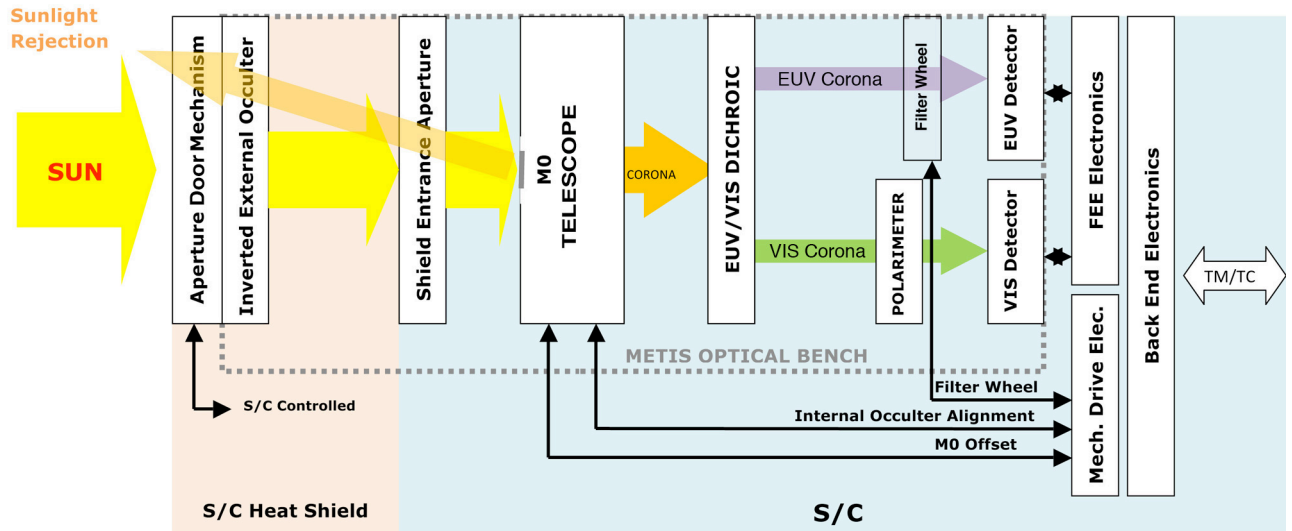


Figure 3.12. METIS functional block diagram.

is an IAPS. METIS derives heritage from the HERSCHEL/SCORE sounding rocket program. A functional diagram of METIS is shown in **Figure 3.12**.

Solar Orbiter Heliospheric Imager (SoloHI). The Solar Orbiter Heliospheric Imager (SoloHI) will image both the quasi-steady flow and transient disturbances in the solar wind over a wide field of view by observing visible sunlight scattered by solar wind electrons. The scientific questions to be addressed with SoloHI include the acceleration of SEPs by imaging CMEs and CME-driven shocks; the evolution of CMEs and CIRs in the inner heliosphere; the origin and evolution of solar wind by remotely measuring the structure and turbulence with solar wind streams; providing context for the other in-situ and remote-sensing instruments aboard Solar Orbiter.

The $40^\circ \times 40^\circ$ SoloHI field of view is centred on the ecliptic plane but is offset by 5° from the Sun centre and covers a range of elongation angles, thereby providing continuous synoptic images of the inner heliosphere with good spatial resolution. SoloHI (**Figure 3.13**) is an evolution of the design from the SECCHI/HI-1 instrument on the STEREO mission. It consists of two units: the SoloHI instrument module (SIM) and the SoloHI control electronics (SCE) (**Figure 3.14**). The SoloHI telescope consists of a wide-angle lens ($f = 59$ mm) of aperture 1.53 cm^2 . The SIM is located behind the heat shield, and a system of baffles provides the required rejection of incoming direct and scattered solar radiation. The average predicted stray light level is $< 5 \times 10^{-13} \text{ B/B}_{\text{sun}}$ at 0.88 AU and $< 4 \times 10^{-12} \text{ B/B}_{\text{sun}}$ at 0.23 AU . Other than the simple one-shot door, which provides protection

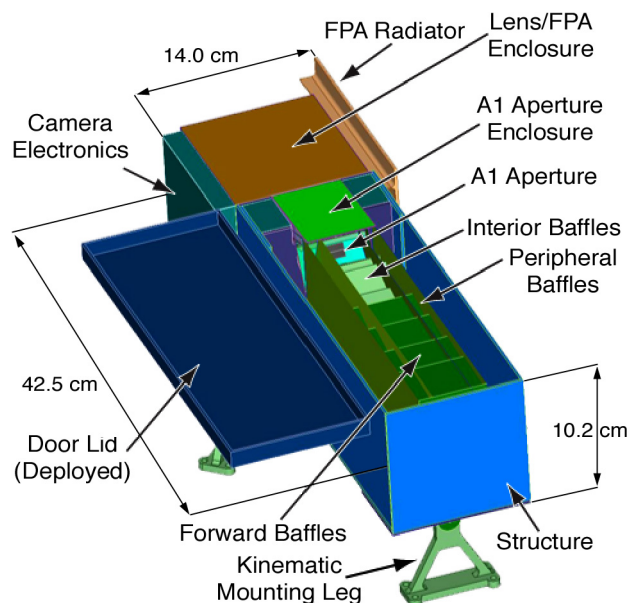


Figure 3.13. 3D view of Solar Orbiter Heliospheric Imager (SoloHI).

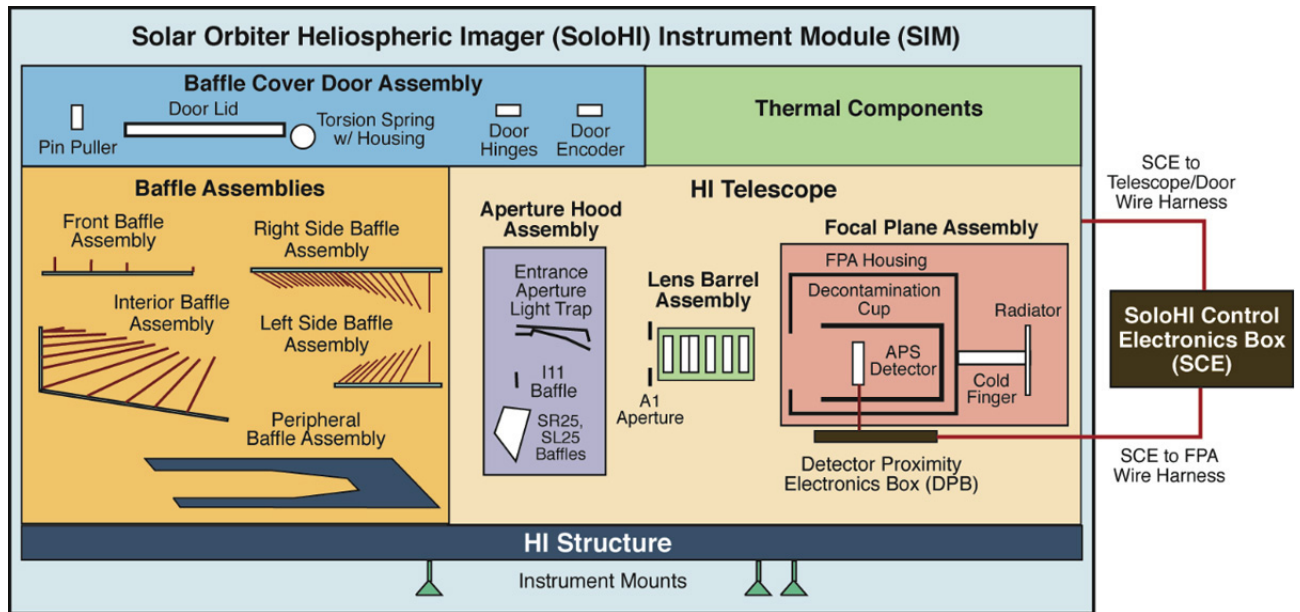


Figure 3.14. SoloHI functional block diagram.

against contamination during AIV and launch, there are no moving parts. The 40° field-of-view is imaged onto a customized APS that is cooled to -60°C to mitigate the effects of radiation damage. The SoloHI observing strategy is very flexible. The standard product will be synoptic images of the full field of view every 30 min. During perihelia SoloHI will obtain high cadence (~ 15 s) images of a subfield nearest the solar limb for solar wind turbulence studies while still providing synoptic images. Other modes (subfields, binned images) are possible depending on the objectives for the current observational window.

3.3 Science Operations Coordination and Science Planning

The science return of the Solar Orbiter mission will be maximized by coordinating operations and data taking among instruments. Every science objective described in Chapter 2 requires coordinated observations among several in-situ and remote-sensing instruments, and the strength of the Solar Orbiter mission stems from the synergy and comparative analysis of in-situ and remote-sensing observations.

The orbits of Solar Orbiter evolve significantly from one to the next (discussed in more detail in the Mission Implementation chapter), as do the designated encounter periods in which Solar Orbiter will be out of contact with Earth. Thus detailed planning by the science working team (SWT) and science operations centre (SOC) will be required for every science orbit. This endeavour will be very similar to what has been used highly successfully in the Joint Observation Programmes (JOPs) of ESA's SOHO mission. Below, we discuss two examples to illustrate how Solar Orbiter's science objectives can be met within the designed mission profile.

3.3.1 Data Rates, Telemetry, Inter-Instrument Communication & Burst Mode

Given the flexibility of the on-board SpaceWire bus, instruments can communicate with each other independently of the spacecraft CPU, making it possible for teams to coordinate operations without incurring additional workload for the spacecraft operations team.

Since the telemetry rates from Solar Orbiter, like those of many missions, are limited, the spacecraft will be equipped with a large (768 Gbit) mass memory that will store up to about two months of data at average rates, to allow for variable downlink speeds. However, the instruments are not limited to taking data at one rate and a number of coordinated and targeted data rate selection mechanisms will be implemented.

Burst Mode. Coordinated burst-mode data acquisition will enable detailed studies of the microphysics of the solar wind. Approximately 10% of the data return is expected to be in burst mode, with ~ 10 times the data rate of normal mode, corresponding to $\sim 1\%$ of the time. For instance, this mode will be used to study solar flares, which explosively release magnetic energy, driving shocks and accelerating particles. STIX will detect the flare's onset

and location and trigger high time resolution measurements by remote-sensing instruments to determine the properties of the flare site and its evolution, as well as measurements by RPW to measure radio emission from accelerated particles and by EPD to measure accelerated particles passing the spacecraft. The burst mode will also be used to study shocks crossing the spacecraft. They will be detected in the magnetic field and plasma and will trigger short burst mode measurements by Solar Orbiter's in-situ suites (MAG, RPW, SWA, and EPD) to quantify shock substructure and the motion and acceleration of particles nearby. Rolling buffers within the instruments will make it possible to store high-cadence data from upstream of the shock trigger time.

Small-scale kinetic processes will be measured using coordinated burst mode measurements of the magnetic and electric fields and particle distributions by Solar Orbiter's MAG, RPW and SWA. By sharing data on local plasma and field conditions, the instruments will trigger short burst mode intervals to ensure a wide coverage of different plasma regimes. In addition, some remote-sensing instruments will take high-cadence measurements of sub-fields of view. These can be planned based on known positions of active regions, but also in response to triggers based on emission levels of rapid changes in observed conditions.

Sharing of Magnetic Field Direction. Magnetic field directions can be shared among the in-situ instruments to produce reduced velocity distribution functions on board Solar Orbiter, thus greatly reducing the telemetry requirements. The local magnetic field direction is important to particle instruments in order to compute reduced data products such as temperature anisotropies or pitch-angle distributions. The Solar Orbiter magnetometer will transmit the measured magnetic field direction in real time to other instruments via the SpaceWire bus. The generation of high time resolution data and accurately reduced distribution functions requires precise timing knowledge between the contributing instruments, which will be achieved by synchronizing instrument clocks with the spacecraft via the SpaceWire bus. An accuracy of ~ 10 ms can be achieved and will be used to ensure synchronization of sampling between instruments. This accuracy is sufficient given the proton gyro-period of roughly half a second at $\sim 50 R_s$ (near perihelion).

3.3.2. Sample Science Orbits

As discussed in more detail in Chapter 4, certain subsections of every 150-day orbit are designated as part of the 'encounter period.' An encounter typically consists of a 10-day window centred around perihelion for high-resolution imaging studies and two 10-day windows centred around the highest latitudinal extents reached during that specific orbit or maximum co-rotation. In-situ instruments operate during the entire orbit whereas the remote-sensing instruments operate primarily during the 30 days within the encounter windows.

The first case to consider is a nominal orbit in which we have the lowest telemetry rate and which therefore places the most severe constraint on choosing what kind of data to acquire. Solar Orbiter has been designed around this 'worst' or nominal case in which in-situ instruments are assumed to be operating along the entire orbit and the remote-sensing instruments are operating for three 10-day periods during the encounter period at the data rates given in **Table 3.7**. Spacecraft memory has been sized to ensure that all data can be transmitted to Earth for this case. All science objectives of Solar Orbiter can be met in this nominal telemetry mode.

There will also be more favourable cases, based on celestial mechanics, where Solar Orbiter will have a higher than nominal telemetry rate. This will be used to increase the measurement opportunities in several ways, which will be determined by the SWT/SOC. For example, some remote-sensing instruments will acquire additional synoptic context images to support the key science goal of Solar Orbiter – how does the Sun create the heliosphere? In-situ instruments will increase the amount of data acquired at enhance cadence to study turbulence, capture fine structure of shocks and current sheets or event onset times. Helioseismological studies will benefit from an increased temporal baseline, and high-resolution studies of solar source regions will be able to extend outside the 10- or 30-day windows. In these orbits, as a baseline, the telemetry allocation of each instrument will be increased proportionally to the overall increase.

3.4. Supporting Observations

3.4.1. Space-Based Observations Supporting Solar Orbiter Science

Solar Probe Plus (status Fall 2009). The NASA Solar Probe Plus mission is highly complementary to Solar

Orbiter. Solar Probe Plus is a ~ 7 year mission to approach the Sun, planned to be launched in 2018 and reaching a $9.5 R_s \times 0.7$ AU orbit with an 88-day period resulting in many close passes to the Sun. Since its scientific payload contains primarily in situ instruments and a single Heliospheric Imager, the two missions can together address many questions in powerful new ways. **Figure 3.15** shows cases of particular interest, which occur about 15-20 times during nominal missions: The left panel shows the case of SPP and Solar Orbiter radially aligned. In this configuration the radial evolution of solar wind properties, including shock and turbulence properties, can be studied directly. The middle panel shows cases of alignment along a nominal IMF spiral, where energetic particles travelling past one of the two spacecraft will later move past the other, permitting direct tests of energetic particle transport and scattering since the source function is determined at one of the spacecraft and result is seen at the other. The right panel shows cases of quadrature alignment, where Solar Orbiter remotely observes plasma low in the corona that later passes by SPP, allowing tests of radial evolution of solar wind plasma, shocks, and other structures. When Solar Orbiter enters the high latitude phase of its mission, alignments with SPP will allow latitude gradient studies. Since both spacecraft's orbital motions are in the same direction, these alignment periods can range from a few days to over a month, depending on the radial distances at the time. Finally, there are many periods with Solar Orbiter, SPP, and Earth lie within a 30° or 60° wedge, which is ideal for studies of larger structures such as high speed streams, or large CME-driven interplanetary shocks.

Solar-C (status Fall 2009). JAXA's Solar-C is a next-generation Japanese solar physics satellite that is presently under study. Following the great success of Hinode, an international Solar-C Working Group is, together with JAXA, developing the mission concept of Solar-C. Many different Solar-C mission concepts have been discussed, and the most current one being considered for Solar-C is an L-5 mission with the Solar-C spacecraft being placed in a halo orbit around the Lagrangian L-5 position (in the ecliptic at 1 AU but either ahead or behind the Earth in heliospheric longitude). Certainly there will be synergies between Solar-C and Solar Orbiter that can be exploited once Solar-C becomes defined.

Other missions in the planning stage may contribute to heliophysical science and will be coordinated under the ILWS initiative.

3.4.2. Ground-Based Observations Supporting Solar Orbiter Science

Ground-based instruments in the visible and radio range will support Solar Orbiter observations. Spectropolarimetric on-disk observations in the visible and infrared will provide the photospheric magnetic field vector from a different viewing angle (with the Advanced Technology Solar Telescope (ATST) and the European Solar Telescope (EST)). Coronagraphic observations of the density and the magnetic field vector in the corona (with the Coronal Solar Magnetism Observatory (COSMO)) will be most valuable, especially during perihelia in quadrature and give plasma properties in the coronal region observed by Solar Orbiter from straight

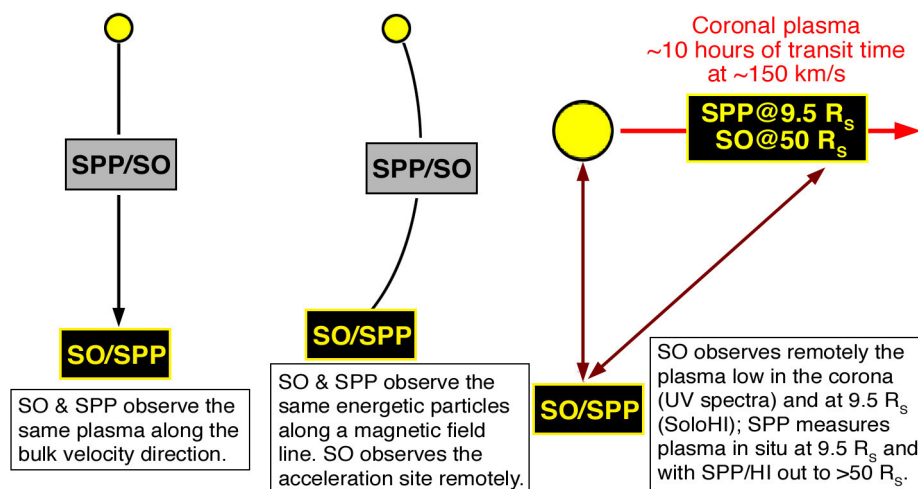


Figure 3.15. Solar Orbiter and Solar Probe Plus will provide multiple opportunities for coordinated observations from complementary vantage points.

above. Radio observations with the large arrays of LOFAR (Low Frequency Array) and ALMA (Atacama Large Millimeter Array) will allow high-resolution observations of the thermal and magnetic structure of the chromosphere and the corona. Availability of the Global Oscillation Network Group (GONG) or a similar successor will make it possible to carry out stereoscopic helioseismology for the first time, probing the deep interior of the Sun.

3.5. Theory, Modelling, and Scientific Closure

Underlying the science objectives of Solar Orbiter are some of the most important outstanding questions in solar and heliospheric physics, and more generally in plasma astrophysics, today. They are also some of the most challenging, namely the complex coupling of physical processes across multiple spatial and temporal scales. Microscopic physical processes lead to the formation of macroscopic solar wind streams; kinetic, small-scale processes combine with large-scale ones (e.g., to accelerate particles in shocks or compression regions); CME evolution is determined by its micro- and macroscopic interaction with the ambient corona and solar wind. The powerful high-resolution and high-cadence measurements during co-rotation will allow Solar Orbiter to discriminate between spatial and temporal variations and to correlate small-scale solar phenomena with larger ones both remotely and in-situ. Solar Orbiter's instrumentation and observational strategy are innovatively designed to tackle these problems, to understand the coupling from the global MHD scales of the Sun's corona to the local kinetic scales of wave and particle distributions in the heliosphere.

However, observations alone will not be sufficient. Theory and modelling will be key to provide the interpretive framework and also be required to elucidate the multi-scale connections among the coronal and heliospheric phenomena observed. Theory and modelling efforts are integral parts of the Solar Orbiter mission and each instrument team has equally talented scientists responsible for the theory and modelling aspects of their investigations.

Moreover, our understanding of both global and local processes has advanced considerably in recent years. Several large-scale programs are under way in Europe, the U.S., and world-wide to develop global MHD models that encompass the whole corona-heliosphere system. At the same time, there have been broad advances in theories for basic mechanisms such as particle acceleration and reconnection in collisionless plasmas. We expect that the theories and models will greatly increase in sophistication during the next five to ten years, and that Solar Orbiter will play a key role in testing and refining these powerful new models. For example, data-driven 3D MHD models of the initiation and development of solar wind streams and CMEs are now being developed and should be in a production state by the time Solar Orbiter delivers data. One of the crucial missing items for such models have been measurements of the photospheric field on the *entire* 4π steradian surface of the Sun, not just the one half which happens to face the Earth at any given time. Thus Solar Orbiter will not only provide fundamentally new and important missing data, but also provide a powerful tool to verify model predictions and provide quantitative information about the state of the heliosphere in a wide range of latitudes and heliocentric distances.

The first attempts of data assimilation in flux-transport models herald a new phase in the development of solar dynamo theory, from probing the fundamental principles to detailed models that embrace the potential for predictions. Observed data are fed as input into such models in order to tie them closely to the actual development of the solar conditions. Helioseismic measurements of sub-surface differential rotation and meridional flow, particularly at high latitudes, together with the detailed maps of the polar magnetic fields that will be obtained by Solar Orbiter, will supply the essential information required to perform critical tests of the central concepts for the flux-transport model and other approaches to understand the solar dynamo. On this basis, Solar Orbiter data will set the stage for quantitative and potentially predictive modeling of the solar cycle.

4.0 Mission Implementation: Mission Design and Operations

The Solar Orbiter mission has undergone extensive study over a period of 10 years, both internally in ESA and in industry, resulting in a mature, detailed design that satisfies the requirements placed on the mission by the science objectives and science implementation plan described in the two preceding chapters and that addresses the key risk areas. The following sections describe the current baseline mission, including the baseline mission profile and spacecraft design. These sections are followed by a description of the mission operations concept, including science operations and science management.

The key mission and spacecraft requirements that flow down from the science objectives and drive the mission and spacecraft design are:

Mission Requirements

- During the nominal operational lifetime, the Solar Orbiter operational orbit shall have the following parameters:
 - Minimum perihelion radius less than 0.25 AU
 - Inclination with respect to solar equator increasing to a minimum of 25° (with a goal of 35° in the extended operational phase).
- At minimum perihelion passage, the spacecraft shall maintain near co-rotation with the Sun's surface to < 6°/day averaged over 10 days.
- The Solar Orbiter system lifetime shall be compatible with a launch delay of 19 months (launch window locked to the next Venus gravitational assist opportunity).

Spacecraft Requirements

- The Solar Orbiter spacecraft shall be a 3-axis stabilized spacecraft using conventional chemical propulsion for orbit manoeuvres and attitude control;
- The Solar Orbiter Spacecraft shall be capable of accommodating the payload complement already selected in response to the ESA AO and NASA SMEX/FOSO;
- The Solar Orbiter spacecraft shall provide the payload with global resources of at least:
 - 180 kg of total payload mass (including payload support elements and system margin);
 - 180 W of total payload power (including system margin);
 - 100 kbps (kilobits per second) average generation rate for compressed scientific data (including 10% system margin).
- For each operational orbit, the Solar Orbiter spacecraft shall allow full operations of the complete payload complement for three continuous periods of 10 days each, with a maximum of 2 periods contiguous, centred on:
 - maximum northern heliolatitude;
 - maximum southern heliolatitude;
 - perihelion passage.
- The spacecraft shall support a data downlink of 150 kbps at a range of 1 AU with the New Norcia ground station based on standard ESA link budget calculations.

4.1 Baseline Mission Design

Two ballistic mission profiles satisfying the above requirements for launches in 2017 and 2018, respectively, have been studied and are described below. The mission profile for the 2017 launch provides the overall sizing parameters, exhibiting a maximum Sun distance of 1.48 AU and a minimum Sun distance of 0.23 AU, with mission duration of 9.6 years up to the end of the extended mission phase. Direct injection into the required operational orbit is beyond the performance of the available launch vehicles (see below) and the capabilities of the spacecraft. Raising the solar inclination angle (with respect to the Sun's equator) to the required value can be achieved, however, by repeated gravity assist manoeuvres (GAM) at Venus, where the relative arrival velocity

of the spacecraft with respect to Venus must be ~ 18 km/s. Direct injection into a trajectory from Earth to Venus, arriving at Venus with the required relative velocity, requires an escape velocity from the Earth greater than 10 km/s, which again is beyond the capabilities of the available launch vehicles. By using a sequence of GAMs with Venus and Earth and deep space manoeuvres (DSM) performed with chemical propulsion, it is possible to leave the Earth within the capabilities of the launch vehicle (velocity about 3.65 km/s) and arrive at Venus with the required high relative velocity. This solution yields a reasonable transfer phase duration of 3.4 to 4.1 years and a reasonable maximum distance to the Sun (although still a driver for the spacecraft design) of just less than 1.5 AU. The initial period of the operational orbit is selected to be resonant with the orbital period of Venus (224.7 days), so that a sequence of Venus GAMs will gradually increase the solar inclination angle of the operational orbit while maintaining the orbital period.

4.1.1 Launch and Launch Vehicle Selection

The Solar Orbiter Spacecraft is planned to be launched by a NASA-provided EELV from Kennedy Space Centre (KSC), USA. The Soyuz-ST 2-B/Fregat launcher from Kourou is currently the back-up launcher. The EELV (i.e., Atlas V and Delta IV) launch vehicles have a significantly greater capacity (both volumetric and mass) than the Soyuz launch vehicle. However, even though it is the backup launch vehicle, the Soyuz is currently used as the sizing case for determining allowable mass and volume. An important point to note here is that the actual performance of Soyuz-ST 2-B from Kourou is not well defined at present, and some considerable uncertainty exists, particularly for launches into high declinations such as will be the case for Solar Orbiter. Furthermore, the launch environment of the Soyuz-Fregat launcher is comparatively benign (this is a man-rated launch vehicle, and therefore has lower design limits to the forces experienced during launch); the launch loads experienced with the EELV are more severe.

4.1.2 Baseline Mission Trajectory (2017 Launch)

The transfer phase of the 2017 baseline mission begins with a launch in January 2017, leaving the Earth at a velocity of 3.64 km/s and declination of 21.45° . This launch window provides a good balance between launcher performance and the spacecraft on-board propulsion capabilities. In fact, for the optimum launch window of 20 days, no deterministic DSM is required. About 3 months after launch, a Venus GAM with a pericentre height of more than 4000 km puts the spacecraft in a trajectory towards the Earth. An Earth GAM 1.4 years later places the spacecraft into an orbit such that another Earth GAM, with a pericentre height of more than 700 km, occurs 2 years later. Less than 6 months after the last Earth swing-by, a Venus GAM, with a pericentre height of 300 km, places the spacecraft into a 4:3 resonant trajectory with Venus. The next Venus GAM, less than 1.9 years later, starts the sequence of 3:2 resonant trajectories that raises the solar inclination angle. The resultant operational orbit has a period of 150 days, corresponding to a semi-major axis of 0.55 AU, a perihelion of 0.23 AU, and a solar inclination angle of 7.7° . A series of Venus GAMs every 450 days increases the solar inclination to its final maximum value of $\sim 34^\circ$. The characteristics of the trajectory are shown in **Figures 4.1** and **4.2** and summarized in **Table 4.1**. The key mission events listed in **Table 4.1** are launch and early orbit phase (LEOP), checkout and verification phase (CVP), cruise, nominal mission phase, and extended mission phase.

4.1.3 Back-up Mission (2018 Launch)

The transfer phase for the 2018 back-up mission begins with a launch in July 2018, with an escape velocity from the Earth of 3.66 km/s and declination of the escape velocity of about -52.97° . In this case, it is not possible to maintain a 20-day launch window without incurring a DSM-penalty: 50 m/s of additional ΔV . About 6 months after launch, a Venus GAM with a pericentre height of more than 9000 km places the spacecraft in a trajectory towards the Earth. An Earth GAM 10.5 months later puts the spacecraft into an orbit with a period such that another Earth GAM occurs 22.3 months later. Less than 3 months after the last Earth swing-by, a Venus GAM with a pericentre height of 300 km, places the spacecraft directly into a 3:2 resonant trajectory with Venus. The characteristics of the 2018 mission profile are summarized in **Table 4.2**. The 2018 option will not impact Solar Orbiter's ability to accomplish the science objectives detailed in Chapter 2.

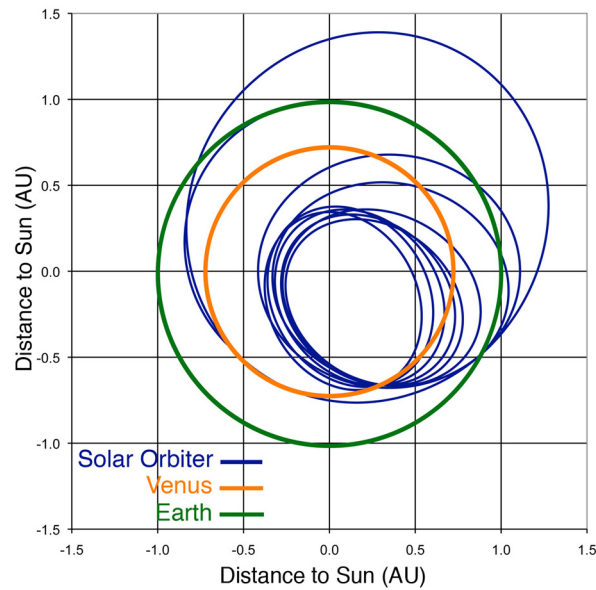


Figure 4.1. Solar Orbiter trajectory viewed from above the ecliptic.

4.2 Spacecraft Overview

The design of the Solar Orbiter spacecraft is driven both by the need to satisfy the mission's technical and performance requirements listed above and also by the need to minimize the total cost of the mission. The design philosophy adopted for Solar Orbiter is therefore to avoid technology development as far as possible in order to maintain the cost-cap of the mission in keeping with its M-class status. The obvious route to achieving this goal is through the use of technologies and engineering design lessons from previous missions. The primary 'source' mission is the BepiColombo project, which is a mission with several similarities to Solar Orbiter in terms of the space environment encountered (e.g., high solar flux). The design of Solar Orbiter has continued to incorporate BepiColombo technology items as the definition has progressed, as discussed in more detail below. Furthermore, design heritage from the Express series of missions, which had the goal of rapid and

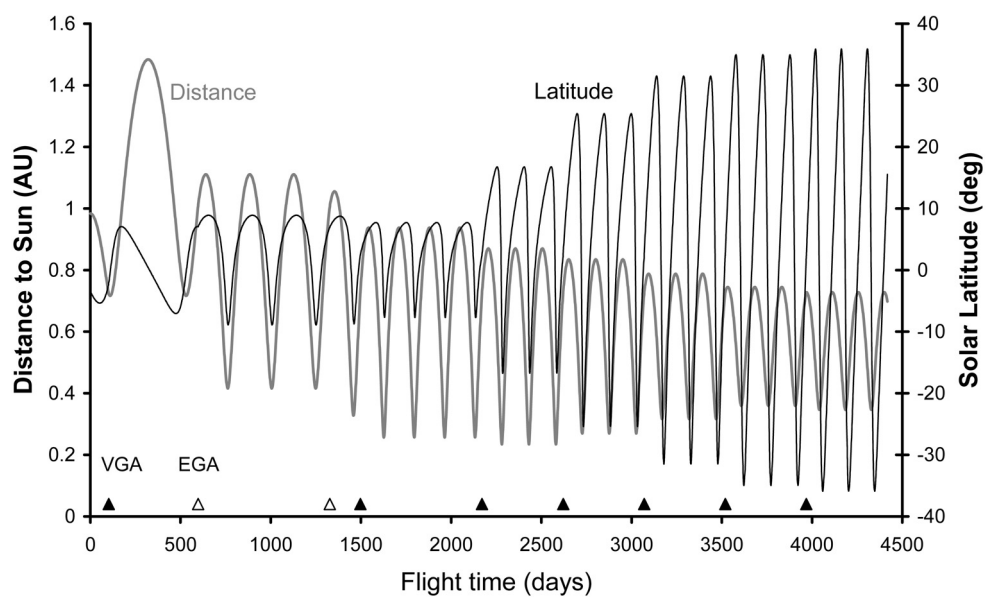


Figure 4.2. The Solar Orbit 2017 mission profile, showing heliocentric distance and solar latitude as a function of time since launch in days. Also indicated are the times at which gravity-assist manoeuvres at Venus (VGA, solid triangles) and Earth (EGA, open triangles) occur.

Table 4.1 04/01/2017 mission summary.

Mission Phase Duration (days)	Event	Date (Calendar)	Flight Time (days)	Ecliptic Inclination (deg)	Aphelion (AU)	Perihelion (AU)
LEOP (7)	Launch	2017/01/04	0	2.27	0.98	0.65
	End of LEOP	2017/01/11	7	2.27	0.98	0.65
CVP (90)	End of CVP	2017/01/11	97	2.27	0.98	0.65
Cruise (1400)	GAM V1	2017/04/15	101	2.22	1.48	0.72
	GAM E1	2018/08/25	597	3.71	1.11	0.42
	GAM E2	2020/08/25	1328	3.46	1.06	0.33
	GAM V2	2021/02/09	1497	2.68	0.94	0.26
	End of cruise	2021/02/09	1497	2.68	0.94	0.26
Full Science Nominal Mission (1229)	GAM V3	2022/12/15	2171	11.14	0.87	0.23
	GAM V4	2024/03/09	2620	19.76	0.83	0.27
	ENM (1st perihelion after GAM V4	2024/06/23	2726	19.76	0.83	0.27
Full Science Extended Mission (881)	GAM V5	2025/06/01	3069	25.84	0.79	0.32
	GAM V6	2026/08/24	3519	29.31	0.74	0.36
	EEM (1st perihelion after GAM V6	2026/11/20	3607	29.31	0.74	0.36

Mission Launch	Absolute Minimum Sun Distance (AU)	Absolute Maximum Sun Distance (AU)	Absolute Maximum Earth Distance (AU)	Max. Ecliptic Inclination (deg)	Maximum Solar Latitude (deg)
2017	0.23 2023/04/04	1.48 2017/11/21	1.98 2020/02/26	30.24 achieved at EEM	35.89 achieved at EEM

streamlined development, has also featured heavily in the Solar Orbiter design.

4.2.1 Spacecraft Description

The solution adopted for the layout of the Solar Orbiter spacecraft must take into account the following key issues:

- Thermal considerations in the allocation of units to the various bays of the spacecraft and external surfaces;
- Thermo-elastic considerations for coalignment and pointing;
- The necessity of an instrument boom to satisfy the following requirements:
 - The field-of-view requirements of all instruments;
 - Magnetic cleanliness requirements of certain key instruments;
- The necessity to protect all the instruments from the solar flux during close approach periods while providing a field-of-view to the Sun for all remote-sensing instruments (except the heliospheric imager) as well as for the solar wind in-situ instrument suite;

Table 4.2 30/07/2018 mission summary.

Mission Phase Duration (days)	Event	Date (Calendar)	Flight Time (days)	Ecliptic Inclination (deg)	Aphelion (AU)	Perihelion (AU)
LEOP (7)	Launch	2018/07/30	0	4.42	1.019	0.69
	End of LEOP	2018/08/06	7	4.42	1.019	0.69
CVP (90)	End of CVP	2018/11/04	97	4.42	1.019	0.69
Cruise (1139)	GAM V1	2019/01/23	177	3.50	1.35	0.72
	GAM E1	2019/12/01	489	0	1.083	0.48
	GAM E2	2021/09/30	1158	0.29	1.017	0.35
	GAM V2	2021/12/17	1236	3.00	0.86	0.24
	End of cruise	2021/12/17	1236	3.00	0.86	0.24
Full Science Nominal Mission (1229)	GAM V3	2023/03/12	1686	13.13	0.83	0.27
	GAM V4	2024/06/03	2135	20.61	0.79	0.32
	ENM (1st perihelion after GAM V4	2024/07/22	2184	20.61	0.79	0.32
Full Science Extended Mission (881)	GAM V5	2025/08/27	2585	24.98	0.74	0.36
	GAM V6	2026/11/20	3035	26.30	0.72	0.39
	EEM (1st perihelion after GAM V6	2027/02/02	3109	26.30	0.72	0.39

Mission Launch	Absolute Minimum Sun Distance (AU)	Absolute Maximum Sun Distance (AU)	Absolute Maximum Earth Distance (AU)	Max. Ecliptic Inclination (deg)	Maximum Solar Latitude (deg)
2018	0.24 2022/01/27	1.35 2019/07/30	1.89 2021/03/26	26.30 achieved at EEM	33.54 achieved at EEM

- The operational constraints of the mission arising from the required movements of key spacecraft appendages, including:
 - The wide range of high gain antenna (HGA) positions required in order to achieve a radio-frequency link with the ground segment;
 - The necessity to stow the HGA for close-approach periods due to the severity of the thermal environment.

The principal features of the Solar Orbiter spacecraft are shown in **Figure 4.3**. Panels A) and B) show the spacecraft in cruise and launch configurations, respectively. The platform is 3-axis stabilized and is Sun-pointed during all mission phases after LEOP. A heat shield protects the platform and sensitive equipment from the extremely high levels of solar flux. Cut-outs with feed-throughs (and doors) in the heat shield provide certain instruments with their required FOV to the Sun. The overall dimensions of the spacecraft, with appendages and solar generators stowed, are approximately 2.5 x 3.0 x 2.5 m.

The spacecraft structure is derived from the MEX/VEX/Aeolus programmes, with internal shear panels providing mounting locations for the remote-sensing instruments and bus units. External mounting locations

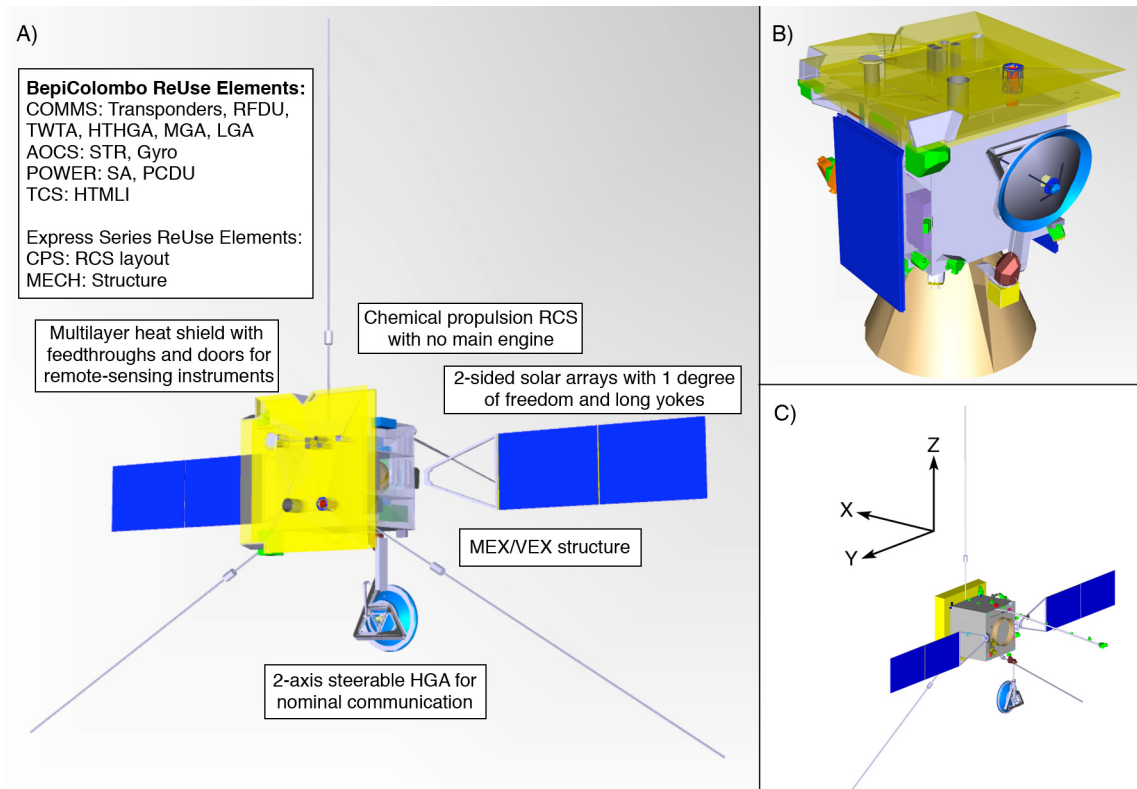


Figure 4.3. A) Solar Orbiter in cruise configuration; inset in the upper left shows reuse of elements from BepiColombo and the Express series. B) The spacecraft in launch configuration. C) The Solar Orbiter physical reference frame and coordinate system. $-Y$ is the ram direction.

are provided on face panels, as well as on a dedicated instrument boom, for the in-situ payload elements. Two-sided solar arrays provide the required power throughout the mission over the wide range of Sun distances experienced. Rotation about their longitudinal axis enables switching between faces as well as control of the solar aspect angle (SAA) to allow management of the array temperature throughout the mission and in particular during close approach to the Sun.

The spacecraft does not require a main engine because the mission does not suffer from gravity losses, and the overall ΔV requirements of the mission are comparatively modest. The rear-panel thrusters are complemented by additional thrusters on side panels in order to provide the capability to perform ΔV manoeuvres whilst maintaining a Sun-pointing attitude when close to the Sun, a critical capability for Solar Orbiter.

An articulated high-temperature high gain antenna (HTHGA) provides nominal communication with the ground station, and a medium gain antenna (MGA) and two low gain antennas (LGA) are included for use as backup and during LEOP.

The Solar Orbiter physical reference frame is defined in **Table 4.3** and shown in **Figure 4.3C**.

4.2.2 BepiColombo Technology Re-use

The re-use of BepiColombo technology (including modifications) features heavily in the design of Solar Orbiter. The inset in **Figure 4.3** summarizes the BepiColombo technology re-use status at present. For example, the X/Ka-band communications subsystem is taken entirely from BepiColombo, as is the power conditioning and distribution unit. The data management subsystem and attitude and orbit control subsystem (AOCS) also borrow heavily from BepiColombo.

4.2.3 Spacecraft Subsystems

Mechanical Subsystem. The Solar Orbiter mechanical subsystem consists of a core structure, an outer structure, brackets, joints, and attachment devices. All of the instruments and accompanying equipment are mounted on

Table 4.3 Solar Orbiter physical reference frame.

Item	Definition
Origin	Point of intersection of the launcher longitudinal axis ($+X_{LV}$) with the separation plane between the launcher and the spacecraft.
$+X_{so}$ (roll axis)	Longitudinal axis of Solar Orbiter, pointing from the origin towards Solar Orbiter, positively upwards (launcher in vertical position), coinciding with the $+X$ axis ($+X_{LV}$) of the launcher.
$+Y_{so}$ (pitch axis) $+Z_{so}$ (yaw axis)	Transverse axes, completing the right-handed orthogonal triad ($Z_{so} = Y_{so} * X_{so}$).

a closed box-type structure; several instruments are mounted on appendages (instrument boom and RPW antennas). A heat shield is mounted on the top panel ($+X$) of the spacecraft, and provides the required shielding from the direct solar illumination. The launcher interface ring is located on the opposite face ($-X$) such that the heat shield is uppermost when the spacecraft is mated to the launch vehicle. Two propellant tanks are accommodated within the box structure.

Heat Shield and Thermal Control Subsystem. The design of Solar Orbiter heat shield and thermal control subsystem (TCS) is driven by the high solar flux experienced at perihelion (hot case), on the one hand, and by the low temperatures experienced during cruise, where the spacecraft reaches a Sun distance up to 1.5 AU (cold case). The overall configuration of the Solar Orbiter TCS is illustrated in **Figure 4.4**.

Heat Shield. Solar Orbiter's heat shield consists of a combination of barriers positioned orthogonal to the incident solar flux, combined with gaps used as lateral paths to space for the heat crossing the barriers (Figure 4.6). Feed-throughs provide the required fields-of-view for the instruments (and Sun sensor) while maintaining the thermal integrity of the heat shield and limiting the flux entering the spacecraft. The feed-throughs may also provide a very limited stray-light reduction. Feed-through dimensions are derived from the instrument pupil dimensions, unobstructed field-of-view angles, distance from instrument pupil to the top layer of the heat shield, heat shield/feed-through thermoelastic performance, and integration/alignment margins plus limited provision for stray light suppression vanes. Spacecraft-provided doors shade the feed-through openings in those cases where required by a remote-sensing instrument. The doors are optimized for shading and may afford only very limited contamination protection, as they are not meant to seal the aperture. They will be capable of multiple operations, again when required by a particular instrument. The door actuation mechanism will be placed in the shade, where temperatures are relatively low, so as to ensure reliable operation.

The components of the heat shield (cf. **Figure 4.5**) are:

- Insulating layers (listed in order of proximity to the Sun): front shield, high temperature heat barrier, and low temperature heat barrier;
- Star-brackets to mount the front shield and high temperature heat barrier on the support panel;
- A support panel used to mount the brackets, the insulating layers and the various feed-throughs of the scientific instruments, and to interface with the spacecraft structure;
- Blades used to mount the support panel on the spacecraft;
- Multi-layer insulation mounted on the spacecraft $+X$ panel;
- Thermal stand-offs between star brackets, feed-through and support panel;
- Temperature sensors and supports for cables of feed-through mechanisms.

Thermal Control Subsystem. The Solar Orbiter elements behind the Sun-pointed heat shield will be in a relatively benign thermal environment. The heat shield is sized to prevent direct solar illumination onto any of the shaded components during nominal pointing and for safe mode events of spacecraft off-pointing up to 6.5° from Sun-centre. However, the spacecraft must also withstand reflected solar flux and high infrared flux from appendages outside the heat shield shadow. The remote-sensing instruments will all receive additional infrared flux from the feed-throughs. Thus, in addition to the heat shield, Solar Orbiter employs a variety of passive thermal control techniques to maintain the spacecraft platform and payload within specified temperature limits and to ensure sufficient heat rejection for the Sun-exposed instruments. These passive control measures include black-painted interiors to maximize internal radiative heat transfer, radiator areas on external panel surfaces using optical solar reflector (OSR) mirror tiles to reject heat dissipated by units, heat pipes to link units to

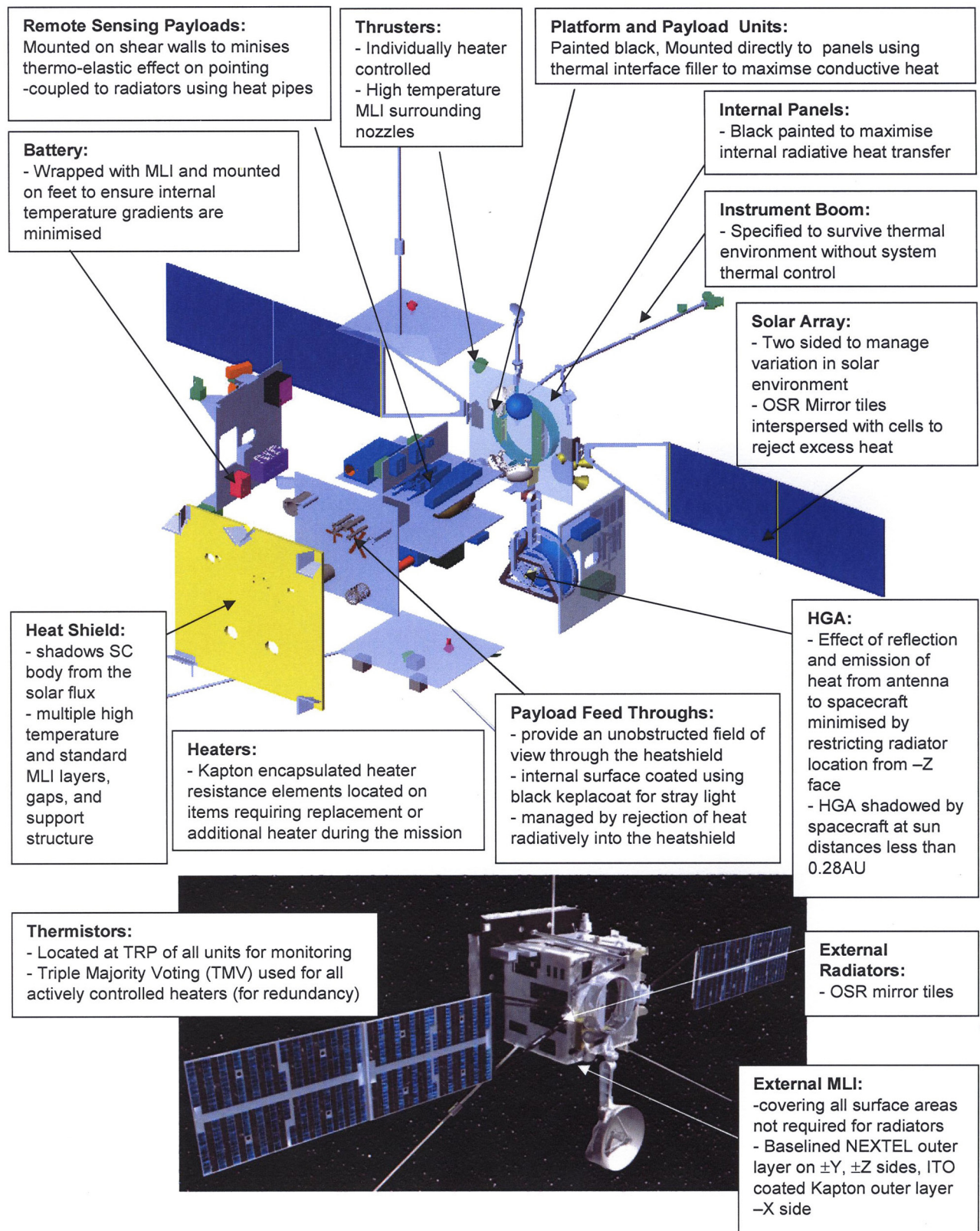


Figure 4.4. Overview of the Solar Orbiter thermal design configuration.

radiating surfaces and multi-layer insulation (MLI) to minimize heat losses from other external surfaces and thereby the use of heaters.

While the heat shield shadows the external radiator surfaces from the Sun, OSR mirror tiles have been selected to minimize the impact of solar flux reflected from external appendages (instruments and antennas)

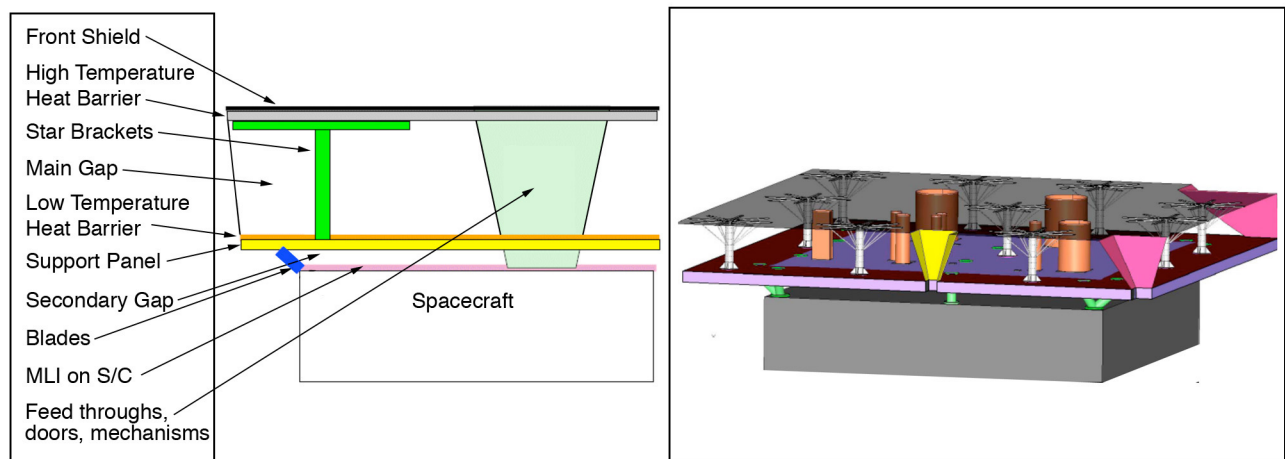


Figure 4.5. Left: heat shield components; right: overall heat shield architecture.

exposed to the Sun. The available radiator area on the spacecraft is greater than that required for the spacecraft power, and the temperature can thus be trimmed up or down before launch by varying the exposed surface.

To further improve heat rejection, the majority of the electronics units are mounted to the panels with thermal interface filler material to improve conductance between the equipment and the structure. The dissipated heat is then rejected via conduction to the panel and subsequently by radiation from the black-painted internal surfaces to the external surface of the panel, and then to space. However, since internal radiation to the external panels does not provide sufficient heat rejection capability, heat pipes are employed to improve the coupling from the payload elements to radiators.

For the cold case, Solar Orbiter requires heaters for active thermal control during the portions of the cruise phase when the spacecraft is travelling at great distances from the Sun. Heater power requirements for the cold case are significant (cf. Section 4.3.2, Power Budget).

Chemical Propulsion Subsystem. Solar Orbiter's modest total ΔV requirement (325 m/s in the worst-case 2018 mission scenario), coupled with the absence of gravity losses, led to the selection of a chemical propulsion reaction control system with no main engine. Solar Orbiter's chemical propulsion subsystem (CPS) is a simple bipropellant helium one-shot re-pressurized system. Monomethyl hydrazine is used as the fuel and mixed oxides of nitrogen, with 3% nitric oxide, are used as the oxidizer. A common propellant storage and feed system supplies the two redundant branches, each having eight 10-N reaction control thrusters. The design builds on the heritage from the Eurostar and ESA programs. The system is designed to operate in two blow-down mode phases with a single, one-shot re-pressurization between the two phases.

Attitude and Orbit Control Subsystem. The Solar Orbiter AOCS design is based on the BepiColombo baseline and aims at a re-use of BepiColombo equipment as far as possible. Solar Orbiter's AOCS comprises three star trackers (one in cold redundancy) on a common mounting integrated with an inertial measurement unit (IMU), rate measurement units, coarse sun sensors, and four 68-Nms reaction wheels. The only significant functional difference from the BepiColombo implementation concerns the survival mode and the safe mode. Instead of the numerous fine Sun sensors and a second inertial measurement unit used on BepiColombo, Solar Orbiter uses coarse sun sensors and rate measurement units in the survival mode. This difference implies that the unit failure control electronics will be different on Solar Orbiter.

Hardwired Failure Detection, Isolation, and Recovery Subsystem. Of particular criticality for the Solar Orbiter mission is the hard-wired failure detection, isolation, and recovery system, which must maintain the attitude of the spacecraft such that the heat shield shades all the sensitive elements of the spacecraft at all times for all credible failures. Accordingly, the design drivers for this system are the failure cases that can lead to off-pointing. Fortunately, the spacecraft inertial rates during the operational phase of the mission are very small, with nominal attitude control provided by the reaction wheels and with periodic off-loading effected by the thrusters. The credible failures include loss of attitude control during Sun-centre to Sun-limb re-pointing manoeuvres, thrusters failing closed during wheel off-loading, thrusters failing open, and reaction wheel blockage. Each of these failure cases has been investigated, and the simulations indicate that the sensitive elements of the spacecraft are protected for all failure cases for the baseline heat shield dimensions.

On-Board Data Handling Subsystem. Solar Orbiter's on-board data handling (OBDH) subsystem is derived mostly from the corresponding BepiColombo subsystem and provides all functionality required for operational access and control of the spacecraft, including AOCS processing and control, interfaces to units and instruments and data storage. The OBDH subsystem is based on three units: the on-board computer (OBC), the remote interface unit (RIU), and the solid state mass memory (SSMM). For the most part, all of these are re-used from the BepiColombo application. As in the case of BepiColombo, Solar Orbiter's OBDH uses the SpaceWire bus to communicate with all instruments.

The OBC is the central control unit for all onboard data handling activities, attitude and orbit control, and the management of the payload. Data management functions consist of command distribution, telemetry acquisition and timing facilities during all phases of the mission. The RIU is the central interface unit of the satellite. The SSMM includes a mass memory array consisting of 3 modules of 256 Gbit each (i.e., 768 Gbit beginning-of-life and 512 Gbit end-of-life, assuming that one of the 3 modules will degrade). The SSMM behaves as a disc unit to the users and supports a simple (flat) filing system with random access, allowing multiple read/write access simultaneously for all possible data sources and destinations. It also allows the ground, via dedicated telecommands, to create, delete, rename and copy files.

Electrical Power Subsystem. The Solar Orbiter electrical power subsystem (EPS) consists of two solar array wings (with two panels per wing); a power conditioning and distribution unit (PCDU); and a battery pack. The solar array wings have a 'hot' side and a 'cold' side. The hot side has a mixture of solar cells and OSRs to cope with the near-Sun environment; the cold side has only solar cells and is used when Solar Orbiter is far from the Sun. The arrays are operated by two solar array driving mechanisms (SADM) with redundant solar array drive electronics (SADE).

The use of the BepiColombo solar array technology and/or design for the Solar Orbiter environment will need to be proven by a future technology development activity. The current baseline design foresees two wings located on the -Y and +Y side of the spacecraft. Although the SADM allows continuous rotation around the Y-axis, only stepwise rotation is foreseen for Solar Orbiter. The PCDU converts the power provided from all power sources (e.g., solar array, battery, simulators) into a $28\text{ V} \pm 0.5\%$ fully regulated power bus for consumption by the various units and payloads on the spacecraft.

Communications Subsystem. Except for the mechanical differences in antenna design, noted below, Solar Orbiter's communications subsystem is a complete reuse of the one developed for BepiColombo, for which the requirements are significantly more severe than those for Solar Orbiter. The communications subsystem comprises a redundant set of X/X/Ka-transponders; fully redundant 35-watt X- and Ka-band travelling wave tube amplifiers (one of each); X-band and Ka-band 3 dB hybrid couplers (one of each); a radio-frequency distribution unit/wave guide interface (RFDU/WUI); and four antennas. X-band is used for uplink, and X-band and Ka-band for downlink. Both downlinks can be active simultaneously. Depending on the mission phase, the transponders can be routed via the radio-frequency switches to different antennas. The telecommunication subsystem provides hot redundancy for the receiving function and cold redundancy for the transmitting function.

Solar Orbiter's high-temperature HGA is a two-axis steerable X- and K-band 1.1-meter reflector, with an antenna pointing mechanism (APM) and associated waveguide rotary joints. It is used for primary communication with the ground and is derived from the BepiColombo HTHGA with modifications. In addition, there are two X-band LGAs, each providing hemispherical coverage (0 dBi) for the near-Earth phase, and one X-band single-axis articulated medium gain antenna (MGA) to provide a contingency communication capability in case of HGA failure.

There are key mechanical differences between the Solar Orbiter and BepiColombo designs. In particular, the Solar Orbiter HTHGA reflector is mounted on a long boom, and the elevation ranges of the HTHGA and MGA APM are different from those on BepiColombo. Both the HTHGA and MGA mechanisms are permanently shadowed by the heat shield in the case of Solar Orbiter, which provides a considerably more benign environment. The MGA mechanism for Solar Orbiter requires only one axis.

4.3 System Budgets

This section describes the current best estimate system-level budgets.

4.3.1 Mass Budget

The overall mass budget is driven by the need to accommodate both the 2017 nominal and 2018 back-up launch opportunities, which correspond to different ΔV requirements and hence propellant loading needs, and the different capabilities of the EELV and Soyuz-Fregat. The following approach has been used to calculate the Solar Orbiter mass budget:

- At equipment level, the ‘basic mass’ figures are given a margin which depends on the unit maturity level (7% for an off-the-shelf unit; 10% for a modified unit; 25% for a new unit). In the case of unit re-use from BepiColombo, the unit maturity margin is applied in addition to the BepiColombo margin. This approach results in a reliable unit ‘nominal mass’.
- For comparison with the performance of the EELV, a system margin of 30% (consistent with NASA requirements) is added. The precise type and version, and hence performance, of the EELV that will be employed is not yet defined; a best-estimate of 2500 kg derived from the Atlas V-401 User’s Manual has been used for the mass budget calculations.
- In view of the status of the Soyuz-Fregat as a back-up launch vehicle and the uncertainties still affecting its performance in the applicable 2-1b version launched from French Guiana, an estimated launch performance of 1318 kg is used and no system margin is added.

The worst-case mass budget (2018 launch with a required DSM) is shown for the EELV case in **Table 4.4**. The overall mass budget shown in **Table 4.4** displays a significant mass margin with respect to the baseline EELV capability. The equivalent budget for the back-up Soyuz-Fregat launch vehicle shows only a very small margin, however.

4.3.2 Power Budget

Table 4.4 Details of Solar Orbiter mass budget (EELV case, 2018 launch).

Subsystem	Mass (kg)	Comment
Structure	236.5	
Thermal	45.2	
Communications	111.9	Including antennas
Data Handling	32.0	
AOCS	75.6	
Power	166.4	Including Solar Generator
Propulsion	66.0	Not including consumables
Payload	180.0	Including instruments and payload support elements
Harness	99.0	
Miscellaneous	19.1	
Heat Shield	82.5	
Total spacecraft dry	1100.9	
System margin 30%	330.3	Applicable to EELV case
Consumables	194.2	
Spacecraft launch mass	1625.4	Without launch vehicle adapter
Launch vehicle adapter	41.0	
Total launch mass	1666.4	

Table 4.5 Power consumption as a function of selected mission modes.

Mode Description	Sun Distance (AU)	Power (W)
Standby (Launcher) Mode	1.0	169
Sun Acquisition Mode	1.0	518
Cruise Mode	0.8 to 1.2	968
Sun-Keeping Mode	0.234 to 0.8	896
Venus Flyby Mode	0.72	826
Science with Comms	0.28 to 0.8	1077
Science No Comms	0.234 to 0.28	783
Cold Science Case	0.8	1024

Since Solar Orbiter will re-use a number of electrical subsystem units developed for BepiColombo (a notable exception being the battery), the values adopted for unit power consumption have generally been derived from those of BepiColombo with an added 5% margin. In the current spacecraft design, the size of the two-sided solar array (8.4 m², or 2.1 m² for each of the four panels) is driven by the power demand of the cold side at the maximum distance of 1.5 AU from the Sun. Heaters to compensate for heat loss through radiators in the cold case also make up a significant proportion of the power budget (~200-250 W). The power consumption for various mission modes is shown in **Table 4.5**.

4.3.3 Link Budget

The link budgets are compliant with the telecommand and housekeeping telemetry needs in all mission phases, even in case of HTHGA failure or non-availability (in the latter case via the MGA) to the New Norcia baseline ground station.

The operational mode telemetry downlink provides the required 150 kbps at 1 AU (reference case) via the HTHGA to New Norcia. The distribution between Ka-band and X-band links varies significantly, from roughly half-half to 2/3 – 1/3, according to the orbital position of the spacecraft.

4.3.4 Data Storage Budget

The storage capacity of Solar Orbiter's solid state mass memory assumes a 2017 launch. The maximum data volume to be stored is 491 Gbits. This value is based on a communications performance of 150 kbps at 1 AU and spacecraft design allocations (i.e., not on instrument-aggregated data production demand). The time profiles of available telemetry data rates and data storage are shown in **Figure 4.6**.

The SSMM is identical to the BepiColombo unit, except for the size of the memory modules. Solar Orbiter uses 256 Gbit modules, which enables the SSMM to meet the maximum data storage requirement throughout the spacecraft life, i.e., assuming the loss of one of the three modules.

4.3.5 Pointing Budget

The absolute pointing error (APE) performance is driven by the thermoelastic deformations experienced as the spacecraft distance to the Sun varies. The current APE computation shows a performance of about 3.3 arcmin in the extreme hot case and 2.5 arcmin in the extreme cold case, versus 2 arcmin required by certain remote-sensing instruments. However, the hot case performance will be improved to compliance by both local thermal design and minor thermal operational changes. The requirement is likely to be relaxed in the extreme cold case, since it does not correspond to any of the remote-sensing science windows. The APE in all other cases meets the requirements.

The relative pointing error (RPE) does not currently meet the original performance requirement of 1 arcsec

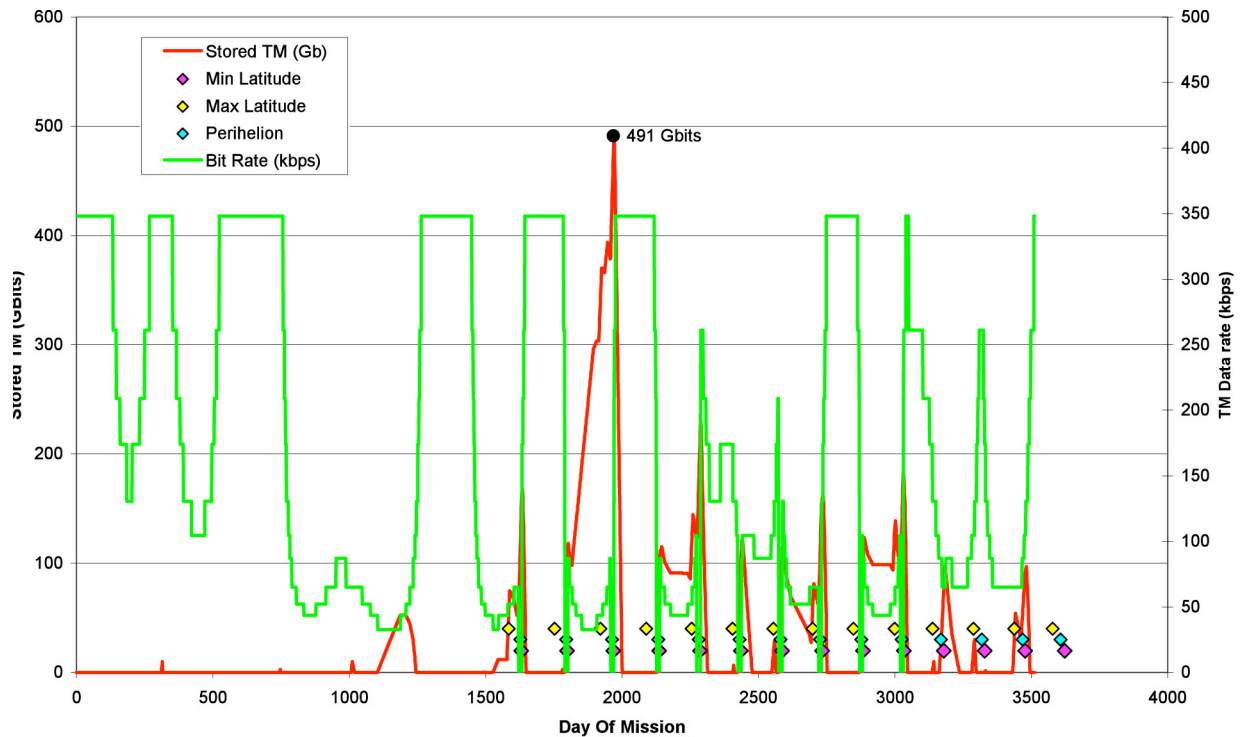


Figure 4.6. Time profile of telemetry data rate and data storage.

per 10 s, mostly because of the performance of the AOCS hardware and estimator. The achievable performance is presently 2.0 arcsec about Y (2.4 arcsec, including margin) and 1.3 arcsec about Z (1.6 arcsec, including margin). The RPE requirement of 2 arcsec about line-of-sight (X axis) is met.

4.4 Technical Challenges

The very nature of the Solar Orbiter mission implies that a number of spacecraft components are technologically critical. This is due to the very large solar flux (20 Earth solar constants) experienced at perihelion, and also to the large variations in spacecraft-to-Sun distance, with the attendant variations in the solar radiation environment. The spacecraft critical items are generally those exposed to the Sun: solar arrays, HTHGA, heat shield, attitude control sensors, and thermal control materials. The TCS design and the ground test facilities will also require critical emphasis.

Solar Arrays. Because of the extremely high solar flux to which Solar Orbiter's arrays will be exposed compared with that experienced by existing solar arrays, a new, dual-side design specific to Solar Orbiter is necessary. The array 'cold side' will be used at large distances from the Sun and is sized by far-Sun power demands; traditional technology will be used for the cold side. The hot side, which will consist of a majority of OSRs and a minority of solar cells, will be used close to the Sun, and tilted around its longitudinal axis to maintain the cell temperature within manageable limits. The design will integrate a partial heritage of units from the BepiColombo mission (solar cells, blocking diodes, shunt diodes, coatings).

High Temperature High Gain Antenna. As noted earlier, the HTHGA reflector will be inherited from the BepiColombo mission but must be adapted (pointing mechanism, coating, mounting frame) to Solar Orbiter, resulting in a higher mass than originally budgeted. For thermal reasons, the HTHGA will likely have to be folded repeatedly to place it in the shade of the spacecraft during the mission.

Heat Shield. The radiative heat shield is a development specific to Solar Orbiter. The choice, development, and verification of the materials and design are critical to the survival of the spacecraft. While the heat shield keeps most of the spacecraft in the shade, some of the baffles, doors, and mechanisms are exposed to the solar flux and have critical interfaces with the scientific instruments. It should be noted that representative heat shield prototypes have already undergone testing.

Attitude Control Sensors. Sun sensors and star trackers will have to be adapted to cope with the solar

Table 4.6 Mission scaling factors.

		Radius (AU)	r ² scaling factor
Total Mission for launch in 2017	Max (min perihelion)	0.23	18.2
	Min (max aphelion)	1.48	0.45
	Mission average *)	0.59	2.84
Nominal Science Phase for launch in 2017	Max (min perihelion)	0.23	18.2
	Min (max aphelion)	0.93	1.14
	Mission average *)	0.52	3.65
Total Mission for launch in 2018	Max (min perihelion)	0.24	16.9
	Min (max aphelion)	1.35	0.55
	Mission average *)	0.59	2.87
Nominal Science Phase for launch in 2018	Max (min perihelion)	0.24	16.9
	Min (max aphelion)	0.86	1.35
	Mission average *)	0.57	3.04

*) calculated as $1/\sqrt{\text{Average}(r^2)}$

environment. In addition, the Solar Orbiter-specific failure control electronics must be able to ensure that the spacecraft remains Sun-pointed at all times when close to the Sun, even in case of failure of the nominal attitude control.

Thermal Control Materials and Subsystem. High-temperature MLI material and coatings will be partly inherited from BepiColombo and adapted to Solar Orbiter requirements. The critical TCS will require extensive use of heat pipes and other high-performance items.

High Solar Flux Test Facilities. A combination of specially adapted, large-size, moderate-to-high solar flux test facilities and smaller, very high flux vacuum test facilities is necessary to verify the spacecraft and unit designs as well as materials properties, interfaces, and local thermal effects.

Radiation Environment. While many units will be re-used or adapted from BepiColombo, the differences between the radiation environments to which the two missions will be exposed must be taken into account for their qualification (see the following section).

4.5 Mission Environment

Very little is known about the space environment in the innermost regions of the solar system. In many cases, observations or models are not available for the range of heliospheric distances covered by Solar Orbiter, and an appropriate scaling has to be applied to a model valid for 1 AU. **Table 4.6** shows the scaling factors given by the trajectory of Solar Orbiter. **Figure 4.7** shows the heliospheric distance distribution of the Solar Orbiter trajectory. The environmental factors of particular relevance to the Solar Orbiter mission are the solar irradiance, the properties of the solar wind, and energetic particle radiation.

Solar Irradiance. The solar flux varies with solar activity, which is highly variable over a solar cycle. **Table 4.7** shows the solar flux for solar minimum and maximum, calculated using the scaling factors given in **Table 4.6**, as well the mission average flux. For thermal analyses or certain special applications, more detailed treatment is required.

Solar Wind. Characteristic mean values for the solar wind environment are given in **Table 4.8** (the values for the different distances from the Sun are derived from the values at 1 AU via simple scaling laws).

Energetic Particle Radiation. **Figures 4.8** and **4.9** show the predicted solar proton fluences and total radiation dose for the Solar Orbiter mission.

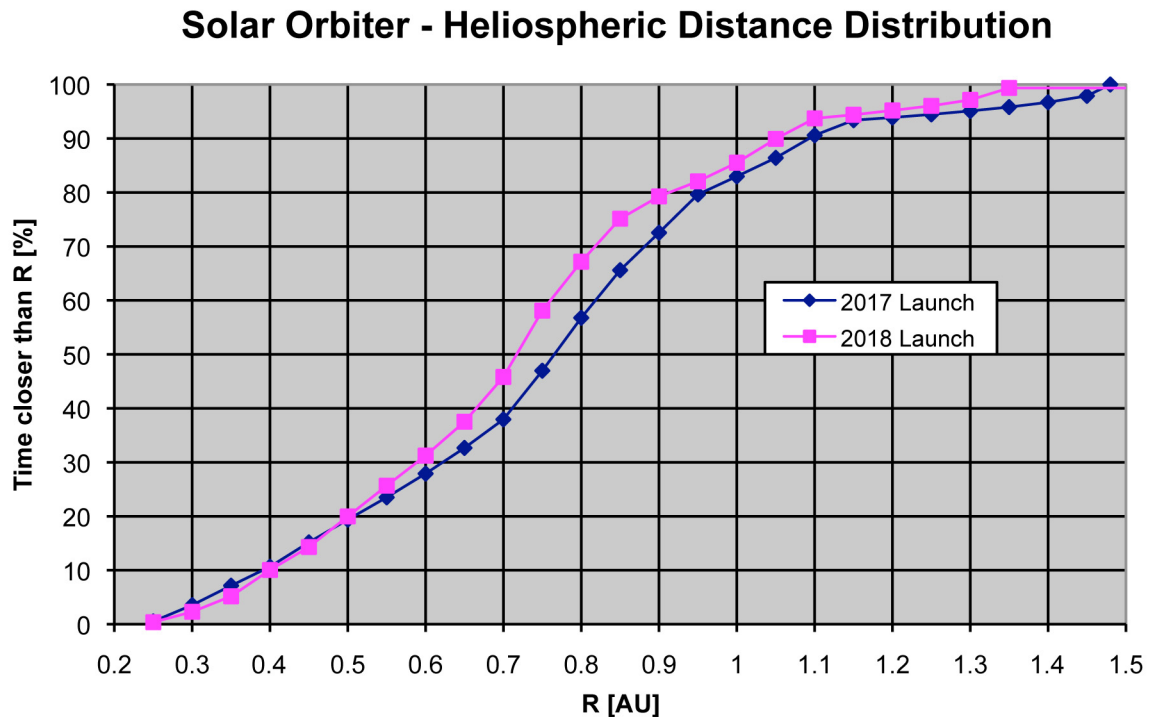


Figure 4.7. Sun-spacecraft distance distribution.

4.6 Mission Operations Concept

The mission operations concept that has been adopted for Solar Orbiter relies on the maximum possible exploitation of commonality with BepiColombo, both in the area of ground segment tools and facilities and in the sharing of manpower and expertise in the development and operations teams. Other principles underpinning this concept include, prior to launch, a joint approach to spacecraft system-level testing between the spacecraft manufacturer and the spacecraft operations team, and maximizing the synergy between spacecraft manufacturer and operators in the preparation of operational documentation, spacecraft user manual, operations database, etc.

In flight, real-time contact during phases of low activity such as cruise (in absence of manoeuvres) and periods where communications are impossible due to solar conjunctions will be minimized. In practice, this means not only that the frequency of contacts will be low, but also that each contact period will be as short as possible. Another underlying principle during flight will be the maximization of off-line operations (e.g., planning, on-board schedule execution), or alternatively, a minimization of the need for real-time interaction with the spacecraft. Regarding spacecraft operability, full, consistent, and intelligent use of the packet telemetry and telecommand concepts in the spacecraft avionics architecture is envisaged.

A clear definition of operations-related responsibilities and interfaces is of paramount importance. In particular, a clear identification (and separation) of responsibilities for payload operations between the Mission Operations Centre (MOC), the Science Operations Centre (SOC) and the principal investigators. Concerning the interface with industry, the MOC has responsibility for on-board software maintenance of the main spacecraft subsystems; industry consultancy support will be requested only on an ad-hoc basis.

Table 4.7 Solar irradiance.

	Solar flux [W/m ²] 2017 Launch	Solar flux [W/m ²] 2018 Launch
Average over the mission	3881	3927
Maximum (at minimum perihelion)	24885 (at 0.23 AU)	23057 (at 0.24 AU)
Minimum (at maximum aphelion)	620 (at 1.48 AU)	747 (at 1.35 AU)

Table 4.8 Solar wind parameters.

Parameter (average values)	1 AU (Earth)	Mission average	0.23 AU (minimum perihelion)
Density (cm^{-3})	8.7	25	158
Speed (km s^{-1})	468	468	468
T_p (K)	1.2×10^5	1.2×10^5	1.2×10^5
T_e (K)	1.0×10^5	1.0×10^5	1.0×10^5
λ (m)	7.3	4.3	1.7
$N_{\alpha}/N_{\text{proton}}$	0.047	0.047	0.047

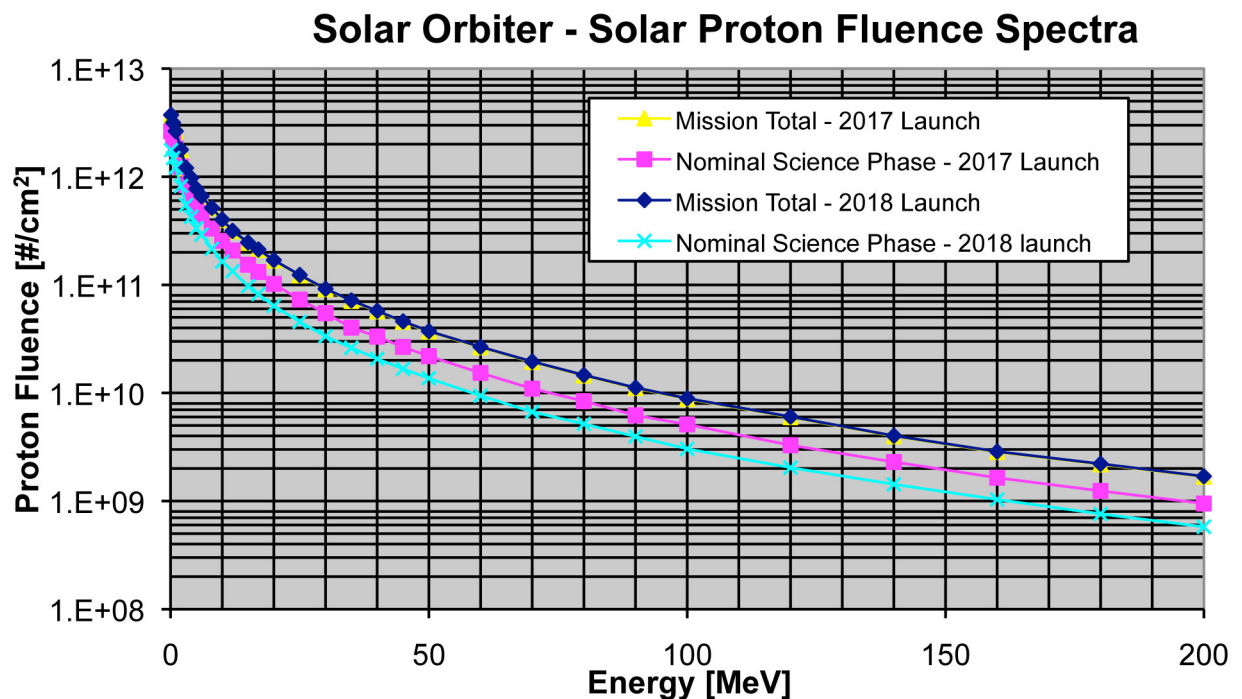
4.6.1 Ground Segment Architecture

The overall ground segment architecture for the Solar Orbiter mission reflects the standard architecture of a typical interplanetary scientific mission and will comprise the ground stations of the ESA network; the MOC, located at the European Space Operations Centre (ESOC) in Darmstadt; the SOC, which will be located at the European Space Astronomy Centre (ESAC) in Villafranca; and the communications network linking the various remotely located centres and stations to support the operational data traffic.

Ground Stations. The Solar Orbiter mission will nominally be supported by a single ESA ground station, except in critical mission phases, where multiple ground station support will be required. The routine ground station for telemetry and telecommanding is the ESA New Norcia 35-m antenna. Alternatively, the new ESA deep space antenna planned to be built in South America may replace New Norcia for the entire mission or part of it, depending on the ESA tracking station network (ESTRACK) load and capabilities at the time of the Solar Orbiter mission.

Where additional tracking support is required (e.g., for high-accuracy tracking in critical phases), the ESA Cebreros 35-m antenna will be used in addition. It is assumed that Cebreros can be used as back-up if required when New Norcia is unavailable because of maintenance.

While no NASA-Deep Space Network (DSN) support is required for nominal and contingency operations, the spacecraft will be compatible with the DSN, since possible use of DSN in support of tracking campaigns

**Figure 4.8.** Solar proton fluence spectra.

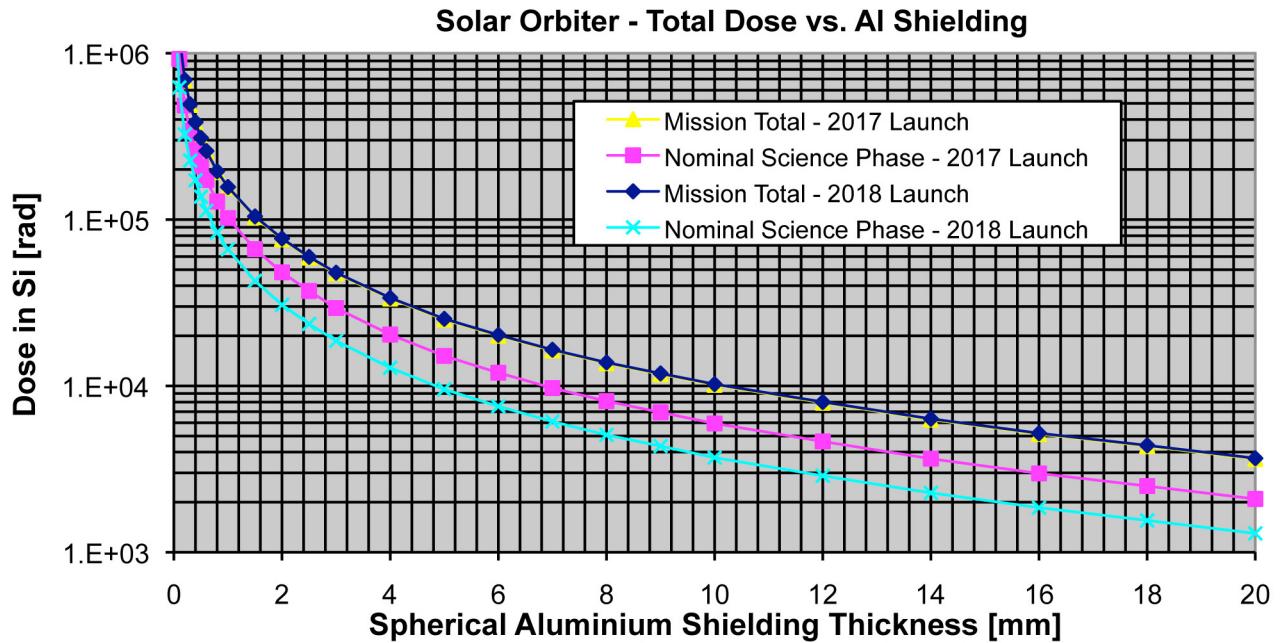


Figure 4.9. Total radiation dose vs. shielding (aluminium).

around planetary flybys or increasing the science data return may be considered when defining the details of the ESA-NASA memorandum of understanding.

The ground station network assumed during launch and early orbit phase (7 days after launch) will consist of the maximum visibility windows of about 10 hours each from New Norcia and Cebreros. The New Norcia ground station will be used over the full visibility of ca. 10 hours per daily pass through the near-Earth commissioning phase (3 months duration). During the cruise phase, 5-hour passes from New Norcia will be taken 3 times per week. For the nominal, full science mission phase after the second Venus GAM, it is assumed that New Norcia will take daily passes of 5 hours duration (4 hours dedicated to science data dump). All ESA stations will interface with the MOC via the OPSNET communications network. OPSNET is a closed wide area network for data (telecommand, telemetry, tracking data, station monitoring and control data) and voice.

Mission Operations Centre. The MOC is in charge of all mission operations planning, execution, monitoring, and control. The MOC includes infrastructure and computer hardware, as well as software for the flight control system, data processing and flight dynamics. The MOC performs the various tasks of operational data processing. It will be staffed by dedicated Solar Orbiter spacecraft operations staff, and experts in spacecraft control, flight dynamics, and network control, who will be shared with other ESA missions. The computer (hardware and software) configuration used in the MOC for the Solar Orbiter mission will be derived from the existing infrastructure and will consist of:

- A mission dedicated control system (workstation hosting SCOS 2000) used for real time telemetry processing and for command preparation and execution, telemetry and command log, archiving, and also for non real-time mission evaluation;
- A mission planning system supporting command request handling and planning and scheduling of spacecraft and payload operations;
- Workstations hosting the flight dynamics system (ORATOS), which supports all activities related to attitude and orbit determination and prediction, preparation of slew and orbit manoeuvres, spacecraft dynamics evaluation and navigation in general;
- Workstations hosting the science telemetry data distribution and instrument command reception system (data servers). The data disposition system supports the acquisition and storage of raw scientific, housekeeping and auxiliary data to be accessible at remote locations;
- A simulation computer, providing an image of the spacecraft system during ground segment verification, for staff training and during operations.

All computer systems in the MOC will be redundant, with common access to data storage facilities and peripherals. External connections to the SOC and PI institutions will use commercial/public networks.

4.6.2 Spacecraft Operations Approach

Owing to the long signal propagation delay, the spacecraft will be required to support autonomous operations. After the initial spacecraft commissioning, all telecommands required to carry out the mission will be loaded in advance on the mission timeline for later execution. All telemetry generated on-board will be stored for later retrieval from the ground. In order to support the off-line operations approach required for a deep space mission, the following autonomy capabilities will be specified for the spacecraft:

- Support of on-board control procedures, as a way to autonomously execute complex procedures including decision loops that cannot be supported from due to the propagation delay. This capability also provides the flexibility required to adjust procedures defined pre-launch to the environment and, over the course of the mission, the aging spacecraft.
- Detection and autonomous recovery from any single failure and reconfiguration to a safe back-up mode in case the detected failure is not recoverable.
- The spacecraft shall be able to continue nominal operations (and generation of mission products) without ground contact during the longest non-communication period. In case of a non-recoverable failure, the spacecraft shall be able to survive for 7 days after the end of the commissioning and up to the 2nd Venus flyby and for at least the duration of the longest non-visibility period by the ground station after the 2nd Venus flyby.

4.7 Science Operations Concept

The science operations concept is described in detail in the Science Operations Assumptions Document (SOAD). A summary of the key aspects are presented in the following.

4.7.1 Science Operations Centre

The SOC will be located at the ESAC in Spain. Its functionality may be augmented by national data centres that act as local sites and, where appropriate, provide specialized data processing and other user services. The SOC is responsible for science operations planning. The requests for payload science operations generated by the individual PI teams will be collected at the SOC and merged in a single payload operations request to be submitted to the MOC on a periodic basis, as part of the mission planning process. The MOC will be in charge of including the requests in the overall mission operations timeline to be uplinked periodically to the spacecraft. In support of the science operations planning process, the SOC will receive raw payload data and auxiliary data from the MOC, including orbit and attitude profiles, event predictions, and other mission-specific information.

The SOC will also construct a mission data archive, including all spacecraft raw data and auxiliary data received from the MOC, plus additional information resulting from basic pre-processing of the science telemetry.

4.7.2 Payload Operations Approach

Operations of the payload instruments will be conducted using the same offline approach and rules as those adopted for the spacecraft. In addition, all scientific operations will be conducted via an offline planning process under the coordination of the SOC. A particular aspect of the Solar Orbiter mission is the fact that, from a science operations standpoint, every science orbit will be different because of the changing orbital conditions (Sun-spacecraft distance, Earth-spacecraft distance, etc.). Thus, effort will be required to organize and plan

each orbit in a timely manner, since this will provide a significant benefit for the science return of the mission. As a baseline, the in-situ instruments will in principle always be switched on during normal operations. The remote-sensing instruments will nominally only operate during pre-defined, high-priority science periods. Within the 150-day orbit, observations with the remote-sensing instruments will be organized into three 10-day intervals centred on the perihelion and maximum and minimum latitude passages (see **Figure 4.10**).

The onboard mass memory will store the accumulated data that cannot be transmitted daily, and these data will be transmitted during the remainder of the orbit. Due to the continuously changing distance of the spacecraft to the Earth, the telemetry rates vary significantly with time. Should telemetry bandwidth and other operational constraints allow for it, there may be opportunities for the remote-sensing instruments to operate during other parts of the orbit. An additional operational constraint is related to the use of the HGA. For thermal reasons, the HGA must be stowed in the shadow of the spacecraft body for those parts of the orbit where the spacecraft-Sun distance is below 0.3 AU (actual threshold distance ~ 0.3 AU). This in turn implies that a number of the perihelion passes will be executed with the spacecraft in autonomous mode, with very limited – if any – ground contact.

Payload instruments contingencies, as well as maintenance and troubleshooting activities (e.g. on-board software updates, anomaly investigations), will be handled outside the normal planning process and with a direct interface between the PI team and the MOC. Presence of the PI team experts at the MOC will occasionally be required to support near-real time decision processes.

4.7.3 Science Management Plan

Following endorsement by the Solar System Working Group (SSWG) and the Space Science Advisory Committee (SSAC), the draft Science Management Plan (SMP) for Solar Orbiter was presented to Science Programme Committee (SPC) at its 120th meeting on 12-13 November 2007. Comments were provided in writing subsequent to the meeting and incorporated in the revised document (ESA/SPC(2007)49, rev.1 Annex dated 4 December 2007), which was then approved via a written procedure. The draft SMP was a reference document for the Solar Orbiter AO issued on 18 October 2007. Key elements of the SMP are summarized below.

The SMP describes the implementation of those aspects of the project, up to and including the post-operational phase, that are required to ensure fulfilment of the mission's scientific objectives, and to optimize its scientific return, with special emphasis on payload procurement, science operations, and data management. Specifically, the SMP summarizes the main aspects of the mission and provides a description of how the scientific community will be involved with the mission, and the selection of the instruments that constitute the Solar Orbiter scientific payload. The plan outlines the role of the Solar Orbiter science advisory structure, and

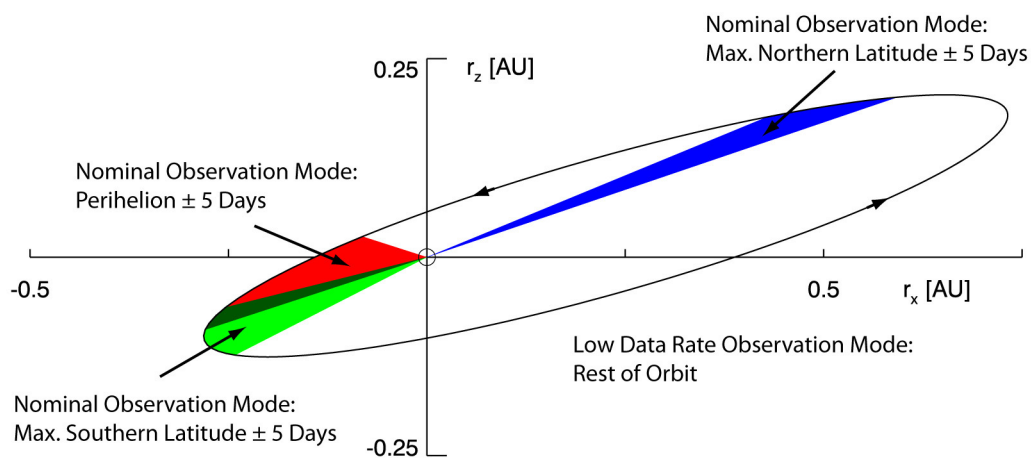


Figure 4.10. Observation modes of Solar Orbiter. Science data is collected at high rate during three 10-day windows of each orbit, centred around the perihelion and the extrema in solar latitude, and at a lower rate during the remainder of each orbit. Shown here is the first orbit that exceeds a heliographic latitude of 25 degrees. The area shaded in dark green indicates an overlap between two nominal observation windows. The r_x axis lies in the ecliptic plane and the r_z axis is perpendicular to it.

the ESA science management tasks from instrument selection to data distribution and archiving. The SMP also addresses the roles of the Solar Orbiter investigators, as well as their interaction with the Solar Orbiter Science Working Team (SWT).

Scientific Participation. As outlined in the SMP, the possible modes of participation in the Solar Orbiter programme are:

- Principal Investigator (PI), heading an instrument consortium providing an instrument;
- Co-Principal Investigator (Co-PI), appointed if a major development is carried out in a country/institution different from the one of the PI; a Co-PI will have similar rights to those of a PI, but the PI will remain the formal interface to the Project Office;
- Co-Investigator (Co-I), a member of an instrument consortium providing an instrument;
- Guest Investigator (GI), participating in the data collection and analysis of one or more instruments;
- Interdisciplinary Scientist (IDS), an expert in specific overarching science themes connected with solar and heliospheric physics.

Guest Investigators will be selected after launch and will be expected to participate in the activities of the Science Working Team, including science communications. It is envisaged that Interdisciplinary Scientists will be selected through an open AO process.

Payload Selection. In accordance with the SMP, and to ensure that the scientific return of Solar Orbiter is of the highest quality, an independent international Payload Review Committee (PRC) reviewed (in close cooperation with ESA technical, programmatic and financial analysis teams, and supported by industry) all instrument proposals submitted to ESA in response to the AO.

Post-Operations Phase and Data Archiving. Data archiving for Solar Orbiter will follow the same model as that used by previous ESA PI missions in the solar and heliophysics domain (e.g., SOHO). Reduction of science data is under the responsibility of PI teams. Following in-orbit commissioning, the PI teams retain exclusive data rights for the purpose of calibration and verification for a period of 3 months after the receipt of the original science telemetry and auxiliary orbit, attitude and spacecraft status information. Upon delivery to the ESA SOC, the data will be made available to the scientific community at large through the ESA science data archive. To enhance the scientific return from the mission, PI teams will also be required to share data with the Guest Investigators and Interdisciplinary Scientists in accordance with procedures to be agreed and formalized within the SWT.

The PI teams will provide records of processed data with all relevant information on calibration and instrument properties to the ESA science data archive. The format for the spacecraft data shall be compatible with those defined for the ESA science data archive. The ESA science data archive will be the repository of all mission products. The ESA science data archive will also be compatible with NASA's National Space Science Data Center.

5.0 Management

5.1 Industrial Organization

The previous industrial study was initiated in March 2008 and was aiming at reaching Phase B1 level by September 2009, with a pre-defined industrial organisation, building on BepiColombo developments. This study was performed by a core team led by Astrium Ltd, Stevenage, and comprising Astrium GmbH, Friedrichshafen, and Thalès Alenia Space Italy (TAS-I), Torino. The initial plan was to have Solar Orbiter mission approved by SPC in 2010, in view of starting its implementation (Phase B2/C/D) the same year. In November 2008, following BepiColombo technical difficulties and launch delay, the SPC took the decision to maintain Solar Orbiter as a potential future science mission, by including it as a candidate M mission for Cosmic Vision slice 1, for a target launch in 2017/2018 and a Cost at Completion to ESA below 450 M€ (e.c. 2008) and assuming a similar NASA provision for the launcher and payload elements. The technical problems encountered during BepiColombo development affected not only the target schedule for Solar Orbiter, but also its technical definition, in particular regarding the solar generator. Therefore, although the link to BepiColombo developments is still valid for Solar Orbiter, in particular for a number of units in the Service Module, it is necessary today to revisit the spacecraft definition and perform key technology development activities to reach the required maturity by end 2011 and enable final adoption early 2012.

As for all other Cosmic Vision missions, the industrial Phase A/B1 will be opened for competition early 2010, with the possibility of running two parallel industrial contracts. The final industrial organization will be completed only in Phase B2, mostly through a process of competitive selection and according to the ESA Best Practices for subcontractor selection, by taking into account geographical distribution requirements. The selection process will, however, be highly constrained by the requirement to re-use existing hardware units to the maximum extent possible, in particular from the BepiColombo project.

5.2 Payload Procurement

The Solar Orbiter payload will be entirely provided by nationally funded institutions. It was the subject of an ESA AO issued in October 2007 and coordinated with the corresponding NASA SMEX/FOSO AO. The responses were evaluated in coordination with NASA. The results were announced by both agencies in March 2009. As a result, 2 of the 10 instruments and (parts of) 2 major sensors of European-led suites are being funded by NASA and will be provided by U.S.-based investigators. The payload details are described elsewhere in the present document.

Although the instrument AO process and selection was performed before Solar Orbiter was placed into the Cosmic Vision plan, it will not be repeated and the current instrument suite will be confirmed for instrumentation activities, should Solar Orbiter be down-selected for a Definition Phase.

5.3 Solar Orbiter Schedule

The Definition Phase (A/B1) system study is expected to start in July 2010 for a period of 16 months, with the objective to enable the mission final adoption early 2012 (**Table 5.1**) It will include two major reviews: the Baseline Critical Review (BCR), to be held by the mid-term of the study, and the System Requirements Review (SRR), which will close the Definition Phase. The Technology Development Activities (TDAs) will be initiated as soon as possible after the mission down-selection in February 2010. These activities will run in parallel with the Definition Phase and their intermediate results will be fed into the System Study as necessary. Output from the TDAs which are critical to ensuring the mission feasibility or its development schedule are expected to be available before the decision for the mission final adoption.

At the BCR, the mission baseline should be well established and documented. It will be critically reviewed, with the aim of confirming the technical and programmatic feasibility of the space segment, and more generally of the overall mission concept. The System Requirements Review will close the Definition Phase by consolidating the overall mission concept for enabling an efficient start of the Implementation Phase, should

the mission be finally adopted.

The mission readiness for starting the implementation phase is essentially dependent on the completion of a number of spacecraft-related Technology Development Activities in the highly critical areas of heat shield items and solar generator and high solar flux test facilities, and to a lesser extent antenna adaptations and several on-board sensor technologies. However, the work done so far provides a good degree of confidence that this mission will reach by end 2011 the maturity level required by the Cosmic Vision schedule. Particular attention will be paid to the environmental test program duration, which is exceptionally long for this spacecraft due to the necessity of multiple spacecraft-level and lower-level thermal tests, including Sun simulation at various solar intensities. Further work during the Definition Phase is planned for speeding up the bottle-neck technology developments and establishing the proper compromises in thermal testing to improve the schedule margins.

Table 5.1 Definition Phase Major objectives

- | |
|--------------------------------------------------------------------------------------------------------------------------------------------------------------------------------------------------------------------------------------------------------------------------------------------------------------------------------------------------------------------------------------------------------------------------------------------------------------------------------------------------------------------------------------------------------------------------------------------------------------------------------------------------------------------------------------------------------------------------------------------------------------------------------------------------------------------------------------------------------------------------------------------|
| <ul style="list-style-type: none"> ● Consolidate the spacecraft design using the results of the Technology Development Activities, including heat shield and solar cells. ● Update the system, subsystem and equipment requirements and interface specifications. ● Assess the preliminary performance of the system. ● Perform a ray trace analysis of the expected refractions and reflections in orbit from the appendages onto the spacecraft (this activity is key to the verification of the spacecraft). ● Perform further detailed mission analysis. ● Issue Requests For Quotations of reusable and modified BepiColombo units in order to consolidate the cost estimate for Phase B2/C/D and be able to start procurement immediately upon kick-off of Phase B2. ● Follow-up of the BepiColombo activities. |
|--------------------------------------------------------------------------------------------------------------------------------------------------------------------------------------------------------------------------------------------------------------------------------------------------------------------------------------------------------------------------------------------------------------------------------------------------------------------------------------------------------------------------------------------------------------------------------------------------------------------------------------------------------------------------------------------------------------------------------------------------------------------------------------------------------------------------------------------------------------------------------------------|

6.0 References

- Aschwanden MJ. 2006. *Space Sci. Rev.* 124:361
- Axford WI, McKenzie J. 1992. In *Solar Wind Seven*, eds. E Marsch, R Schwenn. Pergamon
- Bale SD, Mozer FS. 2007. *Phys. Rev. Lett.* 98:205001
- Beck JG. 2000. *Solar Phys.* 191:47
- Borovsky JE. 2008. *J. Geophys. Res.* 113:A08110
- Breech B, et al. 2008. *J. Geophys. Res.* 113: A08105
- Brun AS, Miesch MS, Toomre J. 2004. *Astrophys. J.* 614:1073
- Bruno R, et al. 2001. *Planet Space Sci.* 49:1201
- Cargill PJ, et al. 2006. *Space Sci. Rev.* 124:249
- Cirtain J, et al. 2007. *Science* 318:1580
- Corbard T. 1997. PhD thesis, Université de Nice
- Cohen CMS, et al. 2007. *Space Sci. Rev.* 130:183
- Cranmer SR, van Ballegoijen AA, Edgar RJ. 2007. *Astrophys. J. Suppl.* 171:520
- De Pontieu B, et al. 2009. *Astrophys. J* 701:L1
- Desai MI, et al. 2006. *Space Sci. Rev.* 124:261
- Dikpati M, Charbonneau PA. 1999. *Astrophys. J.* 518:508
- Dikpati M, Gilman PA. 2008. *J. Astrophys. Astron.* 29:29
- Drake JF, et al. 2009. *Astrophys. J.* 700:L16
- Fisk LA, Schwadron NA, Zurbuchen TH. 1999. *J. Geophys. Res.* 104:19765
- Fisk LA, Zurbuchen TH. 2006. *J. Geophys. Res.* 111:A09115
- Fisk LA, Gloeckler G. 2007. *Space Sci. Rev.* 130:153
- Geiss J, Bochsler P. 1985. In *CNES Isotopic Ratios in the Solar System*, p. 213
- Geiss J, et al. 1995. *Science* 268:1005
- Getman KV, et al. 2008. *Astrophys. J.* 688:418
- Giacone J, Kota J. 2006. *Space Sci. Rev.* 124:277
- Gizon L, Birch AC. 2005. *Living Rev. Solar Phys.* 2 (cited 30 August 2009)
- Gopalswamy N. 2006. *Space Sci. Rev.* 124:145
- Gopalswamy N, et al. 2001. *Astrophys. J.* 548:L91
- Gopalswamy N, et al. 2002. *Geophys. Res. Lett.* 29:106
- Gopalswamy N, et al. 2008. *Astrophys. J.* 674:560
- Hansteen V, Leer E. 1995. *J. Geophys. Res.* 100:21577
- Harvey JW, et al. 2007. *Astrophys. J.* 659:177
- Horbury TS, Forman MA, Oughton S. 2008. *Phys. Rev. Lett.* 101:175005
- Howe R, et al. 2006 *Solar Phys.* 235:1
- Jackiewicz J, Gizon L, Birch AC. 2008. *Solar Phys.* 251:381
- Kleckner BE, Möbius E, Popecki MA. 2006. *Space Sci. Rev.* 124:289
- Kohl JL, et al. 1998. *Astrophys. J.* 501:L27
- Kohl JL, et al. 2006. *Astron Astrophys. Rev.* 13:31
- Lamb DA, et al. 2008. *Astrophys. J.* 674:520
- Lamb DA, et al. 2009. *Astrophys. J.* in press
- Lee MA. 2007. *Space Sci. Rev.* 130:221
- Li X et al. 1998. *Astrophys. J.* 501:L33
- Lin J, Forbes TG. 2000. *J. Geophys. Res.* 105:2375
- Lin RP. 2006. *Space Sci. Rev.* 124:233
- Lites B, et al. 2007. *Publ. Astron. Soc. Japan* 59:S571
- Lockwood M, Stamper R, Wild MN. 1999. *Nature* 399:437
- Lugaz N, Manchester WB, Gombosi TI. 2005. *Astrophys. J.* 634:651
- Lynch BJ, et al. 2004. *Astrophys. J.* 617:589
- Makarov VI, Tlatov AG, Sivaraman KR. 2000. *Solar Phys.* 214:41
- Mann G, et al. 2003. *A&A* 400:329

- Marsch E. 2006. *Living Rev. Solar Phys.* 3
- Marsch E. 2006. *Astron. Astrophys.* 457-699
- Marino R, et al. 2008. *Astrophys. J.* 677 L71
- Martinez Pillet V. 2006. In *Proceedings of the Second Solar Orbiter Workshop*, eds. R Marsden, L Conroy. Noordwijk, ESA
- Mason GM. 2007. *Space Sci. Rev.* 130:231
- Matteini L, et al. 2007. *Geophys. Res. Lett.* 34:L20105
- McComas D, et al. 2008. *Geophys. Res. Lett.* 35:L18103
- McIntosh S, Davey AR, Hassler DM. 2006. *Astrophys. J.* 644:L87
- Mewaldt RA. 2006. *Space Sci. Rev.* 124:303
- Mewaldt RA, et al. 2007. *Space Sci. Rev.* 130:207
- Ontiveros V, Vourlidas A. 2009. *Astrophys. J.* 693:267
- Owens MJ, Crooker NU. 2006. *J. Geophys. Res.* 111:A10104
- Owens MJ, et al. 2008. *Geophys. Res. Lett.* 35:L20108
- Neugebauer M, et al. 1995. *J. Geophys. Res.* 100:23389
- Palmer ID. 1982. *Rev. Geophys. Space Phys.* 20:335
- Parnell CE, et al. 2009. *Astrophys. J.* 698:75
- Patsourakos S, Vourlidas A. 2009. *Astrophys. J.* 700:L182
- Pietarila Graham J, Danilovic S, Schüssler M. 2009. *Astrophys. J.* 693:1728
- Richardson IG, Cane HV. 2004. *Geophys. Res. Lett.* 31:L18804
- Rouillard AP, Lockwood M, Finch I. 2007. *J. Geophys. Res.* 112:A05103
- Schrijver CJ, et al. 1997. *Astrophys. J.* 487:424
- Schrijver CJ, Title AM. 2001. *Astrophys. J.* 551:1099
- Schwadron NA, McComas DJ. 2003. *Astrophys. J.* 599:1395
- Schwadron NA, McComas DJ. 2008. *Astrophys. J.* 686:L33
- Sheeley NR. 1991. *Astrophys. J.* 374:386
- Smith CW, et al. 2001. *J. Geophys. Res.* 106:18625
- Smith EJ, et al. 2000. *Astrophys. J.* 533:1084
- Thieme KM, Marsch E, Schwenn R. 1990. *Ann Geophys.* 8:713
- Telloni D, Antonucci E, Doderio MA. 2007. *A&A* 476:1341
- Thompson MJ, et al. 2003. *Ann Rev. Astron Astrophys.* 41:599
- Tsuneta S, et al. 2008. *Astrophys. J.* 688:1374
- Tu CY, Marsch E. 1990. *J. Geophys. Res.* 98:1257
- Tu CY, et al. 2005. *Science* 308:519
- Tylka AJ, et al. 2005. *Astrophys. J.* 625:474
- von Steiger R, et al. 1997. *Adv Space Res.* 15:3
- Vourlidas A, et al. 2003. *Astrophys. J.* 598:1392
- Vršnak B, Cliver EW. 2008. *Solar Phys.* 253:215
- Wang YM, Sheeley NR. 2006. *Astrophys. J.* 653:708
- Wang YM, Nash AG, Sheeley NR. 1989. *Astrophys. J.* 347:529
- Wang YM, et al. 2007. *Astrophys. J.* 660:882
- Zhang J., Dere KP. 2006. *Astrophys. J.* 649:1100
- Zirin H. 1987. *Solar Phys.* 110:101

7.0 Acronyms

A/D	Analog-to-Digital
AIV	Assembly, Integration, & Verification
ALMA	Atacama Large Millimeter Array
ANT	Antenna (RPW)
AO	Announcement of Opportunity
AOCS	Attitude and Orbit Control Subsystem
APE	Absolute Pointing Error
APM	Antenna Pointing Mechanism
APS	Active Pixel Sensor
ASR	Advanced Study Report
ATST	Advanced Technology Solar Telescope
AU	Astronomical Unit
BCR	Baseline Critical Review
BIAS	Biasing Unit (RPW)
CDPU	Common Data Processing Unit
CDS	Coronal Diagnostic Spectrometer
CIR	Corotating Interaction Region
CME	Coronal Mass Ejection
COMMS	Communication System
COSMO	Coronal Solar Magnetic Observatory
CPS	Chemical Propulsion System
CSL	Centre Spatiale de Liège
CVP	Checkout and Verification Phase
CZT	Cadmium-Zinc-Telluride
DC	Direct Current
DMS	Data Management System
DPU	Data Processing Unit
DPU	Digital Processing Unit
DSM	Deep Space Manoeuvres
DSN	Deep Space Network
EA	Electrostatic Analyser
EAS	Electron Analyser System
EELV	Evolved Expendable Launch Vehicle
EEM	End of Extended Mission
EID-B	Experiment Interface Document, Part B
ENM	End of Nominal Mission
EPD	Energetic Particle Detector
EPHIN	Electron Proton Helium Instrument
EPS	Electrical Power Subsystem
EPT	Electron Proton Telescope
ERNE	Energetic and Relativistic Nuclei and Electron (experiment)
ESA	European Space Agency

ESAC	European Space Astronomy Centre
ESOC	European Space Operations Centre
EST	European Solar Telescope
ESTEC	European Space Research and Technology Centre
ESTRACK	ESA Tracking Station Network
ETH	Eidgenössische Technische Hochschule
EUI	Extreme Ultraviolet Imager
FDT	Full Disk Telescope
FEE	Front End Electronics
FG	Filtergraph
FIP	First Ionization Potential
FOSO	Focused Opportunity for Solar Orbiter
FOV	Field of View
FSI	Full Sun Imager
GAM	Gravity Assist Manoeuvre
GI	Guest Investigator
GONG	Global Oscillation Network Group
HCS	Heliospheric Current Sheet
HELEX	Heliophysical Explorers
HET	High Energy Telescope
HGA	High Gain Antenna
HIS	Heavy Ion Sensor
HMF	Heliospheric Magnetic Field
HMI	Helioseismic and Magnetic Imager
HRI	High Resolution Imager
HRT	Hard X-ray Telescope
HRT	High Resolution Telescope
HTHGA	High Temperature High Gain Antenna
HTMLI	High Temperature Multi-Layer Insulation
IAC	Instituto de Astrofísica de Canarias
IAPS	Intensified Active Pixel Sensor
ICME	Interplanetary Coronal Mass Ejection
ICSTM	The Imperial College of Science, Technology, and Medicine
ICU	Instrument Controller Unit
IDS	Interdisciplinary Scientist
ILWS	International Living with a Star
IMF	Interplanetary Magnetic Field
IMU	Inertial Measurement Unit
ISS	Image Stabilization System
JHU/APL	Johns Hopkins University Applied Physics Laboratory
JPL	Jet Propulsion Laboratory
JOP	Joint Observation Programme
JSTD	Joint Science and Technology Definition Team
KSC	Kennedy Space Center

LASCO	Large-Angle and Spectrometric Coronagraph
LCVR	Liquid Crystal Variable Retarder
LEOP	Launch and Early Orbit Phase
LET	Low Energy Telescope
LF	Low Frequency
LFR	Low Frequency Receiver
LGA	Low Gain Antenna
LOFAR	Low Frequency Array
LOS	Line of Sight
LVPS	Low Voltage Power Supply
LWS	Living with a Star
MAG	Magnetometer
MDI	Michelson Doppler Imager
MEB	Main Electronics Box
MECH	Mechanical (Sub)system
METIS/COR	Multi Element Telescope for Imaging and Spectroscopy
MEX	Mars Express
MGA	Medium Gain Antenna
MLI	Multi-Layer Insulation
MMO	Mercury Magnetospheric Orbiter
MOC	Mission Operations Centre
MPS	Max-Planck-Institut für Sonnensystemforschung
NASA	National Aeronautics and Space Administration
NRL	Naval Research Laboratory
OBC	On-Board Computer
OBDAH	On-Board Data Handling
ORATOS	Orbit and Attitude Operations System
OSR	Optical Solar Reflector
PAS	Proton Alpha Sensor
PHI	Polarimetric and Helioseismic Imager
PCDU	Power Conditioning and Distribution Unit
PCU	Power Converter Unit
PMP	Polarization Modulation Package
PRC	Payload Review Committee
RAL	Rutherford Appleton Laboratory
RCS	Reaction Control (Sub)system
RFDU/WGI	Radio-Frequency Distribution Unit / Wave Guide Interface
RIU	Remote Interface Unit
RPE	Relative Pointing Error
RPW	Radio Plasma Waves (experiment)
RHESSI	Reuven Ramaty High Energy Solar Spectroscopic Imager
S/C	Spacecraft
SA	Solar Array
SAA	Solar Aspect Angle

SADE	Solar Array Drive Electronics
SADM	Solar Array Driving Mechanism
SCE	SoloHI Control Electronics
SCM	Search Coil Magnetometer
SCOS	Spacecraft Control and Operation System
SEP	Solar Energetic Particle
SEPT	Solar Electron Proton Telescope
SIM	SoloHI Instrument Module
SIS	Suprathermal Ion Spectrograph
SMEX	Small Explorer
SMP	Science Management Plan
SOAD	Science Operations Assumptions Document
SOC	Science Operations Centre
SOHO	Solar and Heliospheric Observatory
SoloHI	Solar Orbiter Heliospheric Imager
SOT	Science Operations Team
SOT	Solar Optical Telescope
SPC	Science Programme Committee
SPICE	Spectral Imaging of the Coronal Environment
SPP	Solar Probe Plus
SRR	System Requirements Review
SSAC	Space Science Advisory Committee
SSMM	Solid State Mass Memory
SSWG	Solar System Working Group
STEIN	SupraThermal Electrons Ions and Neutrals
STEREO	Solar Terrestrial Relations Observatory
STIX	Spectrometer/Telescope for Imaging X-rays
STR	Star Tracker
SUMER	Solar Ultraviolet Measurements of Emitted Radiation
SWA	Solar Wind Analyzer
SWRI	Southwest Research Institute
SWT	Science Working Team
TCS	Thermal Control Subsystem
TDA	Technology Development Activities
TDS	Time Domain Sampler
TNR-HFR	Thermal Noise and High Frequency Receiver
TOF	Time of Flight
TRACE	Transition Region and Coronal Explorer
TVLS	Toroidal Variable Line Spaced
TWTA	Traveling Wave Tube Antenna
UCL/MSSL	University College London/Mullard Space Science Laboratory
ULEIS	Ultra Low Energy Isotope Spectrometer
UV	Ultraviolet
VEX	Venus Express